UNIVERSITY OF OKLAHOMA

GRADUATE COLLEGE

AN INTEGRATED PALEOMAGNETIC AND DIAGENETIC INVESTIGATION OF THE BARNETT SHALE AND UNDERLYING ELLENBURGER GROUP CARBONATES, FORT WORTH BASIN, TEXAS

A DISSERTATION

SUBMITTED TO THE GRADUATE FACULTY

in partial fulfillment of the requirements for the

Degree Of

DOCTOR OF PHILOSOPHY

By

DEVIN P DENNIE

Norman, Oklahoma

2010

AN INTEGRATED PALEOMAGNETIC AND DIAGENETIC INVESTIGATION OF THE BARNETT SHALE AND UNDERLYING ELLENBURGER GROUP CARBONATES, FORT WORTH BASIN, TEXAS

A DISSERTATION APPROVED FOR THE
CONOCO PHILLIPS SCHOOL OF GEOLOGY AND GEOPHYSICS

By

_____

Dr. R. Douglas Elmore, Chair

_____

Dr. Michael Engel

_____

Dr. Roger Slatt

_____

Dr. Carl Sondergeld

_____

Dr. Jack Beuthin

ACKNOWLEDGEMENTS

I would foremost like to thank my advisor, Dr. R. Douglas Elmore, for all of this patience, guidance and counsel, and friendship in the preparation and completion of this dissertation. Thanks to Drs. Engel, Slatt, Sondergeld and M. Soreghan for their contributions and reviews and for serving on my examination and advisory committee.

Special thanks to my friends and colleagues: Dr. Shanmugam Johari Pannallal, for his technical assistance and support on many aspects of this project, Mr. Earl Manning for his knowledge of fluids and their inclusions, Mr. John Deng, Dr. Matthew Zechmeister and all of our undergraduate paleomagnetic lab workers. Thanks to Gene Kuhlman and Vy Jordan at OPIC for all their help in retrieving and reviewing well core.

Thanks to the Devon Energy Corporation for funding this research. Special thanks to Jeff Hall for approving and supporting my involvement in this project; to Dale Fritz, for his unwavering support, encouragement and effort to help me get to the finish line, and to Dr. Jack Beuthin, for being a sounding board for geofantasical thinking. Thanks to all of my co-workers who tolerated my absences during work on this project.

Most of all, thanks to my wife, Elizabeth, for her grace and support during this long process; to sons Logan and Morgan, and daughter Alyson for putting up with Daddy working late and going to school all the time; to my parents, R.T. and Paula Dennie for their encouragement and to Mary Ruffel and Lance Ruffel for their generous knowledge and support as well.

Devin Dennie
05/10

LIST OF TABLES

CHAPTER 1

CHAPTER 2

LIST OF FIGURES

Chapter 1

Chapter 2

PREFACE

Shales and mudstones have long been identified as hydrocarbon source rocks, or seals, for other units, but are now viewed as drillable and producible reservoir targets in their own right. Much of the interest in shale oil and shale gas plays is derived from the successful production of natural gas and oil from the Mississippian Barnett Shale Formation of north central Texas. Given the thousands of wells now drilled in the Barnett Shale, questions still remain about the impact of diagenetic alteration of the mudstones, especially impacts, if any, from basin fluids near major faults and karsts developed in the underlying Ellenburger Group carbonates and Precambrian basement rocks. This research focuses on the paleomagnetic, geochemical and petrographic study to attempt to add understanding to the geologic history of both units.

The Barnett Shale is a very tight reservoir rock, with limited permeability and nanoporosity. These characteristics require the artificial fracturing of the rock by high pressure fluids, a process commonly known as “fraccing”, to make an economic well. Lateral and vertical variations in rock character derived from natural geologic variations in the shale and underlying carbonates may significantly impact the ultimate productive nature of a shale gas well.

The origins of these natural variations are not fully understood. Many variations are shown by previous studies to be undoubtedly related to the depositional history and stratigraphic variations of lithofacies. Diagenesis, however, may result in the alteration of depositional lithofacies non-uniformly across the basin, as it is dependant on factors such as burial depth, structural history, rock character (e.g., mineralogy and mechanical behavior) and alteration by burial-related or orogenic fluids. There have been relatively

few studies on the basin-wide diagenesis of the units and how diagenesis can affect reservoir quality and behavior.

Previous studies suggest that thermal maturity anomalies are present within the Barnett shale near major basin faults and near to the Ouachita thrust (Bowker, 2007; Pollastro et al., 2007). These anomalies are hypothesized as related to "hydrothermal" fluids that migrated from the Ouachita thrust collision zone during formation of the Fort Worth Basin. A specific objective of this research is to independently test this hypothesis. This research employed an integrated diagenetic (petrographic, geochemical, and fluid inclusion) and paleomagnetic approach to determine the nature and timing of fluid alteration in the Barnett Shale as well as the underlying Ellenburger carbonates, as well as to understand the ramifications of these fluids on the productivity of the units.

Chapter 1 focuses on identifying paleomagnetic, geochemical, and petrographic evidence for diagenetic alteration and determining the timing of diagenetic events in the Ellenburger Group carbonates underlying the Barnett Shale. In Chapter 2, the study focuses on remagnetization of the Barnett Shale during burial, and post-burial, diagenetic processes. Special focus is given to fracture behavior and orientation versus paleomagnetic timing of diagenesis.

Chapter 1

Diagenesis and Paleomagnetism of uppermost Ellenburger Group carbonates, Fort Worth Basin, Texas.

Abstract

The Ordovician Ellenburger Group carbonates are extensively karsted and brecciated throughout portions of the western half of the Fort Worth Basin, Texas, where it underlies the Mississippian Barnett Shale gas reservoir and source rock. An integrated geochemical/petrographic, paleomagnetic and rock magnetic study was conducted to better understand the nature and timing of diagenetic events in the unit. Samples from three scribe oriented conventional drill cores of the uppermost Ellenburger Group carbonates were analyzed for their diagenetic and paleomagnetic properties. Thermal demagnetization of samples from both units reveals a low-temperature steeply downward viscous remanent magnetization (VRM) as well as several components that are removed at higher temperatures (200-540°C). The higher temperature components reside in magnetite and are interpreted as chemical remanent magnetizations (CRMs) based on low burial temperatures. The specimen directions are streaked from an easterly and shallow direction to a southerly and shallow direction.

The modern VRM was used to orient the CRM data for one of the wells and to test the scribe orienting method. The results confirm that the streak of directions is real. The streak disappears when the directions are grouped by diagenetic facies. Specimens from clasts in the karst breccia facies contain a CRM with easterly declinations and shallow inclinations that fails a conglomerate test and has an Ordovician pole. A mixed dolomite-limestone with shale filled fracture facies contains a pole which falls off of but close to the Late Mississippian-Early Pennsylvanian part of the apparent polar wander path. A group of facies (crystalline dolomite, wavy bedded to argillaceous dolomite, mottled, burrowed dolomite with fine grained breccia

facies, and clastic-rich peritidal carbonates) contains a Late Permian-Early Triassic CRM. Dolomites with vug-fill solution-reprecipitation features contain a Late Triassic-Jurassic CRM. The results from these facies suggest a possible tectonic counterclockwise rotation of the basin by 15 to 20°. The Ordovician CRM is interpreted as related to relatively early diagenetic processes, perhaps associated with Ordovician to early Silurian dolomitization. The Late Mississippian-Early Pennsylvanian CRM is interpreted to represent a mid-Pennsylvanian burial diagenetic event coinciding with burial of the unit to the oil window. The Late Permian-Early Triassic CRM is interpreted as forming from externally derived hydrothermal fluids that may have migrated from the Ouachita thrust zone or along deep basement faults. The Late Triassic-Jurassic CRM may be related to gravity driven fluid migration occurring during basin relaxation and extension during the uplift of the Llano and breakup of Pangea.

1.1 Introduction

The Cambro-Ordovician Ellenburger Group in Texas has undergone significant diagenesis including multiple dolomitization and karsting events (Loucks and Anderson, 1985; Kerans, 1990; Kupecz and Land, 1991). Orogenic fluids from the Ouachita-Marathon mountain front are also hypothesized to have been a major agent of diagenesis (e.g., Kerans, 1990; Combs et al., 2003; Gale and Gomez, 2007). Questions remain, however, about the absolute timing of the diagenetic events. Most of the previous work on the Ellenburger Group has focused on the outcrops in central Texas and in the subsurface of the Permian Basin where the unit is a major hydrocarbon reservoir. Fluids are interpreted to have played a major role in altering the Ellenburger carbonates in west Texas (e.g., Hoak et al, 1998). Less work has been conducted on the Ellenburger Group in the Fort Worth Basin where rocks are confined to the subsurface.

The diagenetic characteristics of the unit are believed to be an important variable in the recoverability of natural gas from the overlying Barnett Shale natural gas wells (Bowker, 2007; Fisher, 2002). It is important to investigate the Ellenberger Group in the Fort Worth Basin not only to better understand the role of fluids and the timing of events but also because it could help to refine exploration and production strategies in the overlying Barnett Shale.

The objective of this study is to conduct an integrated diagenetic and paleomagnetic study of the Ellenburger Group carbonates in the Fort Worth Basin in order to characterize the diagenesis, determine the origin of the diagenetic fluids, determine the fluid pathways (e.g., faults, factures), and the timing of the events. I will test the hypothesis that the carbonates in the Fort Worth Basin have been altered by orogenic fluids originating from the Ouachita thrust zone and compare the diagenetic history between units subjected to early karsting versus tectonically fractured deposits. The data for this study came from five cores in the upper Ellenburger taken from wells that contain evidence of tectonic and karst processes. The wells were collected adjacent and distal to the Ouachita thrust front (Figure 1-1). Petrographic, fluid inclusion, and geochemical analysis were used to identify the diagenetic features and diagenetic facies and construct a paragenetic sequence. Geochemical studies (C, O and Sr isotopes) were used to assess alteration by externally-derived fluids. Paleomagnetic and rock magnetic studies were used to determine the timing of events.

1.2 Geologic Setting of Study Area

The Ellenburger Group is made up of extensive platform carbonates deposited on Precambrian basement on the southern Laurentian passive margin. The carbonate platform was developed during the mid-Cambrian through Lower Ordovician highstand period (Cloud and Barnes, 1948; Bartram, 1950; Barnes et al., 1959; Burgess, 1976). The thick sequence of carbonates is correlative to the Arbuckle and Knox Groups in the central and eastern United States. These rocks are major reservoirs for oil and gas exploration in many hydrocarbon-producing basins in the southern United States and northern Mexico (Gomez et al., 2001; Bradfield, 1964).

Ellenburger carbonates in the Fort Worth Basin of north-central Texas (Figure 1-1) comprise the bulk of the early Paleozoic strata. The Ellenburger Group in the Fort Worth Basin does produce hydrocarbons but the unit is less productive and more water-wet than in the Permian Basin (Pollastro et al., 2007; Jarvie et. al. 2007; Bowker, 2007).

The Fort Worth Basin is one of a series of foreland sedimentary basins associated with the Late Paleozoic Ouachita fold-thrust belt front (Meckel, 1992). The Ouachita fold-thrust front formed during the closing of the Iapetus Ocean during the continental assembly of Pangaea (Walther, 1982). The basin is constrained to the north by pre-Alleghenian uplifts (Figure 1-1), notably the Muenster arch and Red River uplift. These uplifts are related to tectonic inheritance from the southern Oklahoma aulacogen (Thomas, 1993). Paleozoic rocks of the southern Fort Worth Basin onlap onto the Bend arch to the west and the Lampasas - Concho arches to the south; structures related to the northward flank of the Llano Uplift in central Texas (Turner, 1957).

The Muenster Arch is located on the edge of the southeastern extension of the southern Oklahoma aulacogen, and the presence of major basement reverse faults (Flawn, 1961; Henry, 1982) suggests some reactivation of deep basement faults and possible rift inversion during this time (Erlich and Coleman, 2006). Transpressive motions resulted in a NW-SE oriented basin axis southwest of the Muenster Arch prior to subsidence along the frontage of the Ouachita fold-thrust belt (Pollastro et al., 2007).

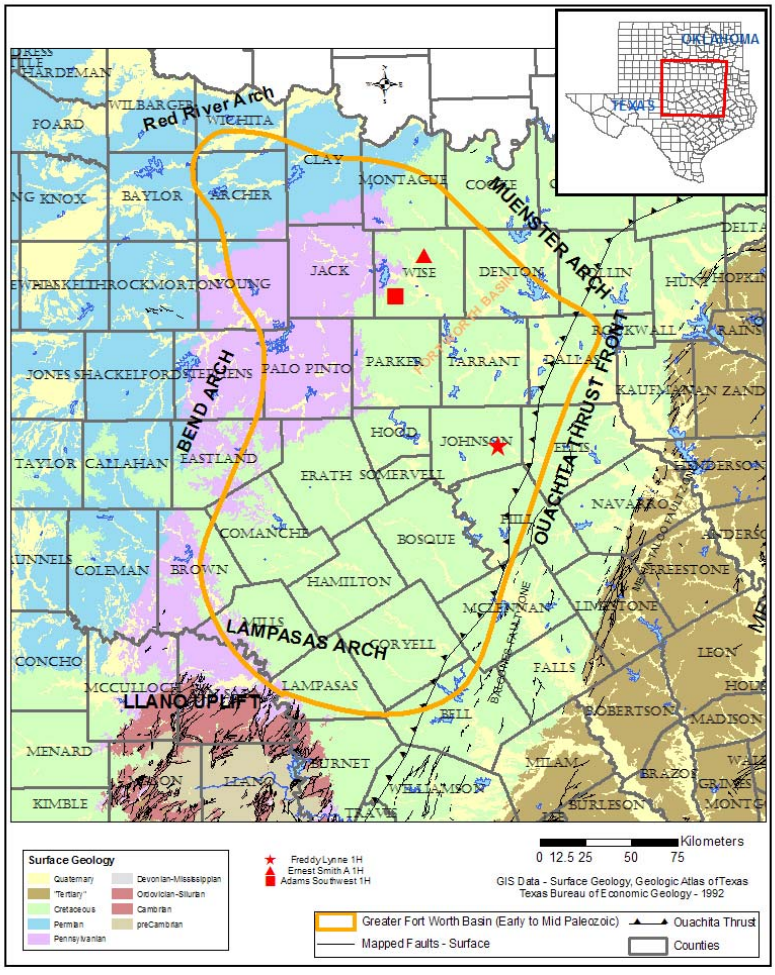

Figure 1- 1. Study area in the Fort Worth Basin showing regional tectonic features and locations of the cores in this study. The inset map is a Texas county map showing the location of the Fort Worth Basin.

The Fort Worth Basin is comprised of rocks from Cambrian to late Cretaceous in age. (Figure 1-2). These basin rocks overlie Precambrian granite and diorite igneous rocks (Pollastro et al., 2007) that may incorporate metasedimentary complexes from the Ouachita thrust belt (Montgomery, 2005). Cambrian-aged Riley Formation sandstones and Wilburn (Hickory) Formation shales and carbonates unconformably cap the basement rocks. These formations are overlain by a thick section of Ellenburger Group carbonates. The Ellenberger Group is found throughout the Fort Worth Basin and is comprised of a complex variety of rock types; tight and porous dolomites, massive to deformed and karsted dolomites, sandstone intervals, dolo-wackestone/packstones and partially dolomitized wackestones/packstones. Most of the units were deposited in shallow-water subtidal to supratidal environments. Most of the rocks of the Ellenburger in the study area are partially dolomitized (Flippin, 1986).

The Ellenburger Group is formally subdivided into three formations: the basal Tanyard Formation, middle Gorman Formation, and uppermost Honeycut Formation, as defined by Cloud and Barnes (1959) from Llano Uplift outcrops in central Texas. The Honeycut is mapped as the formation that subcrops below Upper and Middle Ordovician rocks (Viola and Simpson Groups, respectively) in the Fort Worth Basin. The Tanyard and Gorman formations may be present in the uplifted portions of the Muenster Arch (Bradfield, 1964).

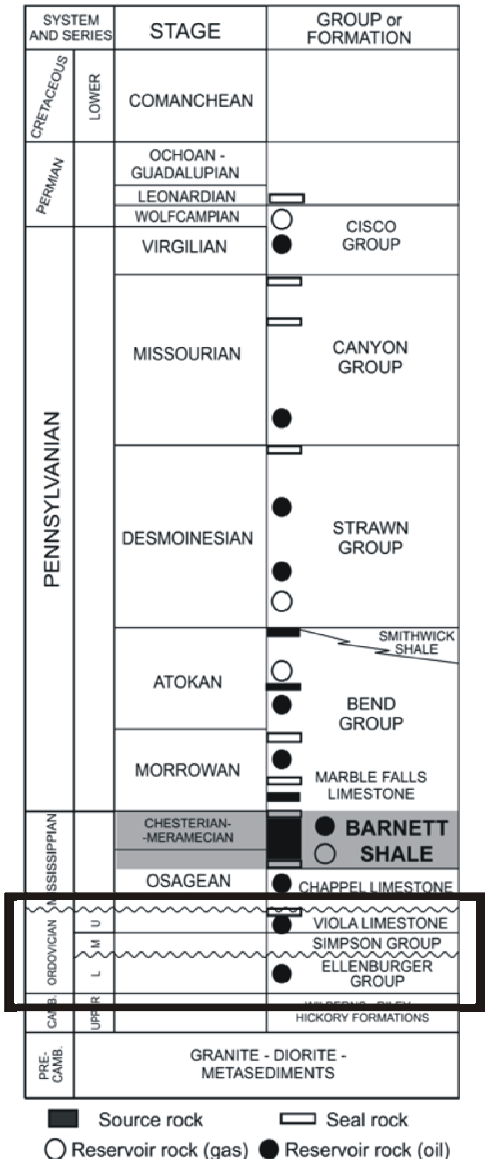

Figure 1- 2. Generalized stratigraphic column for the Fort Worth Basin, modified from Pollastro et al. (2007).

Following deposition of the Ellenburger carbonates in shallow water settings, a sea level fall in the middle Ordovician resulted in exposure of the unit prior to the deposition of Middle Ordovician Simpson Group and Upper Ordovician Viola Group. These two units, deposited on the post-Ellenburger erosional surface (Montgomery, 1995) are preserved in the eastern part of the Fort Worth Basin. After deposition of the Viola Limestone, a second extensive sea level fall resulted in further erosion of the units, forming an unconformity that correlates to the regionally identifiable Ordovician Unconformity (Amthor and Friedman, 1992). This unconformity represents erosion lasting from latest Ordovician to Mississippian time, a period of almost 120 million years.

Beginning in Mississippian time, Mississippian Barnett Shale and the correlative Chappell Limestone build-ups began depositing during submergence of the exposed carbonate platform. The column of Mississippian shale and carbonate that overlies the Ordovician section in the Fort Worth Basin varies from less than 200 feet in western portions of the basin to nearly 1,000 feet in the northeastern corner of the basin near the Muenster arch (Flippin, 1982). Shallow water carbonate deposition became prevalent into Morrowan time with deposition of the Marble Falls Formation, followed by the deposition of conglomerates, sands, and shales of deepwater Ouachita flysch deposition from the mid-Pennsylvanian to late-Permian (Figure 1-3).

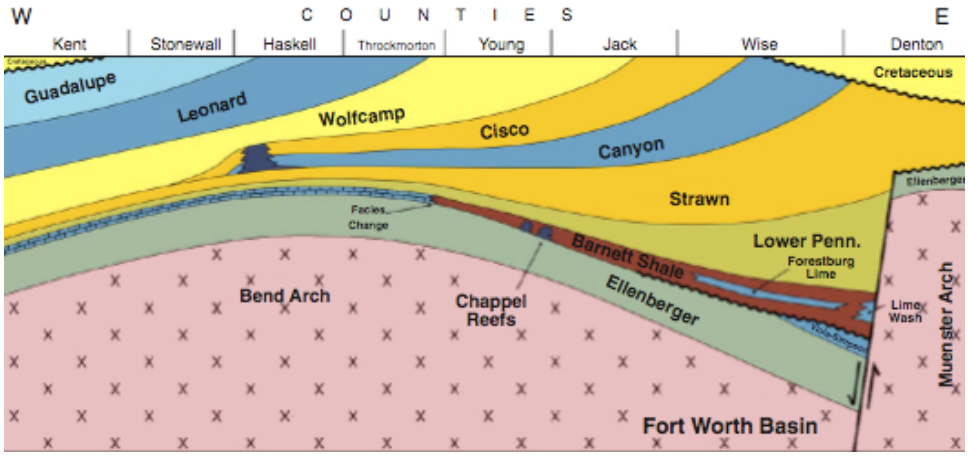

Figure 1- 3. Idealized cross-section from east to west across the northern Fort Worth Basin, modified from Jarvie et al. (2004). Note the preservation of Upper Ordovician Viola and MIddle Ordovician Simpson Groups in the eastern portions of the basin.

1.3 Previous Studies

The Ellenburger Group was the focus of several decades of extensive research with the majority of work centered on burial dolomitization and structural history in the highly productive oil fields in the Permian Basin of west Texas (Hoak et al., 1998) as well as in the outcrop belts of the Llano Uplift in central Texas. Previous diagenetic studies have investigated a range of topics including dolomitization, geochemical characteristics, karst formation and preservation, and the late tectonic structural history of the carbonates.

The Ellenburger Group in the Fort Worth Basin contains numerous faults, flexures, and collapses or sag features (Figure 1-4) that were first identified from seismic data by Hardage (1996). The term “karst” is commonly applied as a catchall

phrase for any semi-circular sag on seismic attribute analysis by a number of studies (e.g., Lacazette, 2004; O'Sullivan et al. 2006) regardless of the geologic process of formation. Geologic processes invoked for karst formation involve meteoric fluids and subaerial exposure, but also late modification through burial dissolution and cementation by internal or externally derived fluids. These fluids have been shown by Smith (2005) and Smith and Davies (2006) to be related to development of faults and fracture systems, and may coincide with large-scale regional orogenic fluid events such as hypothesized by Bethke and Marshak (1990). Evidence that external fluids entered the Ellenburger in the Fort Worth Basin is provided by Papazis (2005), Bowker (2007), and Gale et al. (2008). Other studies have provided evidence that such fluids altered the Ellenburger in west Texas (Kupecz and Kerans, 1987; Kupecz and Land, 1991). Based on this evidence, it is likely that fluid alteration constitutes a significant contributor to the paragenesis of the Ellenburger Group, as well as the overlying Barnett Shale, although the extent of the contribution is poorly understood.

Fractures and faults that form during burial and tectonic activity contain cements that are useful in deciphering the fluid history of the unit in the subsurface of west Texas and outcrop belt of central Texas (e.g., Hoak et al, 1998; Combs, 2003; Loucks et al., 2003; Gale and Gomez, 2007). Brine migration events have been hypothesized as emanating from the Ouachita orogenic front (Bethke and Marshak, 1990) along the fractures and faults. In the Fort Worth Basin, Bowker et al. (2007) and Jarvie et al. (2007) have speculated that late fluid migration events are potentially important to the productivity and thermal maturity of the Barnett Shale. Little is published about the specific timing and possible connections between early karsting, natural hydraulic

fracturing related to hydrocarbon generation, and regional tectonic fluid migration in the Fort Worth Basin. The precise effects of karst-cemented fractures on late fluid modification of these deposits are not fully understood. These connections, however, have important potential impacts on the productivity of the Barnett. For example, fractures in the Ellenburger may originate, penetrate and connect with the overlying Barnett Shale reservoir. Fractures, both open and cemented, are important aspects in the artificial and natural fracture stimulation of shales (Gale et al., 2008).

One line of evidence for a regional fluid event is a pervasive dolomitization of the Ellenburger. Amthor and Friedman (1992) establish a cement stratigraphic framework for dolomites in the Ellenburger of west Texas. Early dolomites are often seen replaced by later replacement dolomite. One theory for the origin of this late dolomitization is that hot aqueous brines moved at shallow depths along conduits and resulted in dolomitization of rocks near to the conduits. Kupecz and Land (1990) and Bethke and Marshak (1990) speculate that these are "orogenic" fluids related to the Ouachita thrust system. Other studies relate the extensive dolomitization of the rocks to internal fluids that were heated by burial (Lee and Friedman, 1988; Amthor and Friedman, 1992).

Late fracture filling hydrothermal dolomite, calcite or silica cements are present in Ellenburger cores and orogenic fluids are also one possible agent (Davies and Smith, 2006). Studies by Gale and Gomez, (2007) and Loucks et al. (2004) distinguished tectonically derived sets of fractures in the Ellenburger from karst-generated fractures. Hardage (1996), McDonnell et al. (2006) and Aktepe (2008) link such tectonic fractures and faults to reservoir scale seismic lineaments at the Ellenburger and basement

horizons, suggesting these may have been pathways that carried these fluid pulses for great distances away from the thrust zone (Figure 1-4).

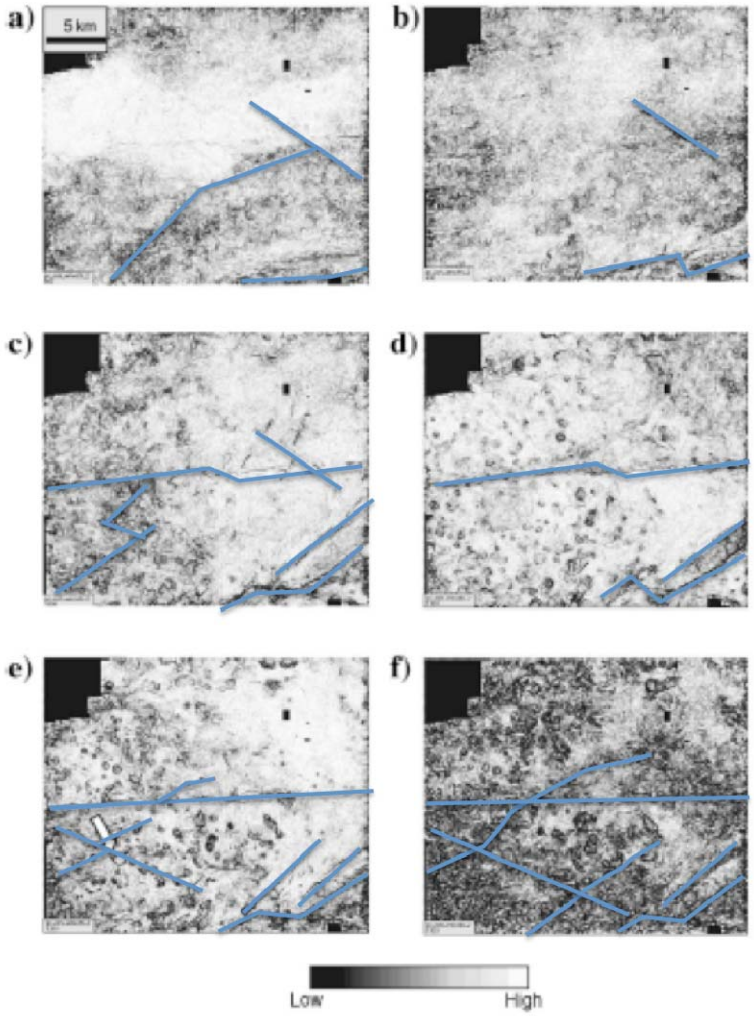

Figure 1- 4. Time slice images through a 3D seismic volume (coherency) in SW Wise County. At a) 0.8 s, _b) 0.9 s, c) 1.0 s, d) 1.1 s, e) 1.2 s (top Ellenburger horizon), and f) 1.3 s. The analysis window is ±10 ms and 9 traces. White arrow in e) indicates location of the ASW core presented in this paper. Linear features (blue lines) are interpreted faults or tectonic structures; circular or semi-circular features are interpreted as karsts or late karst collapse structures. Modified from Sullivan et al., (2006). Scale bar is in amplitude offset between traces.

Karsting could potentially enhance permeability due to faulting or fracturing. Karst fractured facies, termed "paleokarst" facies, have been described in core analysis by Loucks and Anderson (1985) and Loucks et al. (1991) (Figure 1-5). These "paleokarsts" are the result of progressive collapse of a near-surface cave system, in which dissolution voids form near the groundwater table and collapse under burial conditions, resulting in a cave collapse sequence identifiable in well core (White and White, 1949; Loucks and Anderson, 1985) or on seismic as a structural depression (Hardage, 1996). Little is understood, however, about the interactions between these earlier karst structures and the ingress of late fluids along tectonically opened fractures.

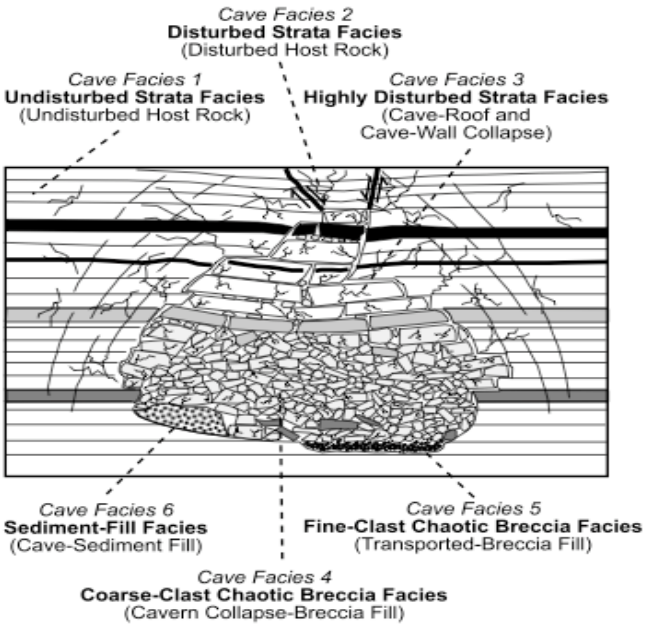

Figure 1-5. Cave collapse "paleokarst" facies after Loucks and Anderson (1985).

Kerans (1990) extended the concept of paleokarst facies to the development of fluid pathways and incorporated the "paleokarst" model into the Ellenburger

paragenesis which links these early karst processes to late tectonic fracturing and dolomitization. Hoak et al. (1998) features a summary of the complete paragenesis of the Ellenburger incorporating of prior works, including karsting, dolomitization and fracturing.

1.3.1 Previous Paleomagnetic Work

Paleomagnetic studies of the Ellenburger Group are limited. A study by Haubold (1999) on Ellenburger outcrops in central Texas and in far west Texas determined that diagenetic alteration of the rocks created authigenic magnetite. The study found correlations between magnetization intensity, magnetic directions, and lithofacies suggesting a permeability control on remagnetization by migrating fluids. The study also found that the amount of remagnetization in the Ordovocian rocks decreased with distance from the Ouachita thrust in a manner consistent with an orogenic fluid event at the thrust margins proposed by Bethke and Marshak (1990).

Elmore (2001) offered a review of work involving paleomagnetic and geochemical studies on remagnetizations in the Arbuckle Mountains in southern Oklahoma north of the Fort Worth Basin. Elmore et al. (1993a, 1998) presented results from the Ellenburger-equivalent Arbuckle Group carbonates in south central Oklahoma and showed that fluids caused remagnetizations near fluid flow conduits.
Regional fluid flow has been proposed as a mechanism for remagnetizations in the Appalachians. For example, Stamatkos et al. (1996) proposed that a single, rapid and pervasive brine migration event through the Appalachian-Ouachita Basins Mountains created a widespread Late Paleozoic remagnetization in the Appalachians. Oliver

(1986,1992) proposed an orogenic fluid hypothesis in which fluids were "pushed in front" of the thrusts and altered foreland basin rocks, a model informally dubbed the "squeegee" hypothesis. Gravitational recharge from mountain highlands by meteoric waters has also been proposed as a fluid flow mechanism (Garvin, 1995).

Other paleomagnetic studies have been performed on older units in Texas and Oklahoma. Loucks and Elmore (1986) studied the Cambrian Morgan Creek Formation, a member of the Wilburns Group sandstone underlying the Ellenburger in central Texas. This study was based on surface exposures. Many of the units in central Texas, including the Ellenburger, experience widespread dedolomitization by recent oxidizing surface fluids. Goethite, a magnetic remanence-carrying mineral is commonly precipitated during this process, obscuring older remagnetization events (Loucks and Elmore, 1986). In this study, subsurface core samples were used to analyze the Ellenburger, in order to obtain paleomagnetic data that were not obscured by a Brunhes (<700,000 year) component in goethite.

1.4 Methods

1.4.1 Core Selection for Study

This study utilizes three conventional, oriented, well cores retrieved by drill stem coring tools at modern reservoir pressure and temperature conditions. Cores were oriented by standard industry down-hole magnetic survey and scribe methods (Nelson, 1987). The well cores in this study were to be Barnett Shale wells, and were designed to retrieve Barnett Shale core as well as approximately 30-35 meters of underlying Ordovician carbonates. Two wells are located in Wise County, Texas, and one in Johnson County, Texas (Figure 1-1).

The Devon Adams Southwest #7 well (ASW) is located in southwestern Wise County and is roughly equidistant from the Muenster arch and Ouachita thrust. It is interpreted as containing an Ellenberger karst breccia zone as interpreted by previous workers (Papazis, 2005; Loucks and Ruppel, 2007). The well contains a major regional Ordovician unconformity and a thin stratigraphic section of relict Viola Limestone (Loucks and Ruppel, 2007). The second well is the Devon Ernest Smith A #1 (ES) which is located in north central to northwest Wise County, approximately 20 miles from the ASW. Based on seismic data analysis near the well location (proprietary, Devon Energy Corp.) the Ellenburger near ES is unkarsted and unfaulted. It is more proximal to the Muenster arch than the ASW.

The third core is the Devon Freddy Lynne 1(FL) located in Johnson County, Texas, approximately 70 miles SE of the ASW well. This location is near the front of the Ouachita thrust zone and is very distal to the Muenster arch. The core is also the

most proximal to the Llano Uplift of all three cores. No karsting was identified based on 3D seismic data at the well location (proprietary data, Devon Energy Corp.).
The cores were described and diagenetic features were identified. The diagenetic facies described in previous studies (Kerans, 1988; Loucks et al., 1999) provided the framework for the facies delineated in this study. Samples were chosen from each core to represent the general diagenetic facies found within the Ordovician carbonates.

1.4.2 Petrographic and Geochemical Methods

Petrographic analysis was conducted on both small and large format thin sections produced from both paleomagnetic core specimens and from samples specially cut from well core. Care was taken to remove a minimal amount of rock and leave a small "footprint" on the core. A total of 25-30 thin sections per well were analyzed, chosen carefully to show specific features or fabrics such as fracture-fill cements, microbreccias, dolomites and vug mineralization. Dolomite textural types were described following Amthor and Friedman (1992). Transmitted light microscopy was conducted using a Zeiss Axio Imager.Z1 petrographic microscope in order to determine lithology and the diagenetic features. Cathodoluminescence microscopy was conducted using an Olympus BX50 system microscope with a CITL CCL 8800 MK4 stage and interpreted per Sommer (1972).

Doubly polished thin sections were created for preliminary fluid inclusion analysis from quartz, calcite and dolomite filled veins, vugs and fractures. Inclusions in the Ellenburger are typically large and plentiful in most diagenetic cement phases with sizes greater than >10μm. Mr. Earl Manning, a MS student, using a Linkam TH-600

heating/freezing stage connected to a Linkam TMS 90 control unit, collected the fluid inclusion data. The homogenization temperature, or temperature at which the vapor bubble disappeared in an individual inclusion, was recorded (T_h). Ice melting temperatures were also successfully obtained on a number of inclusions. These temperatures were recorded sequentially so that lower temperature inclusions were not damaged by unnecessary heating and cooling cycles. Observations were made to look for stretching of inclusions, and if inclusions exhibited stretching they were not included in the final data.

An automated Cameca SX50 electron probe microanalyzer that is equipped with an integrated energy-dispersive x-ray analyzer was used to investigate the nature of minerals observed in the various carbonates, especially the vug fill microbreccias containing possible sulfide mineralization. Backscatter electron imaging (BSEI) was used to image the opaques while energy dispersive x-ray analysis (EDXA) was used for qualitative analysis of the composition of the elements, interpreted for mineral contribution. Scanning electron microscopy was conducted on select specimens using the scanning electron microscope (ZEISS DSM-960A) operated by the Microbiology Department at the University of Oklahoma. Preparation for scanning electron microscopy consisted of sputter coating with a gold target.

Carbon and oxygen stable isotope specimens were sampled using the following procedures. About 200-300 µg of carbonate was loaded into 12 ml borosilicate exetainer vials (Labco 938 W) that were sealed with butyl rubber septa caps. The vials were then placed in a temperature-controlled sample tray heated at 50^0 C and flushed with ultra high purity He (99.999%) using a Thermo Gas Bench II equipped with a

Combi PAL autosampler flushing needle for 360 seconds to remove air. Then 0.4 ml of 100% phosphoric acid was manually injected into the vials with a syringe and the reaction was allowed to proceed for at least 1½ hours. The vials were then sampled with the PAL measurement needle and the headspace CO_2 was analyzed for $\delta^{13}C$ and $\delta^{18}O$ using a Thermo Delta V Plus isotope ratio mass spectrometer. The carbon and oxygen isotopic composition are reported in standard δ-notation: $\delta(\text{sample}) = (R_{\text{sample}} / R_{\text{standard}} - 1)\ 1000$ ‰ where R is C^{13}/C^{12} for carbon and O^{18}/O^{16} for oxygen. The average δ value of 10 sample pulses is expressed relative to VPDB on a scale such that δC^{13} and δO^{18} of NBS-19 is +1.95 ‰ and -2.20 ‰, respectively.

Strontium isotope analysis was performed on representative specimens at the University of Texas-Austin. Twenty samples were processed from carbonates in the Viola-Simpson and the Ellenburger carbonates. Samples were treated with acetic acid for dolomitic specimens in order to dissolve the dolomite per standard procedure. ASW specimens were processed with a NIST SRM 987 standard mean value of 0.710243 ± 0.000007 ($2\sigma = 0.000019$, n = 7). ES and FL specimens were processed at a later time with a NIST SRM 987 standard mean value of 0.710258 ± 0.000012 ($2\sigma = 0.000006$, n= 32). Strontium values were normalized relative to NBS 987 = 0.71014. The $^{87}Sr/^{86}Sr$ values were then plotted versus diagenetic features such as paleokarst facies and tectonic fractures, and were compared to the published values for coeval Ordovician seawater per Denison et al. (1998).

1.4.3 Core Sampling for Paleomagnetic Analysis

Core samples for paleomagnetic and rock magnetic analysis were collected from the three multi-shot magnetic survey oriented and reference scribed 12.16 cm (4 inch) diameter conventional well cores (2/3rds "butt" section only) from the uppermost Ellenburger Group carbonates. The 2.2 cm (0.86 inch) diameter cores were cut with a fixed, variable-speed and water-cooled drill press with a non-magnetic core bit located at the Oklahoma Petroleum Information Center Core Facility, Oklahoma Geological Survey, Norman, Oklahoma. The samples were collected in groups comprised of 2 to 4 cores per 0.91m (3 foot) box. Cores were sampled normal to the corrected tool-face azimuth (corrected true north) as calculated from the reference and scribe data. Since measured wellbore inclinations are small (between one and three degrees from vertical) and beds are near horizontal, this mode of sampling appears to approximate a true "in situ" sample orientation in most intervals.

Orientation of the ES core was an issue because the core was slabbed versus maximum bedding dip as opposed to the orientation scribes. Samples were drilled normal to the slab face as opposed to the orientation scribe lines. The cores were therefore reoriented after measurement based on the near term, modern (<780,000 yr) viscous remanent magnetization (VRM) component as isolated by low temperature demagnetization. This was accomplished using a similar proven technique to that described in detail by Van Alstine and Butterworth (2002). This method was also used to reexamine the orientation of the other cores as a test of the scribe orienting method.

Sixty-six core samples were collected from the Ellenburger dolomite in the ASW well core. Table 1 in Section 1.5 describes each of the diagenetic facies sampled. Samples were taken across fractures as well as in unfractured zones. Six additional samples were recovered from the Viola Group interval in ASW. Forty-seven samples were collected in the ES well. Samples were taken across fractures, clastic-rich zones, and stylolites, as well as in unfractured zones. Additional samples were recovered near the late Ordovician unconformity. In this well a sub-unconformity, carbonate-rich shale was also sampled and is interpreted as the Upper Ordovician Simpson Shale. Twenty-seven samples were collected in the FL core. These samples were drilled in both Ellenburger facies and at the Ordovician Unconformity.

1.4.3 Paleomagnetic Methodology

Plugs were removed from well core normal to the slab face using a water-cooled drill press. The core plugs were measured and cut to samples of standardized length (approximately 2.2 cm) with an ASC Scientific dual blade saw. Samples were measured to determine bulk and total mass magnetic susceptibilities using a Kappabridge mass magnetic susceptibility meter.

Natural Remanent Magnetizations (NRMs) were measured using a 2G-Enterprises cryogenic magnetometer with DC SQUIDs in a shielded paleomagnetic laboratory located at the Sarkeys Energy Center, University of Oklahoma. After the initial measurement of the NRM, some samples were cooled in liquid nitrogen by submerging them twice for two hours and returning them to room temperature in a zero

field, in order to remove the unstable remanence from multi-domain (MD) grains (Dunlop and Argyle, 1991). Other samples were not subjected to low temperature treatment for preservation of viscous remanent magnetization (VRM) information. The NRM was re-measured following each low temperature treatment.

Samples were subjected to stepwise thermal demagnetization in 22 steps from 100 to 580°C using an ASC Scientific Thermal Specimen Demagnetizer. Some samples initially were measured to 680°C with a total of 27 heating steps to test for remanence in hematite; however, the NRM was removed by 480-580°C. In subsequent analysis the numbers of steps were decreased. Additional steps were added at low temperatures on some runs to help delineate the VRM to aid in sample orientation.

Demagnetization data were plotted on vector diagrams as described by Zijderveld (1967) using the Super-IAPD paleomagnetic data analysis software (Torsvik , 1996). This software was also used for Principal Component Analysis (Kirschvink, 1980) to determine the best-fit-line components. Mean angles of deviation (Kirschvink, 1980) are less than 15° for all specimens. Site means and unit means were calculated using Fisher (1953) statistics in Super IAPD. Unit means were calculated by grouping samples by pre-defined (via petrography, geochemistry) lithofacies and/or diagenetic descriptors as described below in the Diagenesis section.

A breccia test (modified conglomerate test per Graham, 1949) was performed on the karst collapse breccia clasts. Samples were collected from chaotic breccia paleokarst facies clasts and matrix from the ASW well core. To determine the timing of remagnetization, facies (Section 1.5) were used to subdivide characteristic remenant magnetizations (ChRMs), and facies means were plotted on an equal area stereonet for

analysis and paleopoles were calculated. The poles were calculated using the PMGSC version 4.2 software program (Enkin, 2004). The poles were then plotted on the Apparent Polar Wander path for North America (Van der Voo, 1993) in order to determine the age of the magnetizations.

In order to investigate the magnetic mineralogy of the samples, isothermal remanent magnetization (IRM) acquisition was performed first by AF demagnetizing samples at 120 mT using a 2G Automated Degaussing System. The specimens were subjected to a 26-step IRM acquisition up to 2500 mT using an ASC Scientific Impulse Magnetometer. The samples were then subjected again to AF demagnetization at 120 mT. LAP-GAP-SAP modeling was conducted on the IRM data using the IRM-CLG 1.0 software generated by Kruiver et al. (2001) to investigate the characteristics of the magnetic mineral coercivity spectrum.

1.5 Results and Interpretations

1.5.1 Diagenetic Facies

The Ellenburger Group carbonates in the Fort Worth Basin can be divided into diagenetic facies based on the core descriptions and petrographic studies (Table 1-1). The facies described by previous studies based on karsting (Loucks et al., 1999), depositional processes (Kerans, 1989) and dolomitization (Amthor and Friedman, 1992) provided the basic framework for the facies delineated in this study. The facies were further delineated by relict depositional features and the diagenetic features observed in this study.

	Diagenetic Facies	ASW	ES	FL
1	Massive to Laminated Dolomite	X	X	X
2	Wavy bedded to argillaceous dolomite		X	X
3	Crackle and Mosaic Karst Breccia (Disturbed Strata)	X		
4	Chaotic Karst Breccia with Clay-rich Cave Fill Matrix	X		
5	Mottled (Burrowed) dolomite with fine grained brecciated intervals	X	X	X
6	Mixed Limestone and Dolomite Facies with or without shale filled fractures	X	X	X
7	Mixed Peritidal sequence carbonates	?	X	
8	Dolomite with Solution-Reprecipitation zones	X	X	

Table 1-1. Summary of Diagenetic Facies and their distribution in the cores.

Dolomites are herein described using a scheme presented in Amthor and Friedman (1992). Table 2 below is provided as a guide of these dolomite types.

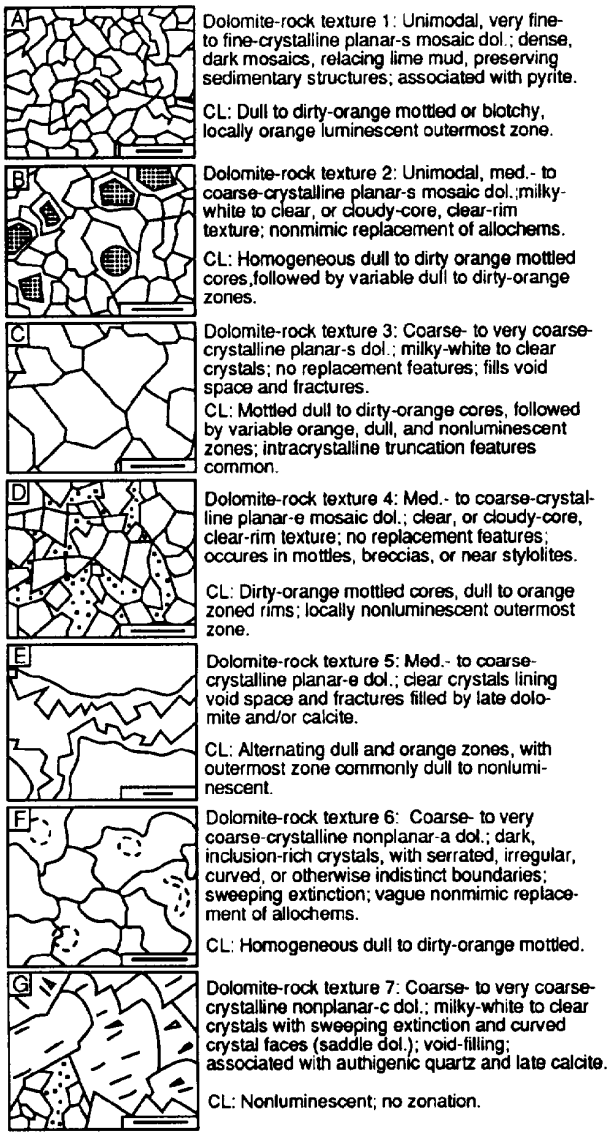

Figure 1-6. Ellenburger dolomite types. Figure from Amthor and Friedman (1992).

Facies 1 – Massive to Laminated Dolomite

This facies contains evidence of algal laminites and dessication cracks, which suggest these rocks were deposited on shallow water tidal flats. The bedding in this facies is mostly horizontal (Figure 1-7) in unkarsted intervals where the facies represents undisturbed host rock. In karsted intervals, the facies may represent large megaclasts dropped into the collapse zone.

A  B 

Figure 1-7. A) Massive to finely laminated crystalline dolomite from Facies 1 with healed fractures in the ES core. B) Finely Laminated dolomites from Facies 1 with open fracture from the FL core. Cores are 10cm wide.

Dolomites found in this facies are Type 1 planar anhedral to subhedral, and represent a syndepositional/very shallow burial replacement of micrite (Figure 1-7). A pervasive Type 2 medium-grained dolomite replaces the Type 1 dolomite. All dolomite types are finely-crystalline. The dolomite has a dull red CL. The facies also contains

extensive vertical fractures in some intervals that are oriented largely northerly or northwesterly and are interpreted as tectonic in origin. The fractures are filled with calcite, pyrite, small amounts of other sulfides, and hydrocarbons are present near the fractures (Figure 1-8).

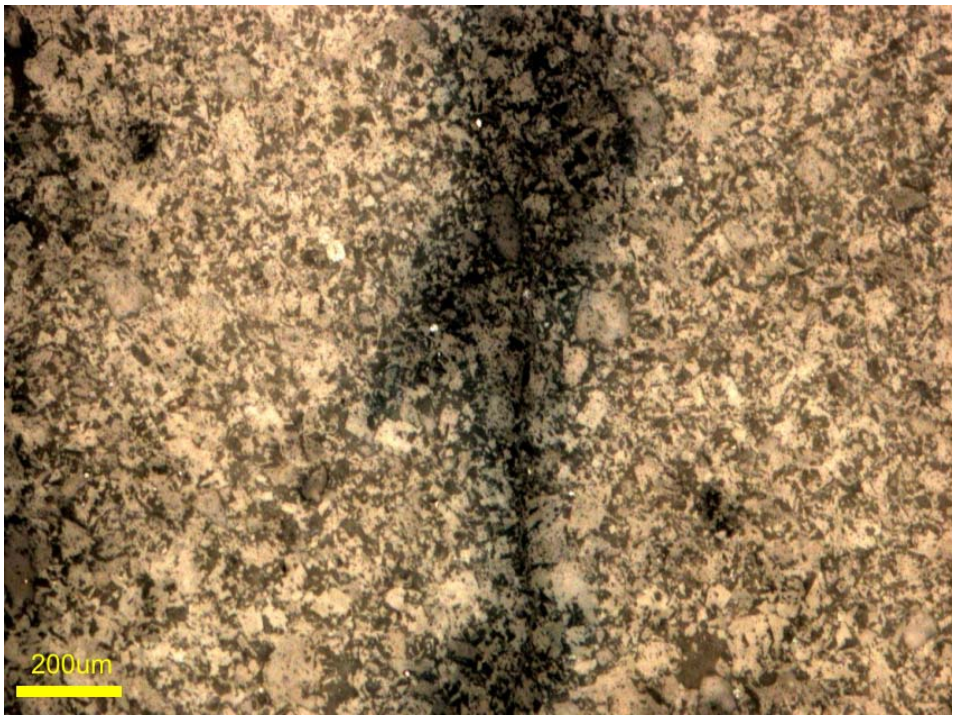

Figure 1-8. Reflected light photo of very fine grained subhedral Type 1 dolomite (brown) with a pervasive subhedral to euhedral Type 2 replacement dolomite (tan) from Facies 1. Note the hydrocarbons (dark brown) found adjacent to the fracture.

Facies 2 – Wavy bedded to argillaceous dolomite

This facies contains numerous argillaceous intervals with muddy laminae interbedded with bioturbated carbonates. (Figure 1-9). The volume of clay in this unit is higher than in other dolomite facies, with the exception of the clay-rich matrix in the chaotic karst breccia facies.

The dolomites are predominantly fine-crystalline planar, subhedral Type 1 dolomite, though some Type 2 medium-crystalline planar-s to planar-e replacement dolomites are seen in near fractures or burrowed intervals (similar to Facies 1). The dolomites have a dark to dull red CL with brighter CL in the fracture fills. The facies contains limited vertical fractures that have a northwesterly azimuth.

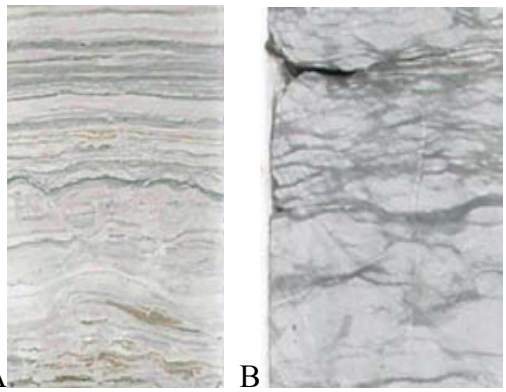

Figure 1-9. A) Core photo showing wavy bedded and bioturbated dolomite in the ES core from facies 2. B) Mud drapes and argillaceous dolostones in the FL core from facies 2 . Both cores are 10 cm wide.

Facies 3 – Crackle and Mosaic Karst Breccia (Disturbed Strata)

This facies contains mostly massive to laminated carbonates that are cross-cut by a network of fractures containing dolomite and calcite fill cements (Figure 1-10A). The network of fractures subdivides the rock into a series of small angular clasts, forming a breccia. There is little to no rotation on the clasts suggesting the rocks are largely in situ. This suggests the rock was karsted cave roof or wall rock that did not collapse. This facies is described by Loucks et al. (1999) as crackle breccia (with no clast rotation) and mosaic breccia (with some clast rotation). The dolomites are predominantly fine-crystalline planar-s Type 1 early dolomite in clasts, and Type 2 medium to coarse-crystalline planar-s mosaic dolomites mainly in burrowed intervals and fracture-fills. The dolomites have a dull red to red-orange luminescence with brighter CL in fracture fills. Fracture walls have zoned CL alternating between red, orange, dull and dark zoning. The facies contain limited vertical fractures that often terminate against the older karst-related fracture set. Early dolomite in fractures that is related to karsting clearly predates the later near vertical tectonic fracturing.

Facies 4 – Chaotic Karst Breccia with Clay-rich Cave Fill Matrix

This facies contains a random, or chaotic, network of clasts (typically greater than 5cm in diameter), matrix and fracture filled by a clay-rich dolomitic mudstone and/or sparry dolomite or calcite cements (Figure 1-10B). The original fabric of the host rock is largely destroyed by the wholesale displacement of clasts. This suggests the rock was formed by the collapse of the cave roof or wall. It is described by Loucks et al.

(1999) as chaotic breakdown breccia. Caves formed along pre-existing northwesterly joints which are visible in the well core and are also observable in the lineation of karsts (Sullivan et al., 2006)(Figure 1-4).

The cave sediment fill which makes up the matrix of the karst deposits was broken out as a separate facies in Loucks et al. (1999). However, here we will only distinguish between karst breccias with little rotation and sediment fill versus those with considerable rotation and abundant fluvial cave sediment fill (Facies 3 versus Facies 4). The internal sediment fills space between clasts in most cases, although in some zones a sparry calcite cement is present. The dolomite clasts are composed of about half fine-crystalline planar-s Type 1 early subtidal dolomite and half Type 2 pervasive replacement (coarser grained) dolomite. The fractures are filled with Type 3 coarse-crystalline planar-e dolomites.

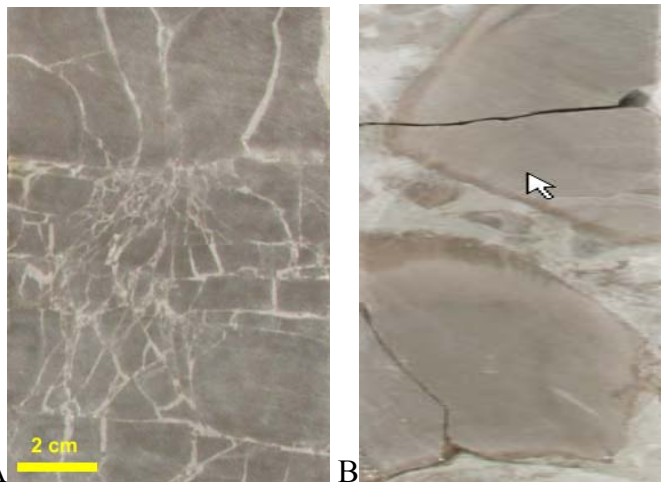

Figure 1-10. A) Core photos showing crackle breccia (Facies 3), disturbed strata paleokarst facies, in ASW core. B) Chaotic breccia with clay-rich cave sediment facies (Facies 4) in the ASW well (scale same as A). Cores are 10 cm wide.

Isolated large vugs are present in ASW 6972'MD in ASW (Figure 1-11). The vug host rock consists of Type 1 (early fine anhedral to subhedral) dolomite and pervasive type 3 coarse replacement dolomites (zoned CL). The vugs are lined with Type 5 (void-lining zoned dolomite); (Figures 1-12A and 1-12B) with minor nonplanar Type 7 dolomite (void filling "saddle" dolomite)(Figure 1-12C), along with pyrite, quartz, sulfides and Fe-calcite cements. The presence of "saddle" dolomite suggests that warm fluids precipitated the cements. Sphalerite (ZnS) and minor Pb-Mn oxides are also found within this vug.

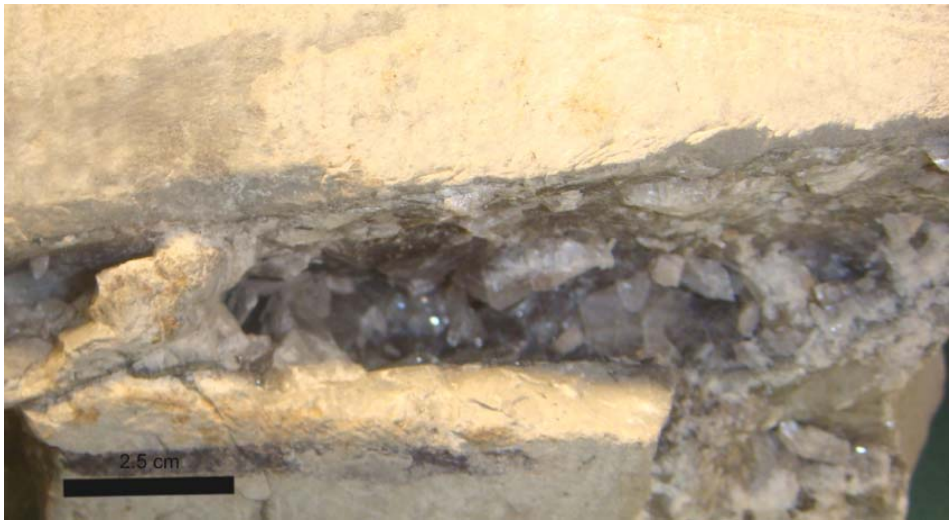

Figure 1-11. Open vug near 6792'MS in ASW from Facies 4, the Chaotic Karst Breccia with Clay-rich Cave Fill Matrix facies. Crystals are sparry calcite, dolomite (including saddle dolomite (pink), quartz and sulfides.

The Type 1 dolomites are non-luminescent and Type 3 replacement dolomite has a dull red to orange homogeneous CL in clasts and host carbonate. Type 5 dolomites that line vug walls have bright zoned CL, alternating between red, orange,

and dark cements (Figure 1-12a-12b). Type 7 dolomites have a dull to non-luminescent character. Quartz and calcite are also non-luminescent.

A 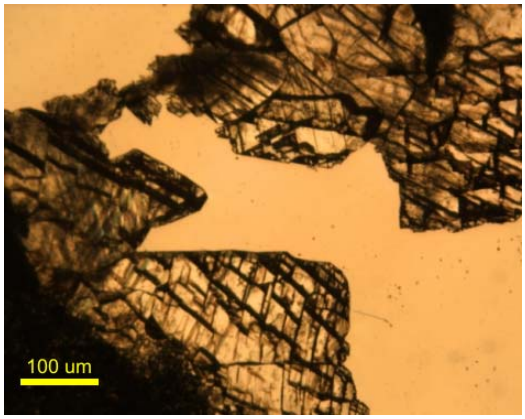

B 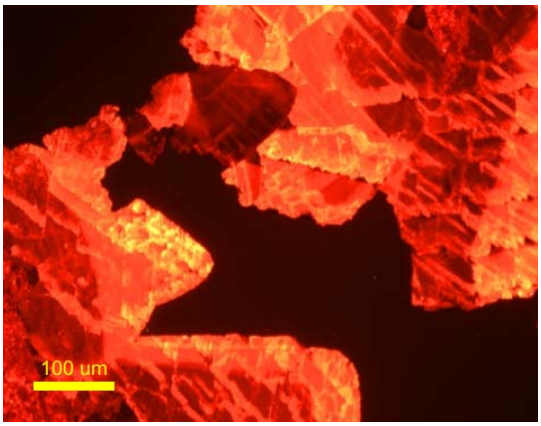

Figure 1-12a and 12b. Photomicrographs of Type 5 and 7 dolomites lining the vug in Facies 4 (chaotic karst breccia). A). Plain light. B. Photomicrograph showing a bright orange CL in dolomites. Interior of vug is filled with late calcite (quenched CL) and open pore space.

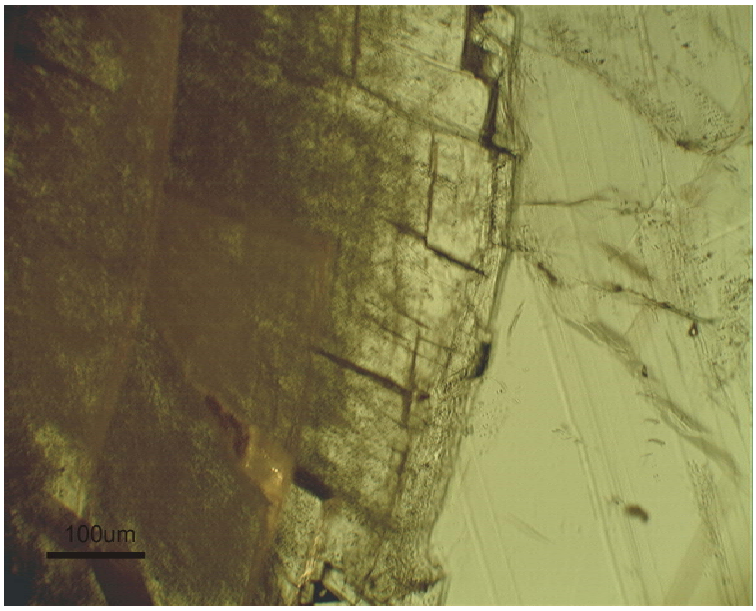

Figure 1-12c. Plain light photo of Type 7 "saddle" dolomite in vug at ASW 6972'MD with late calcite fill (right).

Individual clasts in this facies contain very few vertical fractures that often terminate against the clay-filled breccia matrix. Fracturing is therefore common but through-going early fractures are not, and many local fractures are healed. An early dolomite occurs in some karst related fractures and predates later fracturing. Though the nature of breccia infers an increase in permeability from the original host rock, late cementation and matrix fill have in effect reduced the effective permeability of these breccias to less than the surrounding unbrecciated carbonates.

Facies 5 - Mottled (Burrowed) dolomite with fine-grained brecciated intervals

This facies contains extensive vertical to obliquely oriented borings (*Trypanites?*) and vertical burrows that suggest the rock was deposited on a high energy hardground in an intertidal setting. This facies is extensively dolomitized. In addition to extensive

recrystallization of early dolomite, sulfides such as pyrite and sphalerite, as well as altered carbonates such as rhodochrosite ($MnC0_3$), are present in the FL core (Figure 1-13). In the ASW core, this facies is often interbedded with fine-grained breccias that contain matrix that was apparently locally reworked. These intervals are interpreted to be locally transported material related to karsting.

Dolomites found in this facies represent several types. Type 1 fine-grained early replacement dolomite is present but is pervasively replaced with Type 2 dolomite. In the bioturbated zones, Type 4 (coarse-grained mosaic euhedral dolomite) is found commonly with a mosaic of large and small euhedral crystals (Figure 1-14). In the FL core this is the dominant facies by volume and is composed mainly of Type 4 (mosaic) replacive dolomite.

In terms of CL, the early Type 1 and 2 dolomites have a dull luminescence. Type 4 shows a zoned red and orange CL. Associated late calcite is non-luminescent.

A  B 

Figure 1-13. Facies 5. A) FL core with mottled (burrowed) dolomite with stylolites from facies 5. B) Burrowed and fractured mottled dolomite in ES core from facies 5. Cores are 10cm in width.

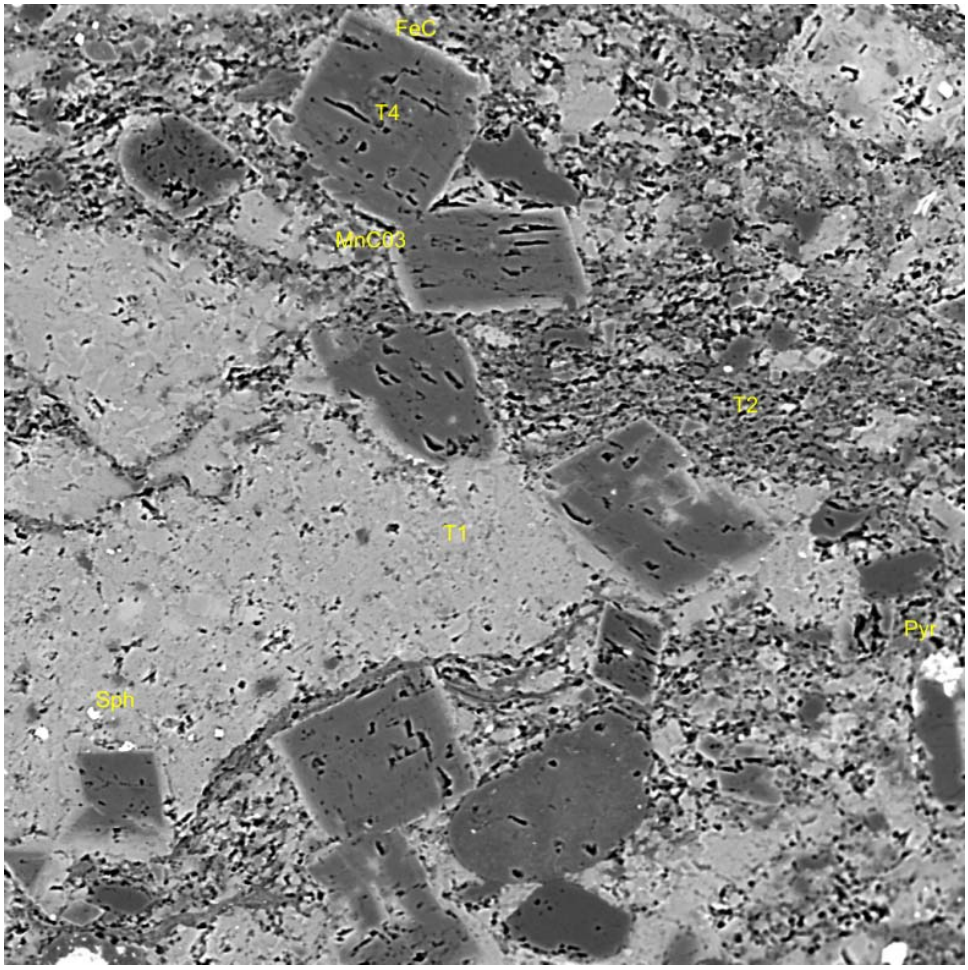

Figure 1-14. Facies 5. 256µm x 250µm SEM image of Type 1,2 and 4 (mosaic)dolomite associated with pyrite (Pyr) and sphalerite (sph), rimmed in a late Fe-Calcite and associated manganese-rich $MnCO_3$ (Alteration rim on dolomite rhombs). FL 8136' MD.

Facies 6 – Mixed Limestone and Dolomite Facies with or without shale filled fractures.

This facies makes up the Viola Limestone (or perhaps, Mississippian Chappel carbonates), and is dominantly a wackestone-packestone that contains some dolomite. The presence of bored and heavily pyritized hardgounds are present as are shelly lag deposits indicating reworking of allochems. Sets of north-south striking, near vertical fractures that increase in aperture upward suggest a paleosurface termination. These factures are filled with the overlying Barnett shale. The fractures are interpreted to have formed on the eroded surface of the Viola and mud washed into them during the first phase of deposition of the Barnett (Figure 1-15).

Dolomites found in this facies are typically replacement Type 2 (medium grained dolomite replacing matrix) and Type 4 (coarse grained mosaic dolomite). The Type 4 dolomites have a dull to medium red CL with zoning. Vertical fractures strike north-south in this zone in ES and ASW cores.

Figure 1-15. Black shale filled in fractures in Facies 6, Viola limestone.

Facies 7 –Mixed Peritidal Sequence Carbonates

This facies is only found in the ES core. The ES core contains a number of depositional and diagenetic textures not seen in the other well cores (Figure 1-16). Core analysis has identified teepee structures, fenestral fabrics, soft sediment deformation, cryptalgal laminites, flat pebble conglomerates, and nodular cherts. These features suggest deposition in a peritidal to supratidal setting. These rocks are arranged in cycles that are capped by an ooid grainstone that is interpreted as a shallowing upward peritidal sequence. This type of sequence has been described in the Ellenburger in west

Texas by Goldhammer (1993) and would place this facies in the uppermost Gorman Formation.

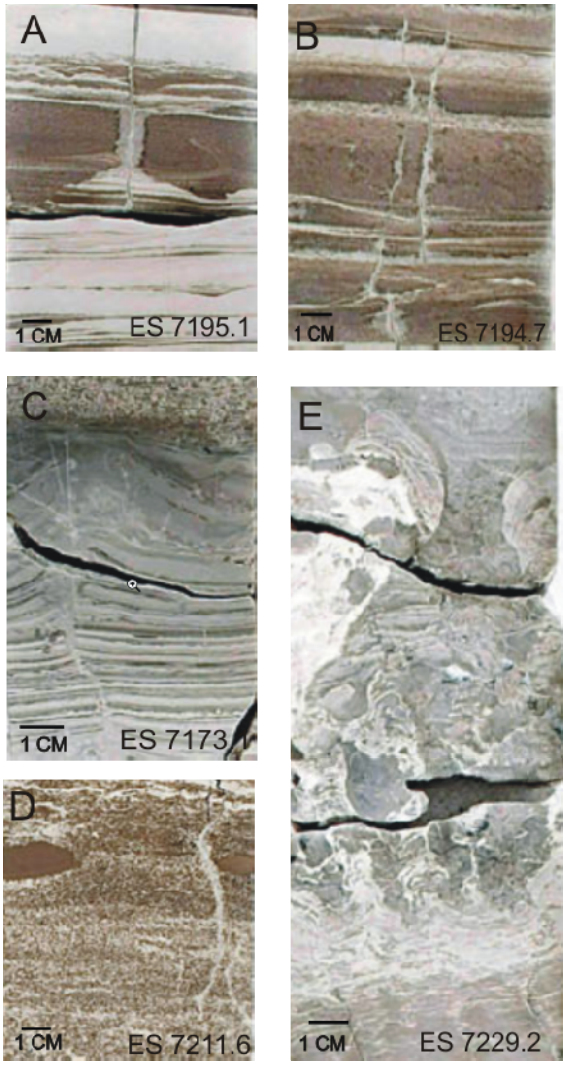

Figure 1-16. Characteristics of Facies 7, ES core. A) Early cementation of a mudstone near a dewatering fracture. B) Alternating light Type 1 dolomudstone and coarser reddish Type 2 and 3 replacement Fe-rich dolomites, with associated pyrites and hydrocarbons. C) Tepee structures D) Early fractures and Fe-dolomite concretions. E) Soft sediment deformation features.

Dolomite is found as iron-poor very fine-crystalline dolomudstones interbedded with coarse, dominantly iron-rich Type 3 replacive dolomites. Type 4 and non-planar Type 6 dolomites are present as vein and fracture fills, and in association with nodular

calcite and cherts. Fe-dolomite commonly is associated with hydrocarbons, and/or pyrite (Figure 1-17). The dolomite has a variable luminescence with Type 2 having weakly zoned medium orange luminescence, Type 4 having a strongly zoned CL, and Type 6 is non-luminescent. Type 6 is also commonly found with authigenic potassium feldspars. The facies also contains extensive vertical fractures in some intervals.

Facies 8 – Dolomites with solution-reprecipitation zones

This facies is primarily associated with Facies 5, and contains dissolution vugs filled with Type 2, Type 4, and minor Type 6 nonplanar dolomite cements. Late Fe-calcites, and authigenic illite (Figure 1-18) can be found with this dolomite. Hydrocarbons and sulfides, including pyrite and sphalerite, are found the center of the vugs. These are interpreted as late diagenetic fluid alteration features.

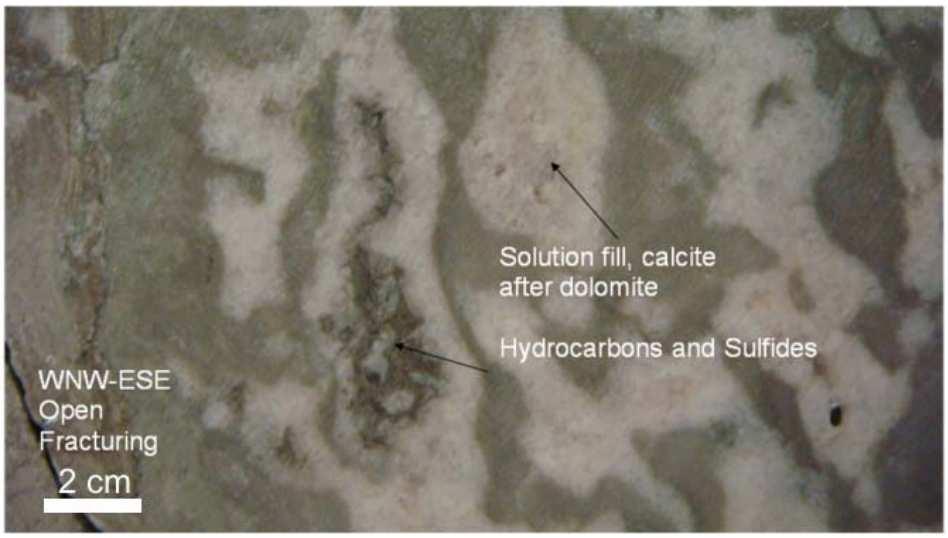

Figure 1-17. Facies 8 with dolomite vugs followed by illite/dolomite cement, then Fe-calcite.. hydrocarbons and sulfides coat the late calcite (brown). Note nearby E-W open fractures.

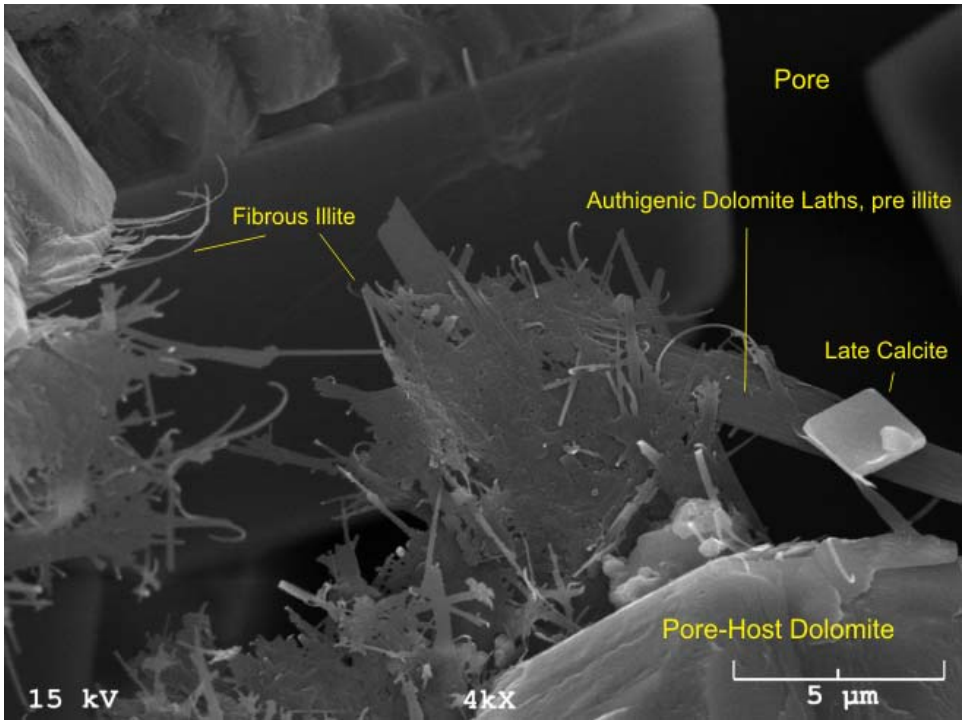

Figure 1-18. SEM image showing cements growing in an open Ellenburger pore at 6874'MD, Facies 8. Late crystalline Fe-calcite is shown on dolomite and authigenic illite.

Mississippi Valley–type (MVT) Zn-Pb-Cu Mineralization

Several facies (Facies 4 , 5, 7, and 8), contain minerals commonly associated with hydrothermal Mississippi-Valley type ores. Barite, sphalerite, chalcopyrite, lead and manganese rich minerals, are found with late replacement dolomites in fractures and vugs (Figure 1-19A,B). These minerals are all associated with intervals that contain the Type 7 saddle dolomite and are interpreted as related to migration of late fluids.

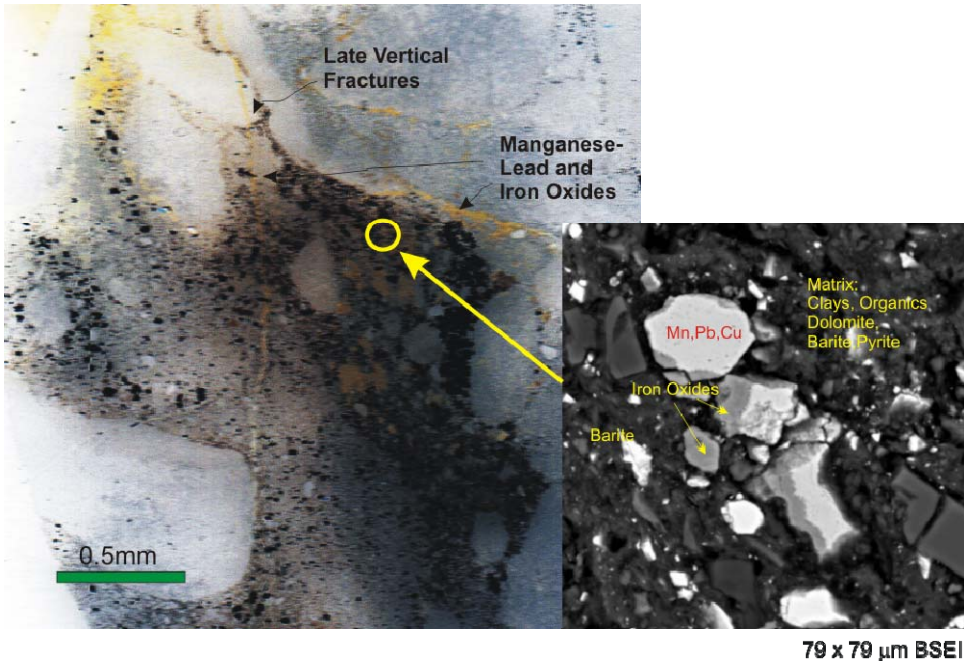

Figure 1-19a. False color CPX image of MVT and oxide minerals in an open vug near ASW 6792.0.

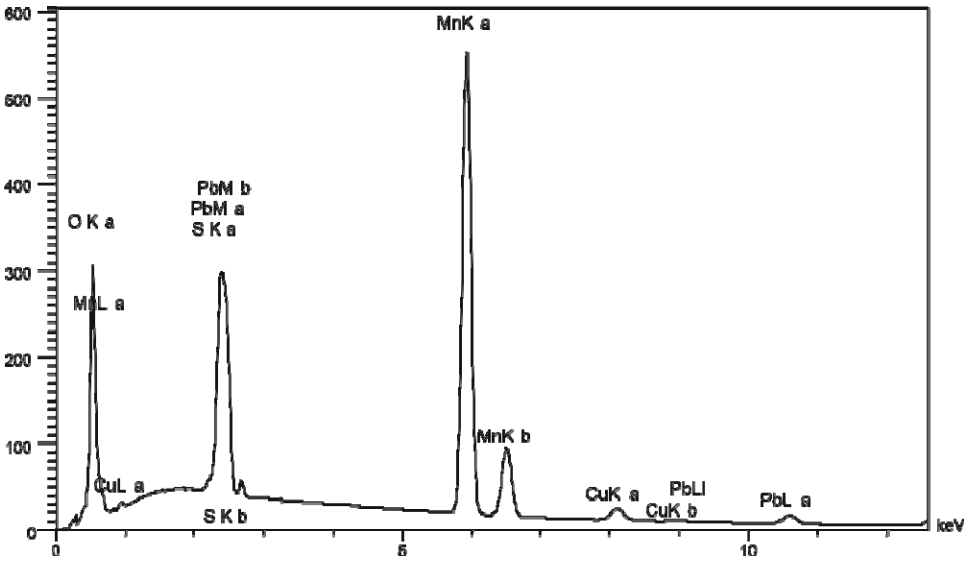

Figure 1-19B. Energy dispersive spectra from SEM analysis demonstrates the presence of lead, manganese, minor copper and sulfur from the grain labeled "Mn,Pb,Cu" in Figure 1-22B.

Other diagenetic Features

Stylolites are common in all of the Ellenburger and they are more commonly found in highly dolomitized and clay zones such as Facies 1,2,5,7 and 8. Facies 8 in ASW near 6874' is very near two stylolites that appear to have been reactivated by east-west oriented shear fractures.

Open faults and shear fractures are most common in clay-poor Facies 1 and Facies 5. For example, in the ASW both facies contain a dense set of open to partially open fractures from the base of Facies 4 (chaotic collapse breccia) down to the top of the Facies 6 near 6925' MD. Formation microimager (FMI) data (not shown) confirms that east-west fractures both occur near this depth. Shears and fractures in general are not common in Facies 4 karsted intervals.

Hydrocarbons occur in all facies, commonly as solid pyrobitumen. These hydrocarbons have a cracked and desiccated appearance in thin section. Liquid hydrocarbons are seen in the ES core in association with late coarse replacement dolomite porosity. In some portions of the basin, Ellenburger porosity may be a producible reservoir of oil (Bradfield, 1964).

1.5.2 Geochemistry and Fluid Inclusion Analysis

Strontium Isotopes

Strontium isotope ratios (**$^{87}Sr/^{86}Sr$**) were collected to determine if externally derived fluids had altered the rocks. The $^{87}Sr/^{86}Sr$ values for most dolomites and karst breccias are coeval and were not altered by externally derived fluids per processes described in Gao et al., (1992). Conversely, fractured and vuggy zones in the ASW contain radiogenic values of $^{87}Sr/^{86}Sr$ that indicate the influence of orogenic fluids or basement brines (Figure 1-20; Table 1-2). This is due to the contribution of igneous or metamorphic feldspathic rocks (Burke et al., 1982). Zones containing vugs filled with saddle dolomite and Fe-calcite such as at ASW 6972' MD contain the most radiogenic strontium values, and Facies 8 (Solution-reprecipitation zones) also contains elevated values of $^{87}Sr/^{86}Sr$.

Ellenburger rocks in the FL core are all radiogenic (>0.709) suggesting that fluids with a radiogenic signature altered the entire core. Since this well is relatively close to the Ouachita thrust, the fluids are interpreted to be interacting with uplifted feldspathic meta-sedimentary units from the Ouachita thrust or from basement rocks. Fluids in the ASW and ES could have been sourced from the thrust and moved along permeable zones (i.e. the Ordovician Unconformity) or along deep basement faults.

Facies	Mean 87Sr/86Sr	Min	Max	Number / Samples	Radiogenic?
1	0.70924	0.70889	0.70983	3	YES
2	0.70813	0.70800	0.70827	2	NO
3,4	0.70865	0.70827	0.70893	2	NO
5	0.70878	0.70878	0.70914	2	SLIGHTLY
6	0.70846	0.70843	0.70850	2	YES
7	0.70895	0.70892	0.70897	2	NO
8	0.70919	0.70904	0.71005	3	YES

Table 1-2. $^{87}Sr/^{86}Sr$ values for diagenetic facies 1 through 9. Coeval values for Ellenburger range from 0.70870-0.70920. Coeval values for Viola is 0.7075-0.70795.

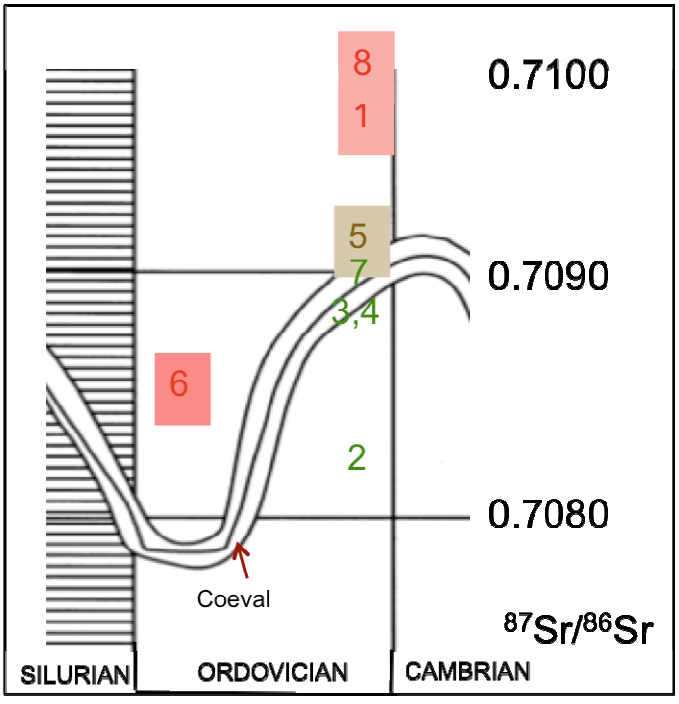

Figure 1-20. $^{87}Sr/^{86}Sr$ ratios for the diagenetic facies 1-8. Modified from Denison et al. (1998). Coeval values for early Ordovician range from 0.70870-0.70920.

Carbon and Oxygen Stable Isotopes

Most samples from the Ellenburger contain slightly depleted values in both carbon and oxygen stable isotopes (Figure 1-21). Some cements have highly depleted in δ^{18} O values (Figure 1-21)), especially karst cement. This suggests that meteoric fluids altered the rock. Some dolomite cements show depletion in δ^{18} O up to -8 to -10 per mil (PDB). Late cements show small variation in δ^{13} C although some values are light (-4 to -6 per mil (PDB) suggesting hydrocarbons may have influenced the precipitation of the cements.

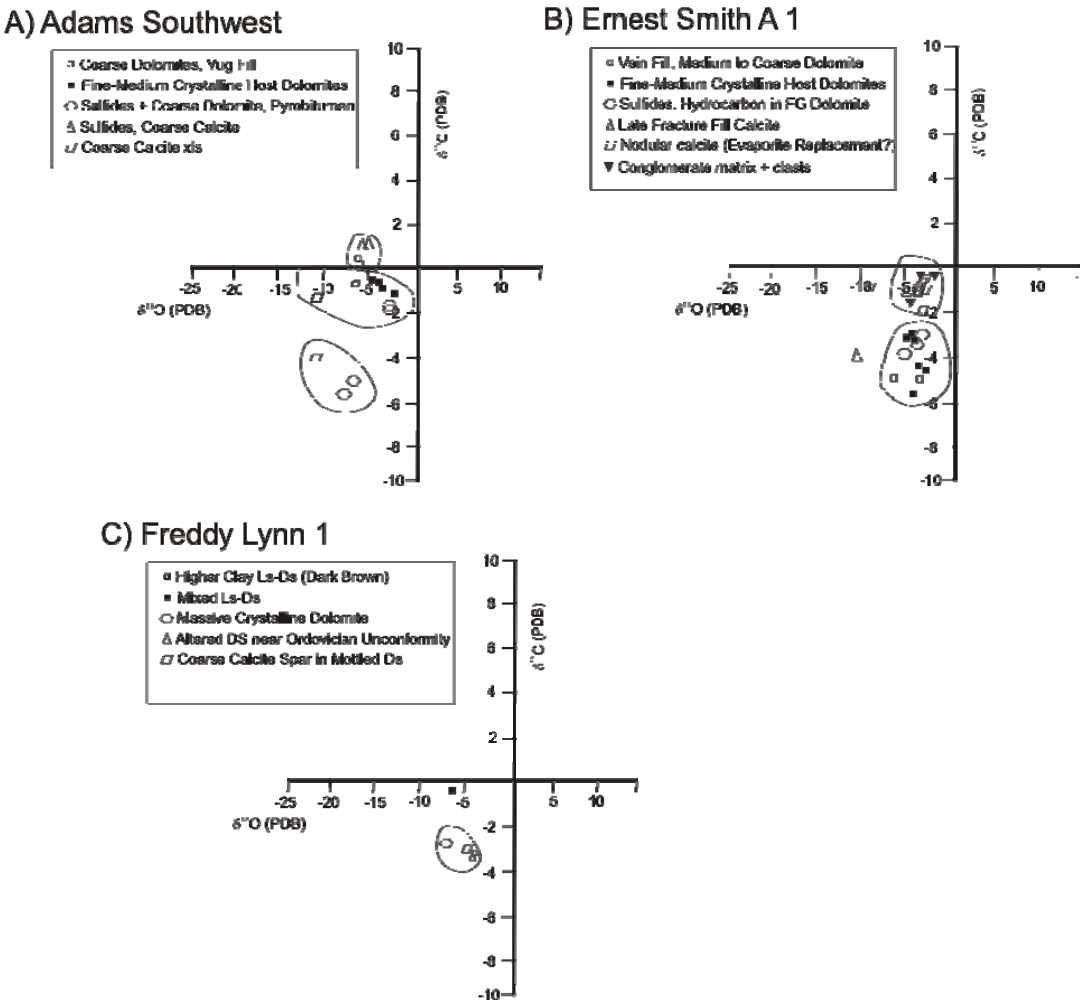

Figure 1-21. A) Carbon and Oxygen Stable Isotope Composition for the Ellenburger - ASW well core. B) ES. C) FL.

Fluid Inclusion Analysis

Fluid inclusion data were gathered from fracture and vug cements from the uppermost breccias in the ASW core. The rocks with these cements contain petrographic evidence of both early and late dolomitization, calcite and quartz cementation, and sulfide mineralization. Most viable primary inclusions had temperatures of homogenization on the order of 100-120°C (Figure 1-22). The inclusion fluids are aqueous brines of high salinity (-25% NaCl weight equivalent). A second cluster of inclusions appears to contain hydrocarbon phases due to very low ice melting temperatures (Figure 1-22).

High salinities may indicate dissolution of evaporates in the Ellenburger section or influx of external high salinity brines. A few inclusions extend to high temperatures near 220°C, but they do not contain hydrocarbons, and may be an artifact of inclusion stretching.

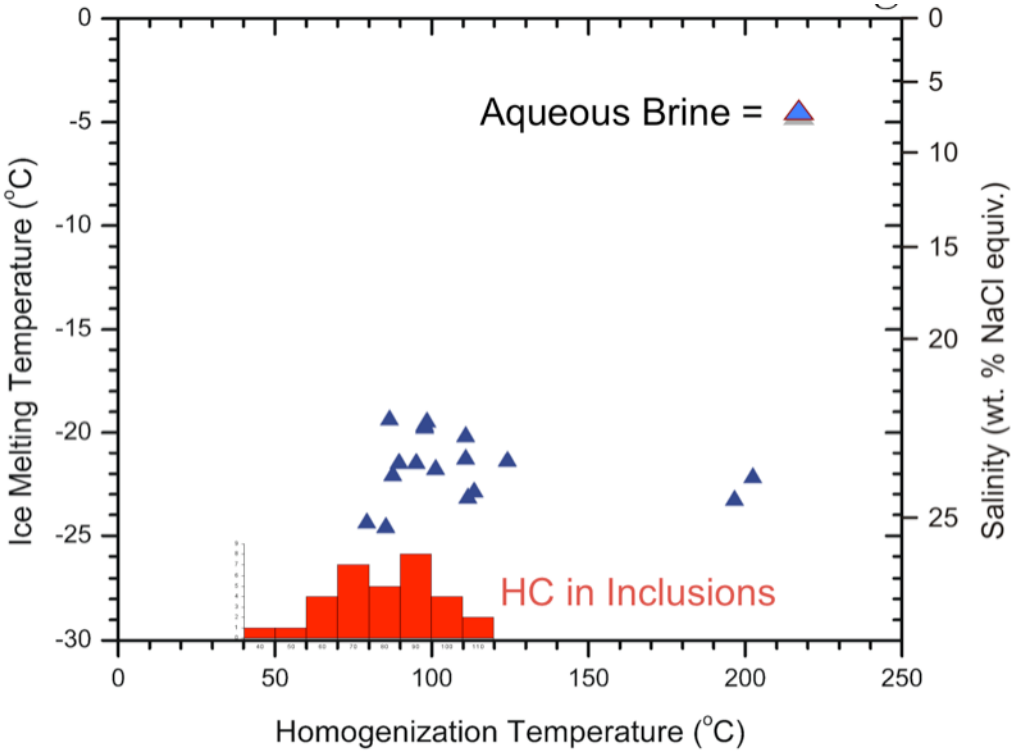

Figure 1-22. Fluid inclusion data from saddle dolomite vug cement in Facies 4, near 6972'MD in ASW. The histogram shows the relative abundance of hydrocarbon filled inclusions (interepreted due to very low ice melting temperatures near -120°C) versus normal aqueous brine fluids (blue triangles).

1.5.3 Results and Interpretations – Paleomagnetism

Magnetic components were defined from data collected during stepwise thermal demagnetization of the Ellenburger specimens. The low temperature treatment resulted in the loss of between 7 and 11% of the NRM on the first cycle and 5 to 9% after the second cycle. Maximum total loss of the natural remanent magnetization (NRM) was 21.3% on one doubly cooled sample indicating that multi-domain magnetite does contribute to the total natural remanence of some specimens. A larger (>75%) portion of the remanence is not removed. The remaining remanence is interpreted to reside in single domain or pseudo-single domain grains.

Thermal demagnetization removed a component interpreted as a modern viscous remanent magnetization (VRM) at low temperatures (<280°C) and a characteristic remanent magnetization (ChRM) between 330° and 530°C in most specimens (Figure 1-23A,B,C). The VRM resides in unstable grains that acquire the Earth's magnetic field as it changes over time (Tauxe, 2002). In most studies the VRM is considered magnetic "noise" but in this study it is important because it can be used to check the orientation of the core specimens. The VRM preserves an average magnetic field orientation over the last tens to hundreds of thousands of years that is a good average approximation of the modern magnetic direction. Multiple demagnetization steps below 300°C allow the VRM to be determined.

The ChRM has easterly to southerly declinations and shallow inclinations (Figure 1-23A,B,C). The magnetization decays to the origin by 500°C in most specimens, although maximum unblocking temperatures extend up to 530°C in some

specimens. The fact that the ChRM decays by 530°C suggests that it resides in magnetite.

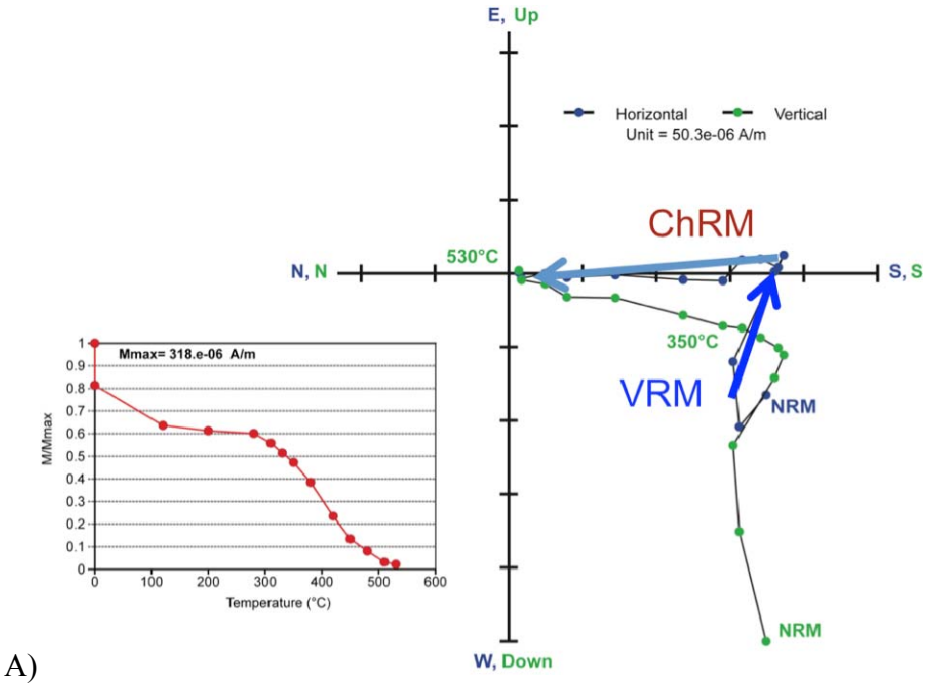

A)

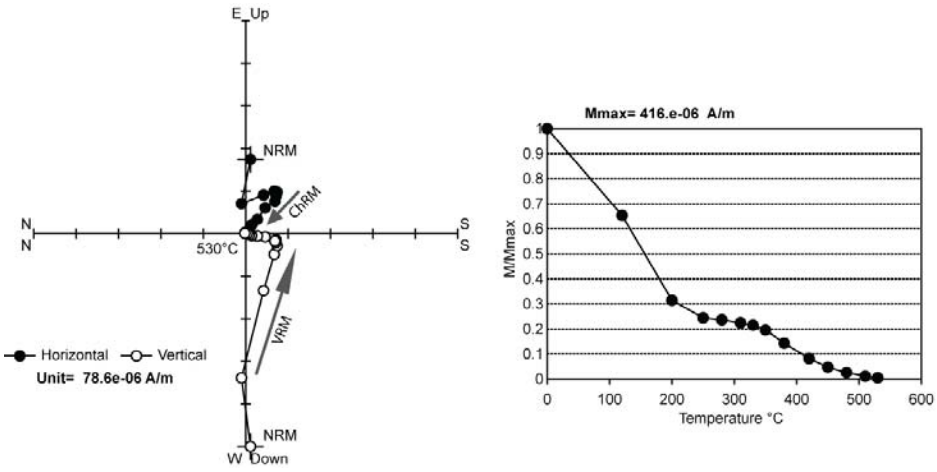

B)

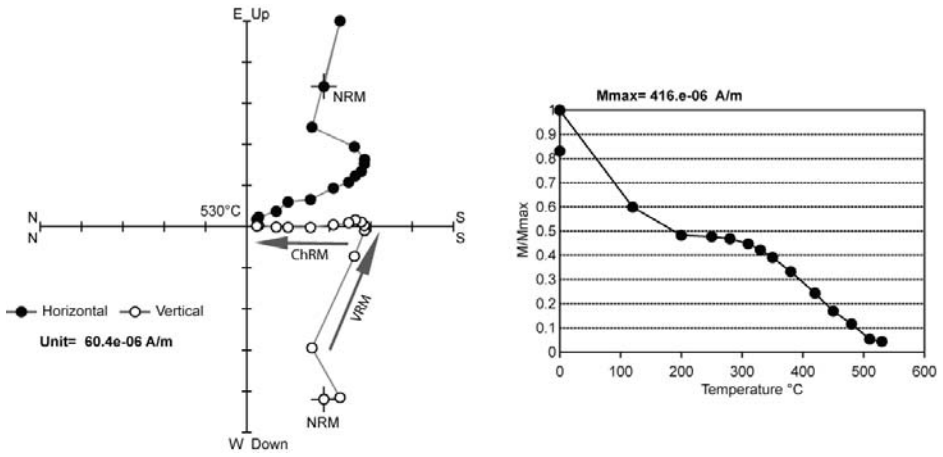

C)

Figure 1-23A-C. Zijderveld diagram (right) and specimen thermal decay curve (left) showing the VRM and ChRM in a representative specimen. Arrows show the VRM and ChRM components. The VRM is a secondary magnetization used for core orientation and the ChRM carries the principle characteristic remagnetization directions.

The ChRMs from the ASW and FL specimens were oriented using the scribe method and plot with southeasterly to southerly declinations and generally shallow inclinations (Figure 1-24A-B). For the ES core, the VRM was independently used to orient the core, yielding similar results (Figure 1-25). Based on this analysis, the paleomagnetic specimen directions are clearly streaked, defined as the statistical grouping of points shows a relatively linear distribution. The ASW core contains the greatest spread of directions in the Ellenberger with a cluster of easterly specimen directions that is not found in the other two wells. The specimen directions in the FL core, by comparison, are only slightly streaked.

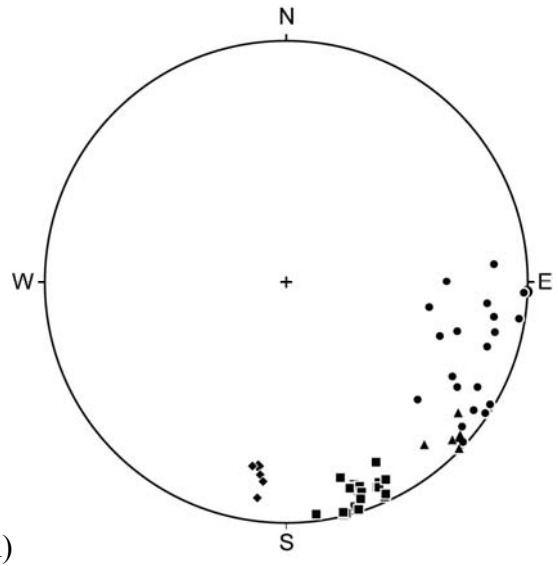

A)

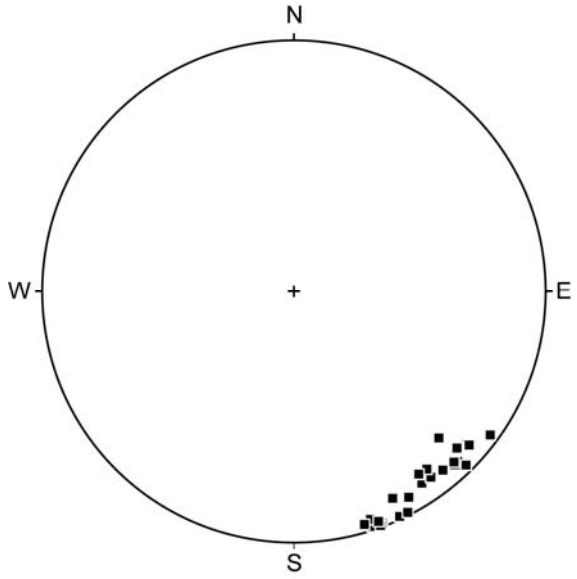

B)

Figure 1-24A-C. Specimen directional data from the Ordovician rocks in each sampled core. Filled squares are lower hemisphere directions (down) and open squares are upper hemisphere directions (up). A) ASW. B) FL. Note the distribution of data points resembles a "streak" of data in the ASW and the ES wells, and FL data are more grouped.

The origin of the streak is a crucial issue. The streak could be caused by rotation of the cores during the acquisition process that would result in "false" directions. In

order to test if the streak is a true representation of the data, the orientation of the core segments in the FL cores was tested by calculating the VRM and correcting the ChRM for the modern direction following the procedure used to orient the ES core (Figure 1-26A). The modern VRM in the FL core approximates the current magnetic field direction at the sample location (5° declination and 63° inclination). Rotating the direction back to the modern direction produces a streak similar to that of the oriented core. The scribe method, therefore, does orient the cores correctly. This indicates that the streak represents real data.

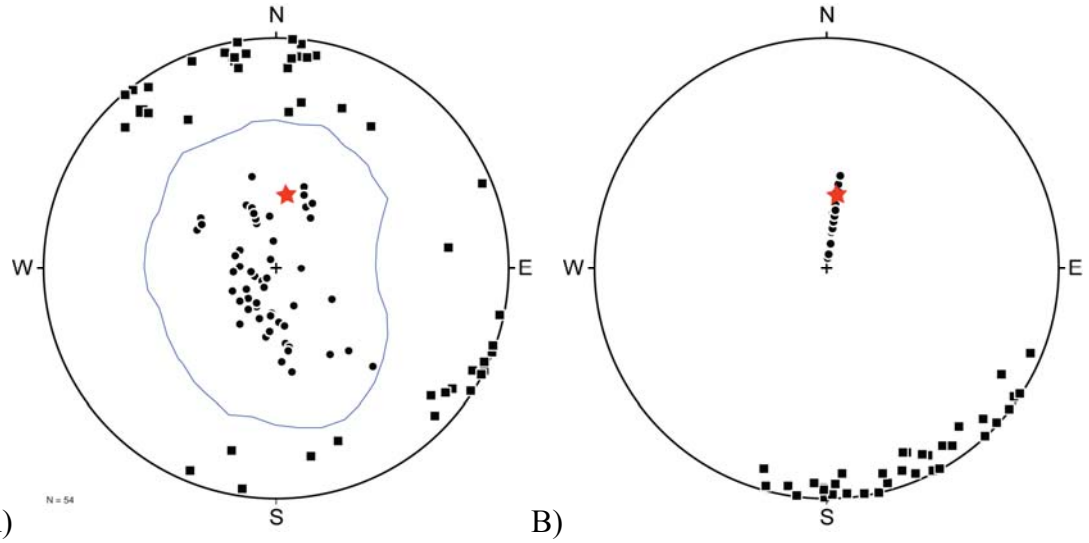

Figure 1-25A-B. Uncorrected VRM and ChRM versus data corrected to the modern VRM for the ES core. A) Uncorrected VRM (in contour) and the ChRM (black). B) ChRM after the VRM has been rotated by declinations back to the Modern direction.

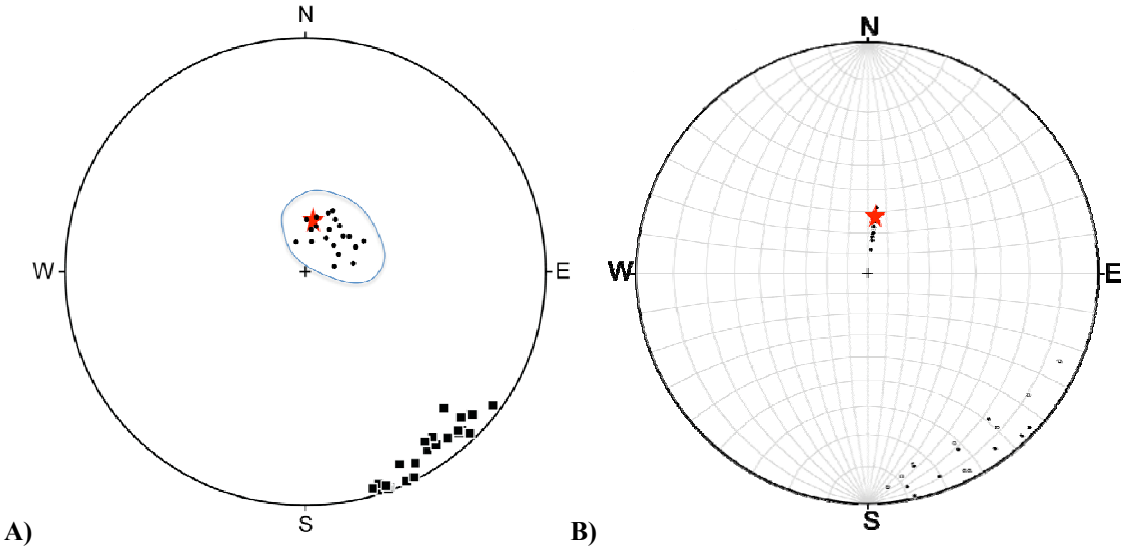

Figure 1-26. Comparison of the core orientation methods, FL well core. A) Comparison of VRM data points from scribe oriented core. B) Results of rotating by VRM to the modern. Streak is similar to the unoriented core in Figure 1-25.

There are several other explanations for the streak in directions. Overlapping components that are unresolved during demagnetization could cause the streak, but this is considered unlikely because the ChRM displays linear decay in the orthogonal projections. Alternatively, the streak could represent distinct elliptical groups of data that only appear linearly streaked due to overlap between magnetizations. In order to test this hypothesis, the specimen directional data were subdivided into groups based on the diagenetic facies. This results in the creation of unit means based on the diagenetic facies (Table 1-3). The specimens from the different facies group into clusters (Figures 1-27, 1-28,1-29, 1-30). For example samples from the paleokarst facies 4 “chaotic breccia” all are grouped, just as facies 1 “massive dolomite” is grouped together. If more than one facies have similar directions, they are grouped together as a unit.

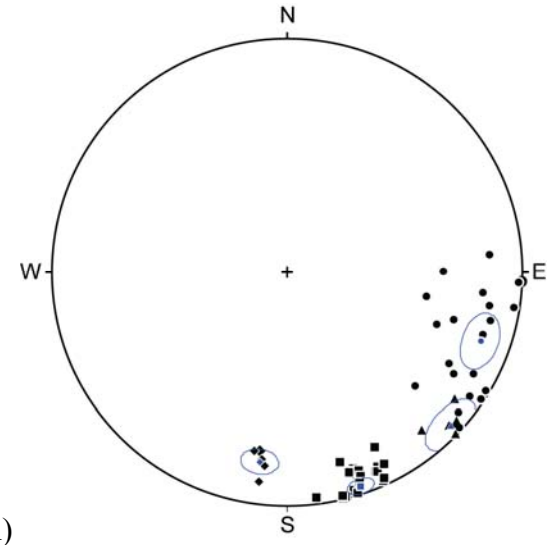

A)

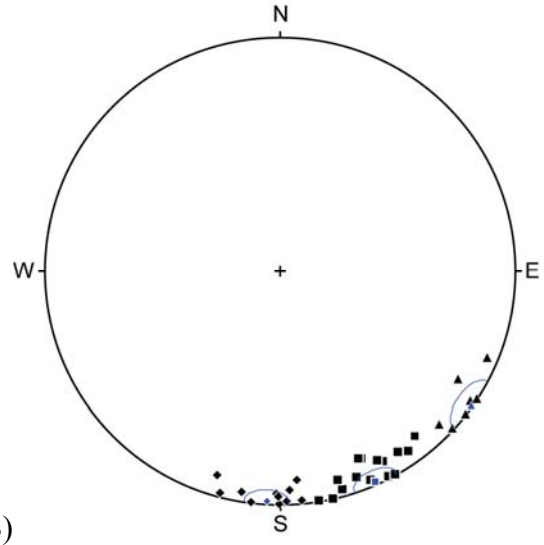

B)

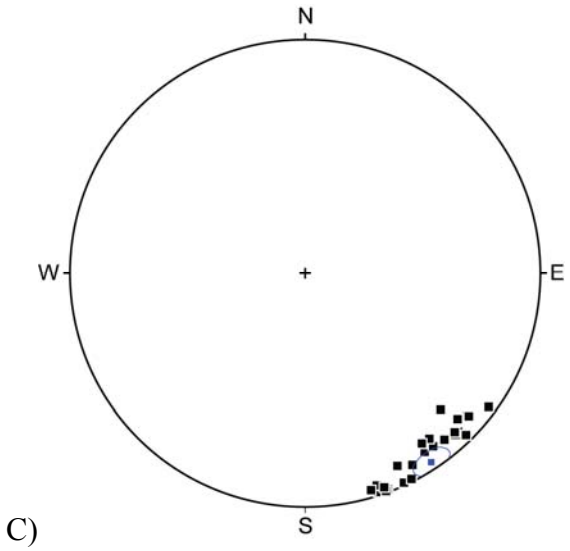

C)

Figure 1-27A-C. Equal area stereonet plot of specimen directions and unit means for ChRMs identified in all three cores. A) ASW. B) ES. C) FL.

Dec°	Inc°	a95	k	N sites	Facies	Description	Paleo Latitude	Paleo Longitude	dp	dm	AGE
132.8	5.9	2.0	816.2	2	6	Dolostone W Shale fill fractures	32.7	141.8	4.4	8.8	IP
200.8	-0.5	11.8	61.9	4	3	Vug Bearing Interval	51.8	47.2	5.9	11.8	P-J
100.3	24.3	20.3	37.9	3	3,4	Breccia Clasts	1.5	155.1	11.6	21.7	Ord
124.2	16.5	9.0	105.5	4	4	Coarse Breccia Clay Matrix	22.7	143.8	4.8	9.3	Ord
162.5	-2.4	6.4	65.3	9	1,2	Crystalline Dolomite	54.1	112.2	3.2	5.4	P

	-					Dolomite -					
178.4	10.4	16.4	32.3	4	8	Diss./Reprecip.	62.2	86.2	8.4	16.6	Tr-J
						Mottled					
54.1	9.4	12.9	36.1	5	5	Carbonate	32.3	8.5	6.6	13.0	P
						Mixed Peritidal					
267.2	-6.0	20.7	148.1	2	7	Carbonates	4.0	350.3	10.4	20.8	P

Table 1-3. Unit Means ChRM Directions and Paleopole Data.

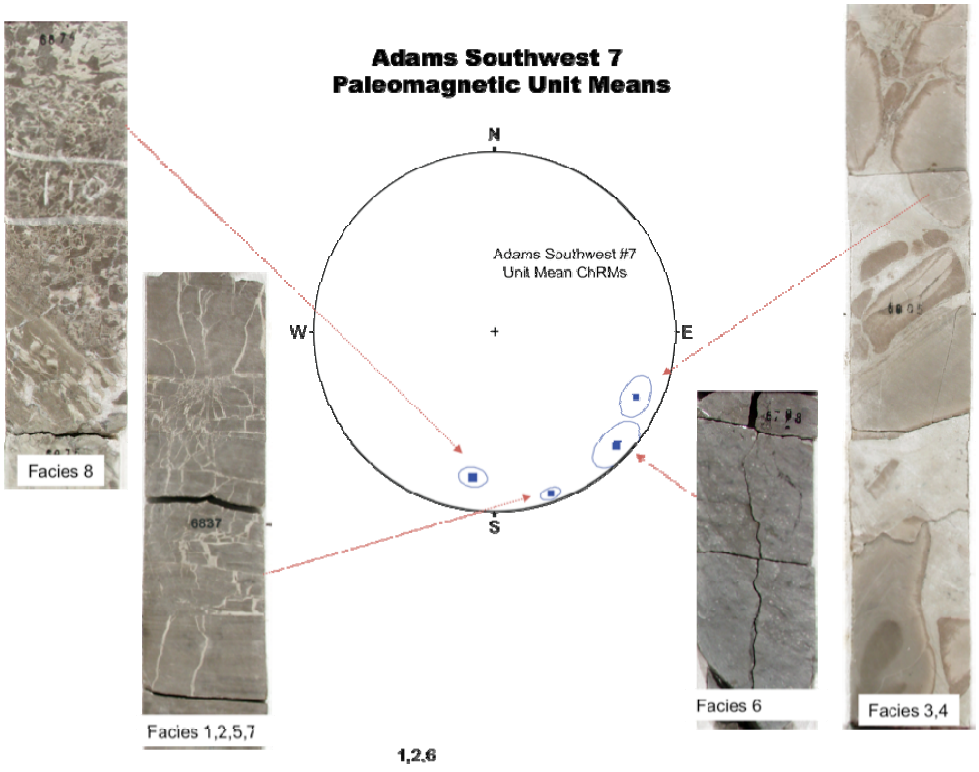

Figure 1-28. Unit means based on the facies in ASW with representative core photos.

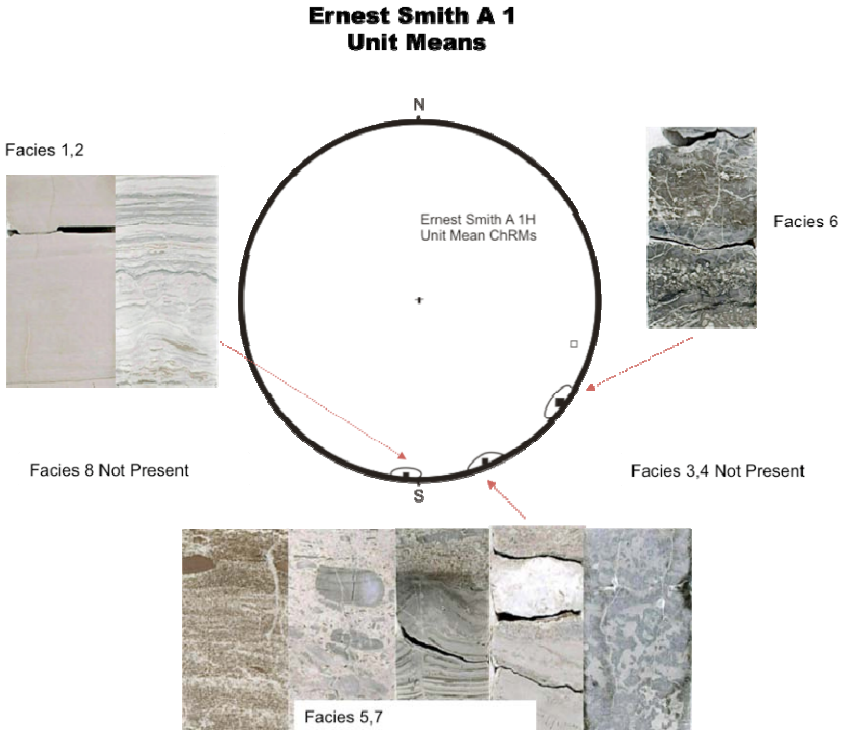

Figure 1-29. Unit means based on the ES core with representative core photos.

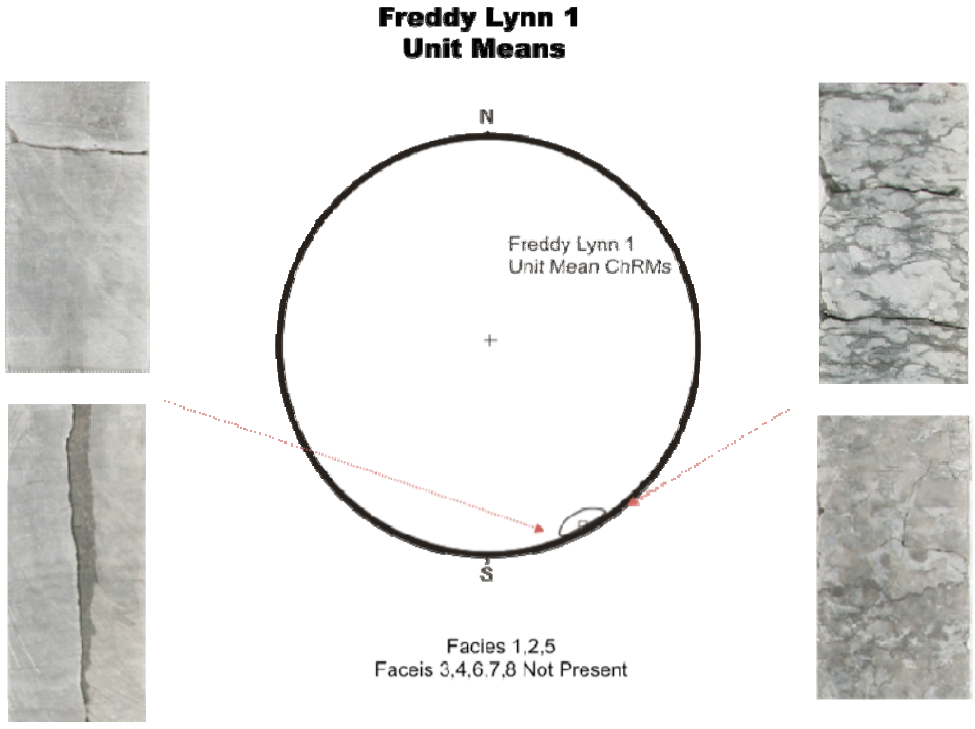

Figure 1-30. Unit means based in the FL core with representative core photos.

Clasts from the Facies 4 (coarse chaotic breccia) were sampled in the ASW core in order to perform a breccia (conglomerate) test. A breccia test allows the discrimination of a post-depositional remanent magnetization from a pre-depositional remanent magnetization. If magnetizations in the clasts are randomly oriented, the ChRM is inherited from the parent rock, and the rock was not remagnetized. If, however, clasts contain a common magnetic declination and inclination, then the rock was remagnetized at some time after the formation of the breccia deposit (Figure 1-31). In this case the direction and paleopole of would set a minimum age (younger) for the brecciation.

Specimens from individual clasts share a common east-southeasterly and shallow down direction (Figure 1-32). The pole for this direction plots along the Late Ordovician portion of the apparent polar wander path (APWP) (Figure 1-33).

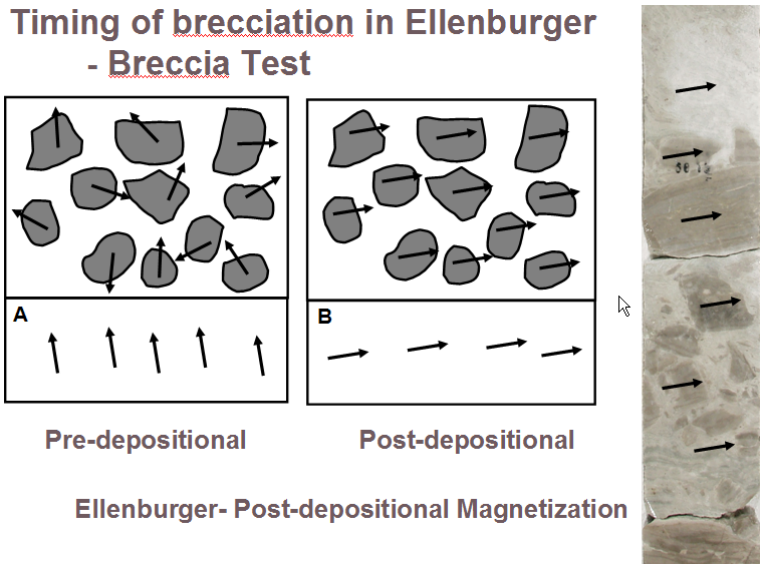

Figure 1-31. Schematic diagram illustrating the breccia paleomagnetic test.

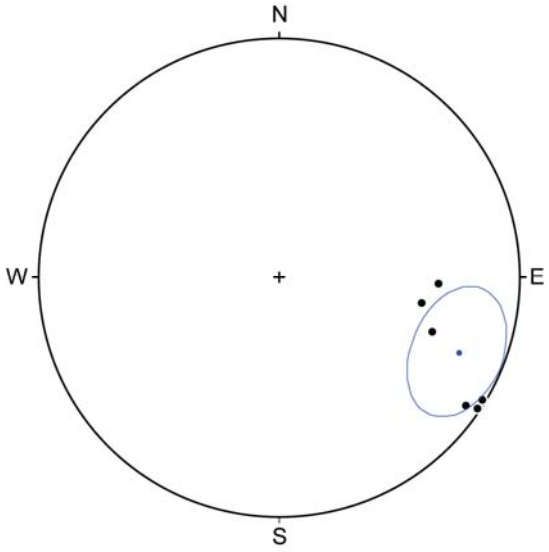

Figure 1-32. Specimen directions from individual breccia clasts group with a mean D=121.2 I=7.3 a95=10.5, n=8. The paleopole of the remagnetization is off the Upper Ordovician APWP (see 1.6.4).

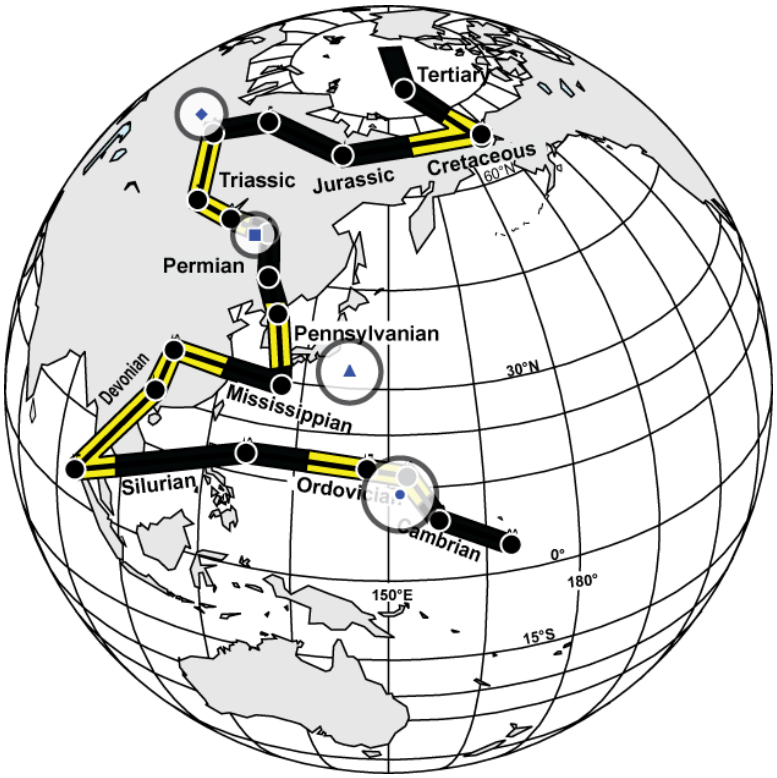

Figure 1-33. Ellenburger magnetic directions vs. the apparent polar wander path (APWP) by Van Der Voo, 1993. Each symbol corresponds to a separate unit mean or means. Squares are Facies (1,2,5,6); circle is karst breccia facies (3,4), triangle is shaly mixed lime dolomite facies (7) in green, and diamond is dissolution-precipitation facies (8) in purple. Each circle represents the ß95 error in degrees latitude and longitude. The inset shows that this path actually is a field, whose width is the error in calculation reflected in the variable width of the path.

The diagenetic facies subdivisions (based on breccias, fractures, dolomites and mineralization) result in consistent groupings of directions in all three wells (Figure 1-27A-C). For example, each core contains fractured, fine-grained crystalline dolomite facies (Facies 1 and 2) that contains a common southeasterly and shallow up direction.

The karst breccia facies (Facies 3 and 4) within the ASW core contain an easterly and shallow up direction. The paleopole falls on the Late Ordovician part of the APWP (Figure 1-33). It is the oldest paleopole found. This remagnetization is interpreted as being related to the cementation associated with healing of karst fractures and breccias in the late Ordovician, following the initial exposure and weathering of the surface during the middle Ordovician lowstand event (Kerans, 1990).

The Middle and Upper Ordovician rocks of the Simpson and Viola Groups that cap the Ellenburger in the ASW and ES (Facies 6; Mixed Limestone/Dolomite with shale filled fractures) contain a magnetization with southeast declinations and shallow inclinations. This direction corresponds to a pole that falls slightly east of the path (Figure 1-33) but close to the Mississippian-early Pennsylvanian part of the path. These rocks contain fractures that appear associated with the younger Mississippian (pre-Barnett Shale) unconformity, as Barnett Shale deposits are found infilling fractures in

this interval. This may suggest why the Viola contains a younger remagnetization than Ordovician.

A number of facies contain a similar south southeasterly and shallow down direction that correlates to the mid-Permian to early Triassic part of the APWP (Figure 1-33). The facies that contain this component are: Facies 1 (crystalline (incl. vuggy/fractured) dolomite), Facies 2 (Laminated dolomites), Facies 5 (mottled mixed limestone and dolomite with finer breccias), and Facies 7 (Clastic-rich mixed peritidal carbonates). The common factor between these facies appears to be coarse dolomite recrystallization and the presence of hydrocarbons and late sulfide minerals. Facies 8 (Dolomites with solution-re-precipitation) in the ASW and ES contain a south southwesterly and up direction which correlates to the Late Triassic to Jurassic part of the APWP (Figure 1-33). This facies is unique to these cores. Hydrocarbons and sulfides may be seen lining the interiors of these solution cavities, but volumetrically are minor. Fe-calcite and Fe-dolomite are present as vug and pore fill, as well as abundant porosity-occluding authigenic illite. Stylolites are common above and below the intervals with these facies, as are east-west open shear fractures.

The ASW and ES poles for the facies 6; mixed limestone/dolomite are off of the path by about 10-15° longitude. The late Permian-Triassic ChRM, however, is not off the path. A) 10-15° clockwise rotation could account for the pole being off the path for Facies 6 (Figure 1-34). A rotation of the pole for facies (6) would place the remagnetization in the late Pennsylvanian. A rotation of the pole for the karst facies (3,4) would place the remagnetization of karst breccias in the early Silurian.

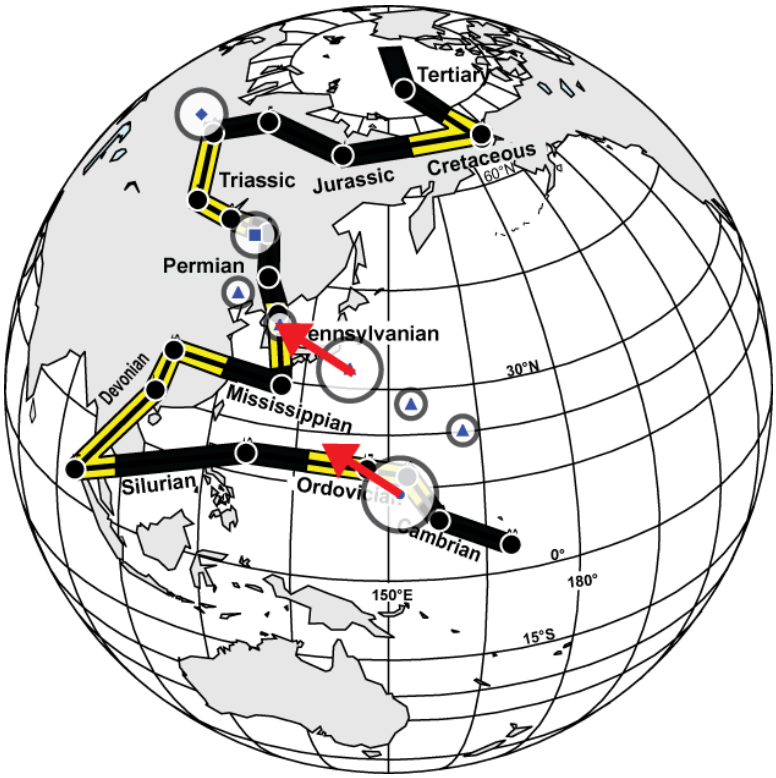

Figure 1-34. Moving the "off the path" pole 10-15 degrees brings the pole back to the late Pennsylvanian part of the path, which is potential evidence of a late Pennsylvanian - early Permian tectonic rotation counterclockwise by 10-15 degrees off the path during the Ouachita orogeny prior to the Permian period. Small cirecles with triangles show the great circle path of rotation that would be experienced by the paleopole during a hypothetical tectonic rotation.

1.5.4 Results and Interpretations – Magnetic Mineralogy

Isothermal remanent magnetization (IRM) acquisition curves for specimens from the study area commonly reach saturation by about 300-500 mT suggesting the presence of a low coercivity magnetic mineral phase. A slight rise above 500 mT suggests the presence of a higher coercivity mineral such as hematite. The IRM acquisition curves can be further evaluated by modeling the curves using linear/gradient/standardized acquisition plots (LAP-GAP-SAP) analysis (Kruiver et al. 2001).

The results of the LAP-GAP-SAP analysis of the Ellenburger suggest magnetite is the primary magnetic carrier in most of the carbonates (Figure 1-36), with lesser pyrrhotite and minor hematite and goethite in some zones (Table 1-4). In at least one zone at the basal Ordovician Unconformity in the ASW, a non-remanence bearing hematite accounts for up to 40% of the total coercivity of the Ordovician rocks.

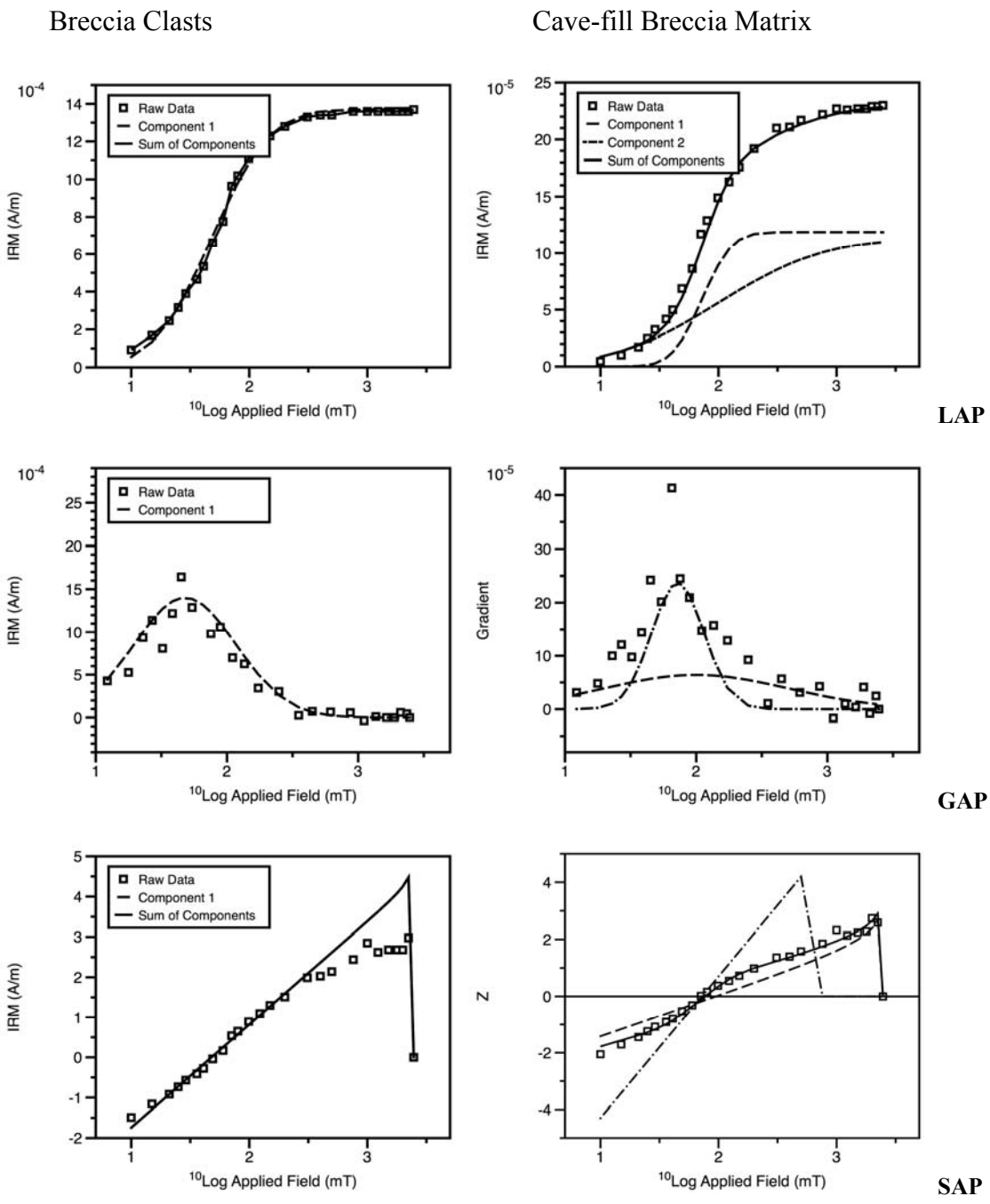

Figure 1- 35. LAP-GAP-SAP acquisition curves show saturation near 13x10-4 Ampere/meters for magnetite in ASW breccia clasts, ASW Core (6816 MD), and mixed magnetite and pyrrhotite in cave sediment fill (6814 MD).

Sample	Depth (Ft)	Components	Contribution (Percent)	SIRM A/M10-4	B1/2 (mT)	Magnetic Mineralogy
81004	6784.07	1	75.4	5.69	56.8	Magnetite
		2	24.6	1.86	279.1	Hemetite
81121	6789.01	1	87.6	4.40	57.5	Magnetite
		2	12.4	0.62	398.1	Hemetite
81531	6798.02	1	91.4	5.55	61.7	Magnetite
		2	8.6	0.52	1412.5	Goethite?
82103	6814.07	1	51.3	1.19	72.4	Magnetite
		2	48.7	1.13	100.0	Pyrrhotite
82201	6816.08	1	100.0	13.70	47.9	Magnetite
90412	6830.04	1	92.8	8.11	61.0	Magnetite
		2	7.2	0.62	724.4	Hemetite
100302	6873.02	1	86.1	12.00	47.6	Magnetite
		2	13.9	1.94	126.5	Pyrrhotite
100412	6874.02	1	96.3	12.70	50.1	Magnetite
		2	3.7	0.49	217.3	Hemetite

Table 1-4. Contributions of magnetic minerals per LAP-GAP-SAP analysis.

1.6 Discussion

I interpret the ChRMs identified within the Ellenburger as residing in magnetite based on unblocking temperatures below 580°C, the Curie temperature for magnetite, and the rock magnetic data. The magnetic data also suggest the presence of some pyrrhotite and hematite or goethite in some samples. All carriers are volumetrically measurable in parts per million in terms of rock volume. These minerals are not interpreted to carry a stable remanence.

Paleotemperatures for the basin are estimated between 100°C and 180°C based on organic geochemical data (Jarvie et al., 2009) and Ro data (Jarvie et al., 2001; Pollastro et al., 2003; 2004; Zhao, et al., 2007). Based on comparisons with the unblocking temperature-relaxation time curves (e.g., Dunlop et al., 1999), the maximum unblocking temperature of 530˚C is too high for the ChRMs to be a thermoviscous remanent remagnetization (TVRM). Therefore the ChRMs are interpreted as chemical remanent magnetizations (CRMs).

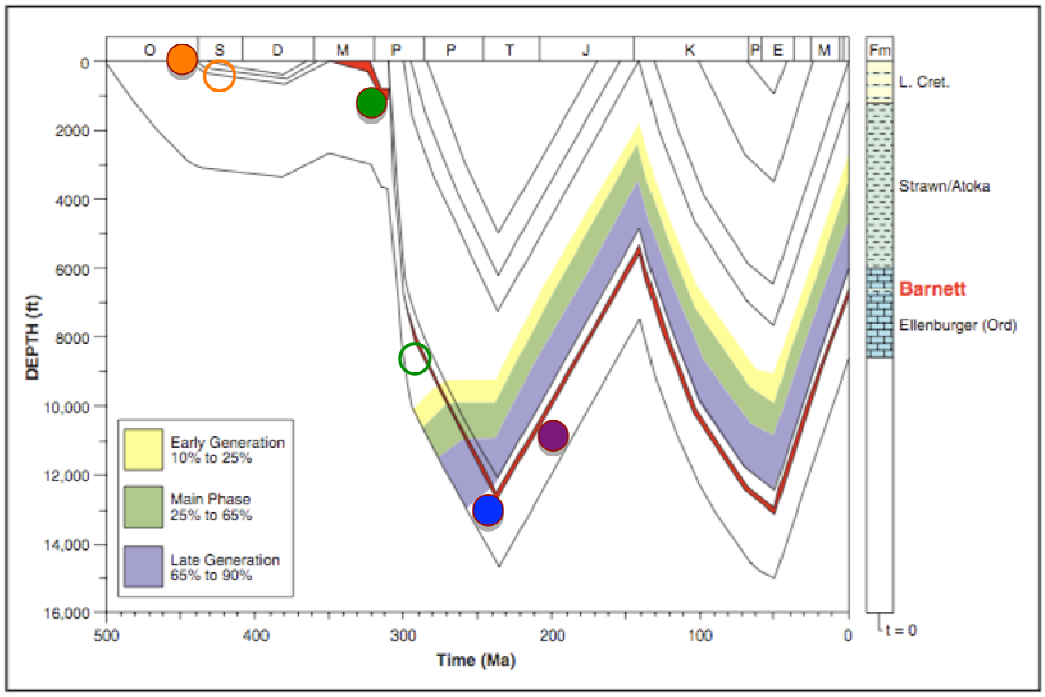

Figure 1-36. Age of remagnetizations versus burial history and thermal maturation chart for Wise County, TX. The orange dot shows the Ordovician post-karsting remagnetization as measured near late Ordovician-early Silurian CRM (not factoring in block rotation). Orange circle shows the block rotated CRM pole for the same post-breccia remagnetization. Green dot shows the Late Mississippian-early Pennsylvanian CRM pole as measured. Green circle shows the age of the same Pennsylvanian CRM with block rotation to the late Pennsylvanian-early Permian path. Blue dot is the late Permian-early Triassic pervasive CRM measured in all wells. Purple dot represents the late tectonic CRM (Late Triassic to Jurassic) possibly related to regional uplift and basin relaxation. Burial curve modified from Jarvie, (2004).

The origin of the CRM's is a critical issue for dating the timing of fluid diagenesis in the unit. The paragenesis of the Ellenburger in the Fort Worth Basin is summarized in Figures 1-37A and B. The late Ordovician (or early Silurian) CRM resides almost exclusively in paleokarst breccias, especially those containing clay-rich sediment in the breccia matrix. The late Ordovician-early Silurian age is correlative to some burial of the unit under Simpson, Viola (and Silurian?) rocks (Figure 1-36). The CRM is interpreted as related to early burial fluids associated with relatively early karst breccia and fracture cementation. It is worth noting that the karsts that preserve this Ordovician-Silurian magnetization are relatively unfractured and are well-cemented, suggesting that low paleopermeability after cementation/early dolomitization shielded the rocks from later remagnetizing fluids. In clay-rich cave fill deposits, it appears that late fluids did not remagnetize these rocks. In other zones, with open or partially mineralized fractures or breccia fill, a late Permian CRM is common (see below.) Open fractures are present in the Ellenburger below these karsted zones suggesting that late opening-mode fractures may have controlled these later post-Ordovician CRMs.

The early Pennsylvanian CRM is found defined only in Facies 6 (Viola-Simpson) in the ASW and ES wells. Specimens that contain this CRM are relatively rich in clays and organic matter. For example, the basal Barnett and Viola-Simpson sections preserve this CRM and include shale-filled solution cavities in the carbonates. The rocks which contain this CRM have $^{87}Sr/^{86}Sr$ isotopic results which are coeval and do not indicate alteration by externally derived fluids. This CRM is interpreted to have formed from burial processes, perhaps the smectite-to-illite conversion, or maturation of

organic matter. The acquisition time is a bit early compared to the burial history (Figure 1-36) though with the suggested block rotation correction this pole moves to correspond closely to the oil window for the unit. It is possible, therefore, that it could be related burial-related fluid pulse that moved along the Ordovician unconformity zone.

All the wells contain a large number of specimens with a late Permian to early Triassic CRM. The CRM is the most pervasive in the FL core (close to the Ouachita thrust zone) and least in the ES core (furthest from Ouachita Thrust). It is also found in rocks with Zn-Pb-Cu sulfides and radiogenic Sr values which suggest it is related to externally derived fluids, perhaps. The timing of the CRM also coincides with the end of the Ouachita orogeny in the early-mid Triassic so it is possible that the CRM is related to maximum burial and to the beginnings of Triassic-Jurassic regional uplift (Ewing, 2005). The timing of acquisition of the CRM coincides with the maximum depth of burial (Figure 1-36). The rocks with this CRM also contain hydrocarbon-filled fluid inclusions, authigenic K feldspars and abundant sulfides (pyrite plus sphalerite and trace Zn-Pb-Cu minerals). This suggests that the CRM could be related to organic matter maturation or hydrocarbon migration (Garven, 1985) through meteoric gravity-driven flow off of the highlands associated with the Ouachita belt. I interpret that the CRM is related to organic matter maturation/migration of hydrocarbons and/or external fluids from the Ouachita thrust belt.

The late Triassic-Jurassic CRM is found in zones containing dissolution textures associated with the mottled dolomite facies in the ASW and ES wells. This zone contains dissolution cavities filled with sparry calcite cements as well as some relict

hydrocarbons. Strontium isotope values are only slightly radiogenic (Figure 1-20). This CRM is interpreted based on the burial history curve position to be associated with fluids that may have migrated off of the Ouachita highlands by gravity-driven flow (e.g. Garven 1985) during extension of the basin during uplift of the Llano Uplift region and initial break-up of Pangaea.

East-west oriented open fractures are seen in core in the vicinity of these dissolution cavities on the core scale. East-west lineaments occur near the location of the ASW well core (Figure 1-4). Proprietary seismic data (provided by Devon Energy) confirms that faults of this orientation are also located near the ES well but not near the FL well. In the ES well, the late Triassic age is derived from a highly fractured zone at 7191-7192' MD in only a few samples near fractures. The E-W fractures/faults could have been a conduit for fluids, with the last remagnetizing fluid occurring in the late Triassic-Jurassic. More work is needed to test this hypothesis.

There is possible evidence for tectonic block rotations in the Fort Worth Basin based on paleomagnetic data. The poles for the Facies 6 fall to the east of the APWP. In contrast, the younger poles fall directly on the path with tight groupings. There are several potential reasons that the Facies 6 pole falls off the path. For example, it could have been acquired in a relatively short period of time that did not average out secular variation. Alternatively, the rocks with this CRM may have been tectonically rotated. A 15-20° counterclockwise rotation would move the pole off of the path to its present position. If this occurred, the block rotation must have occurred prior to the Permian because the younger poles are on the APWP. This block rotation interpretation is intriguing as it begins to suggest a mechanism for creating the complex fault

distributions seen in the Fort Worth Basin. Structural data interpreted from seismic (Sullivan et al., 2006) discussing a rotation of stress during development of the basin may support the block rotation hypothesis. Rotation of that stress would cause a change in the azimuth of these structures with time that is seen in lineament rotation in (Figure 1-4).

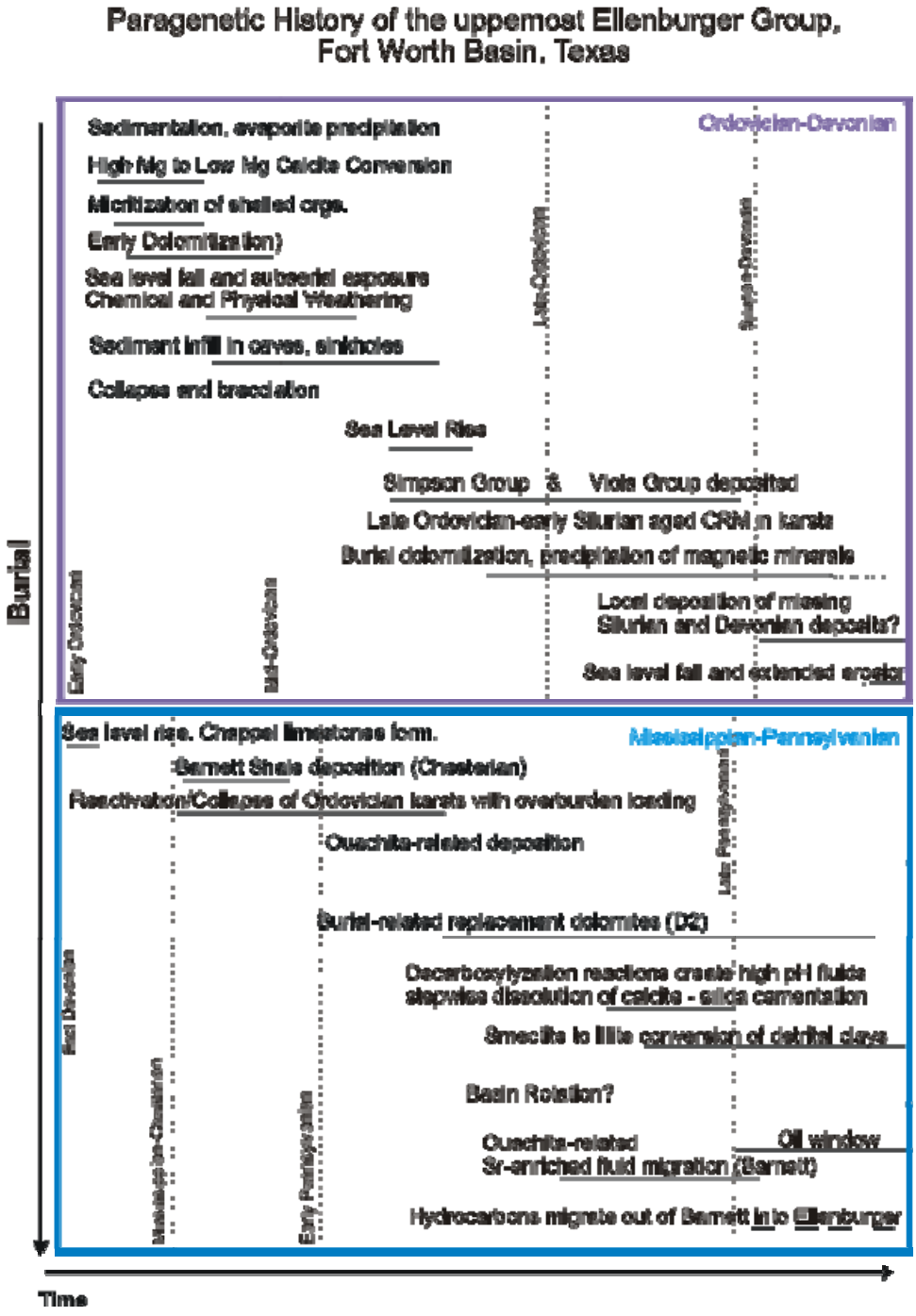

Figure 1-37A. Summary of Ordovician through late Pennsylvanian paragenesis for the uppermost Ellenburger Formation, Fort Worth Basin, Texas

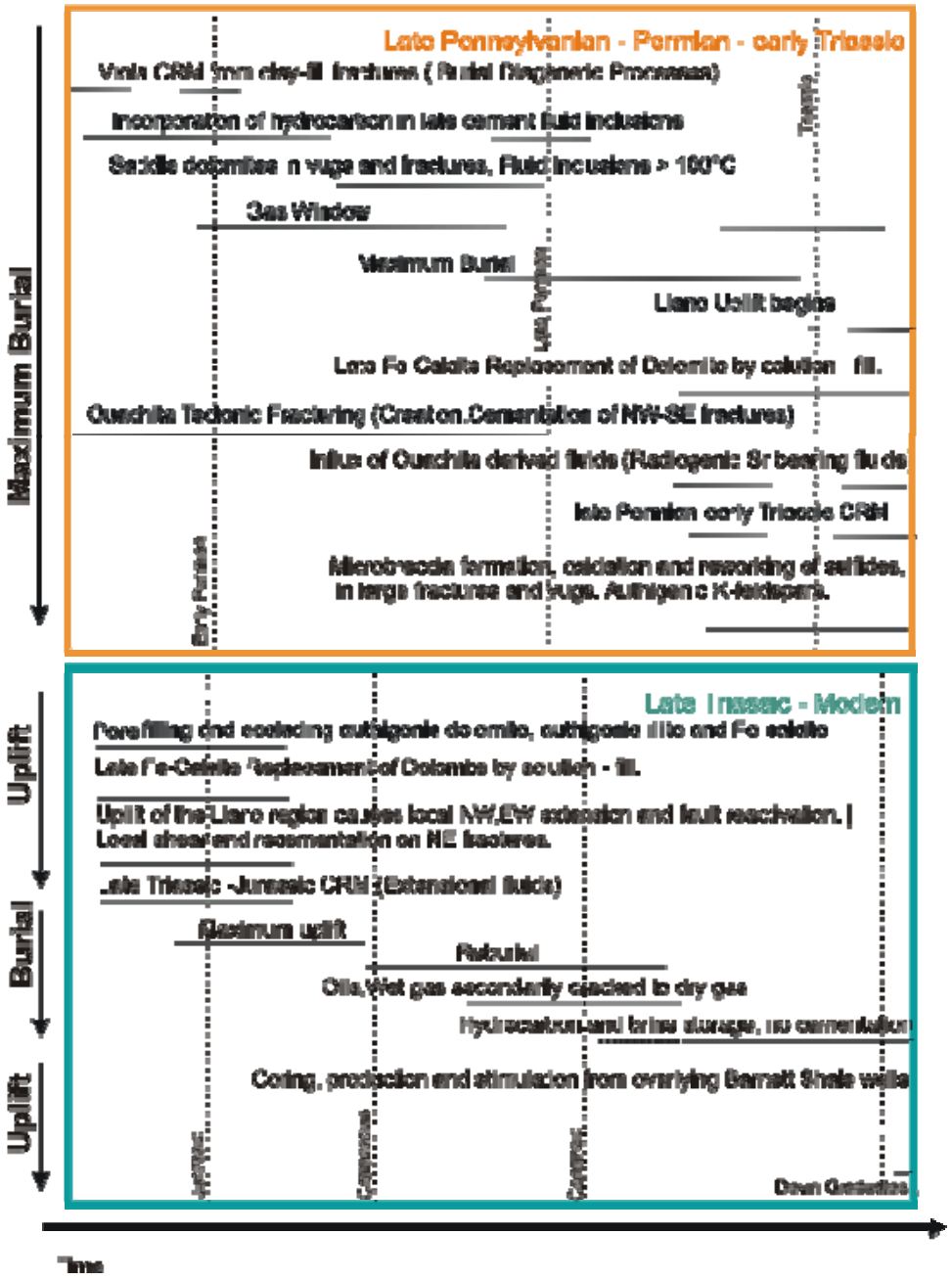

Figure 1-37B. Summary of Permian through Modern paragenesis for the uppermost Ellenburger Group, Fort Worth Basin, Texas.

1.7 Summary and Implications

The Ellenburger is shown to have experienced at least 4 major chemically induced remagnetization events. Mid-Ordovician karst structures were mostly cemented by magnetite precipitating-fluids in late Ordovician to early Silurian time. During burial, from early Pennsylvanian through Permian time, fractures were likely cemented, dissolved and re-cemented further with several successive generations of dolomite and calcite as well as minor quartz, feldspar, and volumetrically minor Zn-Pb-Cu bearing sulfides. Late structural collapse of caves during burial of karst structures could have periodically created enhanced permeability to dissolving and cementing fluids as well as for migration of hydrocarbons; many of these fractures were likely healed in Permian time, as facies containing the Permian remagnetization have largely healed fractures. Block rotations in the Late Pennsylvanian-early Permian are possible based on paleomagnetic data. In the late Permian, regional orogenic fluids from the Ouachita thrust altered rocks in the cores. Northwesterly faults near the Muenster Arch and or basement-linked faults may have been involved in this flow as the Permian-Triassic CRM is common in the NW part of the basin. More work is needed near the Arch to test this hypothesis. A final remagnetizing fluid occurred in late Triassic- Jurassic time. It may have been related to basin relaxation and gravity-driven flow off the Ouachita highlands during the uplift of the Llano region.

The remagnetization of the Ellenburger by fluids appears to have ended during the uplift in late Jurassic and Cretaceous time, although fluids were still stored in Ellenburger pores. Evidence of water can be seen on well logs and highly saline water is

produced from Barnett shale wells whose artificial fractures communicate with late tectonic fracture sets in the Ellenburger.

This study of the Ellenburger ties in well with previous studies of the Ellenburger. Timing of karsting and brecciation supports a subaerial exposure event for the creation of most breccias, although the presence of vugs and hydrothermal alteration suggests modification of these breccias at depth has occurred in some zones. The carbonates have undergone extensive burial dolomitization. A late Triassic-Jurassic pole related to uplift and extension of the region may suggest that further study in late extensional periods of the Fort Worth basin may yield clues to the variable productivity of some parts of the basin.

The Ellenburger, as a foundation for the Barnett shale gas plays, has undergone distinct periods of structural deformation, cementation, dissolution and uplift. The mechanisms and timing of these events are now better known, and such information may be useful in determining which faults or fractures sets in the Ellenburger are water wet and open, and which support the preservation of hydrocarbons.

1.8 Future Work

I recommend further study on the following aspects of paleomagnetism and diagenesis in the Ellenburger Group in the Fort Worth Basin.

1) Additional work is needed in the southwestern parts of the Fort Worth Basin, well as along the Muenster Arch, to better define source of diagenetic fluids.

2) Develop a better understanding of the distribution, volume and occurrence of MVT type minerals and hydrothermal dolomites along major regional faults (e.g. Smith and Davies 2007), whether or not these were possibly involved in the creation of hydrothermal dolomite plays in the basin. Hot fluids require cooling to precipitate minerals; the low volume of MVT minerals may suggest that the temperatures were simply too hot for precipitation, which does not preclude the development of HTD porosity. Further research on the few fluid inclusions samples which reached 220°C would help better define the temperature range of fluids for the basin.

3) Integration of clay XRD data in cave sediment fills to better understand the nature of the altering.

4) Understand the nature and distribution of liquid versus gaseous hydrocarbons versus paleomagnetic data, to test to see if late secondary cracking of oils to gas results in any paleomagnetic signal in the Mesozoic.

5) Further analysis of the VRM and its application as an orientation tool for fracture and fault studies, as well as rock fabrics.

6) Better mapping of the outliers of the Simpson and Viola Groups and their role in early cementation of the Ellenburger prior to deposition of the Barnett.

7) Hydrologic studies of vertically fractured crystalline dolomites versus irregularly-fractured dolomites to better understand the mechanisms of water transmissibility.

1.9 References for Chapter 1

Adams, J.E., 1954, Mid-Paleozoic Paleogeography of Central Texas: Shale Shaker. v.4, no.6, p.4-9

Aktepe, S., Marfurt, K., and Perez, R., 2008, Attribute expression of basement faulting--Time versus depth migration. The Leading Edge, Tulsa, OK, 27. p.360

Amthor, J. E., and G. M. Friedman, 1991, Dolomite-rock textures and secondary porosity development in Ellenburger Group carbonates (Lower Ordovician) west Texas and southern New Mexico: Sedimentology, v. 38, p. 343 – 362

Barnes, V. E., P. E. Cloud, L. P. Dixon, R. L. Folk, E. C. Jonas, A. R. Palmer, and E. J. Tynan, 1959, Stratigraphy of the pre-Simpson Paleozoic subsurface rocks of Texas and southeast New Mexico: University of Texas at Austin, Bureau of Economic Geology, publication no. 5924, 837p

Bethke, C. M., 1985, A numerical model of compaction-driven groundwater flow and heat transfer and its application to the paleohydrology of intracratonic sedimentary basins. J. Geophys. Res. 80: pp. 6817-6828

Bethke, C.M., and Marshak, S., 1990, Brine migrations across North America-the plate tectonics of groundwater; Annual Review of Earth and Planetary Sciences, v.18 (1), pp. 287-315

Bartram, J. G., Imbt, W.C., and Shea, E.F., 1950, Oil and gas in Arbuckle and Ellenburger formations, Mid-Continent region: Am. Assoc. Petroleum Geologists Bulletin, v. 34, pp. 682-700

Blumstein, R.D., Elmore, R.D., Engel, M.H., Parnell, J, and Baron, M., 2005, Multiple fluid migration events along the Moine Thrust Zone, Scotland: Journal of the Geological Society, vol. 162 (6) pp. 1031

Bolton, A., and Maltman, A., 1998, Fluid-flow pathways in actively deforming sediments- the role of pore fluid pressures and volume change: Marine and Petroleum Geology, v. 15 (4), pp. 281-297

Bowker, K.A., 2003, Recent developments of the Barnett Shale play, Fort Worth Basin: West Texas Geological Society Bulletin, v. 42, no. 6, p. 4-11

Bowker, K.A., 2007, Barnett shale gas production, Fort Worth basin issues and discussion: AAPG Bulletin, vol. 91 (4) pp. 523

Bradfield, H.H., 1964, The Ellenburger Group of North Central Texas. Tulsa Geological Society Digest, v.32, pp. 112-118

Burgess, W.J., 1976, Geologic evolution of the Mid-Continent and Gulf Coast areas - A plate tectonics view: Trans. Gulf Coast Assoc, of Geol. Soc, v. 26, pp.132-143

Cloud, P.E. Jr., and Barnes, V.E, 1948. The Ellenburger Group of central Texas: University of Texas, n.4621, 473 p

Combs, D. M., Loucks, R.G., and Ruppel, S.C., 2003, Lower Ordovician Ellenburger Group collapsed paleocave facies and associated pore network in the Barnhart field, Texas, in T. J. Hunt and P. H. Luftholm, eds., The Permian Basin: Back to basics: West Texas Geological Society Symposium: Proceedings, West Texas Geological Society Publication 03-112, p. 397 – 418

Smith, L. B. Jr., and Davies, G.R., 2006, Structurally controlled hydrothermal alteration of carbonate reservoirs: Introduction: AAPG Bulletin, v. 90, p. 1635 – 1640

Denison, R.E., Koepnick, R.B., Burke, W.H., and Hetherington, E.A., 1994, Construction of the Cambrian and Ordovician seawater 87Sr/86Sr curve: Chemical Geology, vol. 152 (3-4), pp. 325-340

Dunlop, D. J., and Argyle, K.S., 1991, Separating Multi-domain and Single-Domain-Like Remenances in Pseudo-Single-Domain Magnetites (215–540 nm) by Low-Temperature Demagnetization, *J. Geophys. Res.*, *96,* (B2), pp.2007–2017

Elmore, R.D., 2001(a), A review of paleomagnetic data on the timing and origin of multiple fluid-flow events in the Arbuckle Mountains, southern Oklahoma: Petroleum Geoscience, vol. 7 (3), pp. 223

Erlich, R., and Coleman, J., 2005, Drowning of the Upper Marble Falls carbonate platform (Pennsylvanian): Sedimentary Geology, 175, p. 479-499

Ewing, T. E., 2006, Mississippian Barnett Shale, Fort Worth Basin: North-central Texas: Gas-shale play with multi-TCF potential - Discussion: AAPG Bulletin, v. 90, p. 963 – 966

Fisher, R.A., 1953, Dispersion on a sphere: Geophysical Journal of the Royal Astronomical Society, v. 217, p. 295–305

Fisher, M., Wright, C., Davidson, B., Fielder, E., Buckler, W., Steinsburger, N., 2002. Integrating fracture-mapping technologies to optimize stimulations in the Barnett Shale: SPE Annual Technical Conference and Exhibition. SPE 77441.

Flawn, P. T., Goldstein, Jr., A., King, P.B., and Weaver, C.E., 1961, The Ouachita system: University of Texas, Bureau of Economic Geology, Report n.6120, 401p, 6 sheets

Flippin, J. W., 1982,The stratigraphy, structure, and economic aspects of the Paleozoic strata in Erath County, north-central Texas, in C. A. Martin, ed., Petroleum geology of the Fort Worth Basin and Bend arch area: Dallas Geological Society, p. 129 – 155

Gale, J.F, and Gomez, L.A., 2007, Late opening-mode fractures in karst-brecciated dolostones of the Lower Ordovician Ellenburger Group, west Texas: Recognition, characterization, and implications for fluid flow. AAPG Bulletin, v.91, 7, pp.1005

Gale, J.F., Reed, R.M., and Holder, J., 2007, Natural fractures in the Barnett Shale and their importance for hydraulic fracture treatments. AAPG Bulletin vol. 91 (4) pp. 603.

Gomez, L. A., Stowell, J.F.W., Ruppel,S.C., and Laubach,S.E., 2001, Fracture characterization using rotary-drilled sidewall cores: An example from the Ellenburger Formation, west Texas, in Proceedings, West Texas Geological

Society fall meeting: West Texas Geological Society, n.01-110, p. 81 – 89 in Texas Geological Society Publication 03-112, p. 231 – 252

Hardage et al., 1996. 3-D seismic evidence of the effects of carbonate karst collapse on overlying Clastic Stratigraphy and Reservoir Compartmentalization. Geophysics. DOE Report. Web: http://www.netl.doe.gov/publications/ proceedings/97/97ng/ng97_pdf/NG4-1.pdf

Haubold, H., 1999, Alteration of magnetic properties of Palaeozoic platform carbonate rocks during burial diagenesis (Lower Ordovician sequence, Texas, USA): Geological Society, London, Special Publications, v.151; p.181-203

Henry, J. D., 1982, Stratigraphy of the Barnett Shale (Mississippian) and associated reefs in the northern Fort Worth basin, in C. A. Martin, ed., Petroleum geology of the Fort Worth basin and Bend arch area: Dallas Geological Society, p. 157 – 178

Hoak, T.E., Sundberg, K.S., Ortoleva, P. and Shebl, M., 1998, Fracture Characterization and Discrimination Criteria for Karst and Tectonic Fractures in the Ellenburger Group, West Texas - Implications for Reservoir and Exploration Models: DOE-OSTI Technical Report, DOE/PC/91008--23-Pt.6, 63p

Jarvie, D.M., Hill, R.J., Ruble, T.E., and Pollastro, R.M. 2007, Unconventional shale-gas systems: The Mississippian Barnett Shale of north-central Texas as one model for thermogenic shale-gas assessment: AAPG bulletin, vol. 91 (4) pp. 475

Kerans, C., 1988, Karst-controlled reservoir heterogeneity in Ellenburger Group carbonates of west Texas: AAPG Bulletin, v.72, (10), pp. 1160-1183

Kirschvink, J.L., 1980, The least-square line and plane and the analysis of paleomagnetic data: Geophysical Journal of the Royal Astronomical Society, 62, pp.699–781

Kupecz, J.A., Kerans, C., and Land, L., 1988, Deep-burial dolomitization in the Ordovician Ellenburger Group carbonates, West Texas and southern New Mexico; discussion and reply: Journal of Sedimentary Research, v.58, (5), pp. 908-913

Kupecz, J. and Land, L. 1991, Late-stage dolomitization of the Lower Ordovician Ellenburger Group, west Texas: Journal of Sedimentary Petrology, v. 61, pp. 551–574

Lacazette, A., 2004, These “Karst” Features in the Ellenburger Are Really Pull-apart Basins. Abs., AAPG Annual Meeting, 2004, Dallas, Texas.

Lee,Y., and Friedman, G., 1988, Deep-burial dolomitization in the Ordovician Ellenburger Group carbonates, west Texas and southeastern New Mexico—reply: J. Sedimentary Petrology, v.58, pp. 910-913

Loucks, R.G., 1999, Paleocave carbonate reservoirs; origins, burial-depth modifications, spatial complexity, and reservoir implications: AAPG Bulletin v. 83, (11), pp.1795-1834

Loucks, R. G., and Anderson, J.H., 1980, Depositional facies and porosity development in Lower Ordovician Ellenburger dolomite, Puckett field, Pecos County, Texas, in R. B. Halley and R. G. Loucks, eds., Carbonate reservoir rocks: SEPM Core Workshop No. 1, p. 1 – 31

Loucks, R.G., Mescher, P.K., and McMehan, G., 2004, Three-dimensional architecture of a coalesced, collapsed-paleocave system in the Lower Ordovician Ellenburger Group, central Texas: AAPG Bulletin. v.88, (5), pp. 545-564

Loucks, R.G., and Ruppel, S.C., 2007, Mississippian Barnett Shale: Lithofacies and depositional setting of a deep-water shale-gas succession in the Fort Worth Basin, Texas: AAPG Bulletin. v.91, (4), pp. 579

Loucks, V., and Elmore, R.D., 1986, Absolute dating of dedolomitization and the origin of magnetization in the Cambrian Morgan Creek Limestone, central Texas: Bulletin of the Geological Society of America. v.97, (4), pp.486

Lowrie, W., 1990, Identification of ferromagnetic minerals by coercivity and unblocking temperature properties: Geophysical Research Letters, v.17, p.159–162

Lu, G., McCabe, C., Hanor, J. S. & Ferrell, R. E., 1991, A genetic link between remagnetization and potassic metasomatism in the Devonian Onondaga formation, Northern Appalachian basin: Geophys. Res. Letters, 18, pp.2047-2050

McDonnell, A., Loucks, R.G., and Dooley, T. 2007. Quantifying the origin and geometry of circular sag structures in northern Fort Worth Basin, Texas: Paleocave collapse, pull-apart fault systems, or hydrothermal alteration?. AAPG Bulletin. vol. 91 (9) p.1295

Meckel Jr., L.D., Smith, D., and Wells, L., 1992, Ouachita foredeep basins: regional paleogeography and habitat of hydrocarbons, *in* Foreland Basins and Fold Belts: American Association of Petroleum Geologists, Memoir vol. 55, pp. 427□444

Montgomery, S. L., Jarvie, D.M., Bowker, K.A., and Pollastro, R.M., 2005, Mississippian Barnett Shale, Fort Worth Basin, north- central Texas: Gas-shale play with multi-trillion cubic foot potential: AAPG Bulletin, v. 89, p. 155 – 175

Nelson, R. A., Lenox, L. C., and Ward, B. J., Jr., 1987, Oriented core: Its use, error, and uncertainty: AAPG Bulletin, v. 71, p. 357-367

Oliver, R., 1986, Fluids expelled from tectonically orogenic belts: there role in hydrocarbon migration and other geologic phenomena: Geology, 14, pp. 999-1021

Oliver, R., 1992, The spots and stains of plate tectonics: Earth Science Reviews, n.2, pp.77-106

Sullivan, E.C., Marfurt, K.J., Lacazette, A., and Ammerman, M., 2006, Application of new seismic attributes to collapse chimneys in the Fort Worth Basin: Geophysics, v.71, pp. B111-B119

Papazis, P.K., 2005, Petrographic characterization of the Barnett Shale, Fort Worth Basin, Texas: Master of Science Thesis, The University of Texas at Austin, Austin, 142p

Pollastro, R., Hill, R., Jarvie, D., Henry, M., 2003, Assessing undiscovered resources of the Barnett–Paleozoic total petroleum system, Bend Arch–Fort Worth Basin province, Texas: American Association of Petroleum Geologists Convention presentation, Fort Worth, Texas, American Association of Petroleum Geologists/Datapages, vol. 18, Search and Discovery Article #10034, pp.1-17

Pollastro, R.M., Jarvie,D.M., Hill, R.J., and Adams, C.W., 2007. Geologic framework of the Mississippian Barnett Shale,Barnett-Paleozoic total petroleum system, Bend arch–Fort Worth Basin, Texas. AAPG Bulletin. vol. 91 (4) pp. 405-436

Smith Jr., L.B., and Davies, G.R., 2006, Structurally controlled hydrothermal alteration of carbonate reservoirs- Introduction: AAPG Bulletin. v.90, (11), pp. 1635

Sommer, S. E., 1972, Cathodoluminescence of carbonates: Chemical Geology, v. 9, p. 257-284

Stamatkos, J., Hirt, A., Lowrie, W. 1996, The age and timing of folding in the central Appalachians from paleomagnetic results: Geological Society of America Bulletin, 108, pp. 815-829

Tauxe, L., 2002. Paleomagnetic principles and practice: Kluwer Academic Publishers, Boston, p.299

Thomas, 1993, Low-angle detachment geometry of the late Precambrian-Cambrian Appalachian-Ouachita rifted margin of southeastern North America: Geology, v. 21, (10), pp 921-924

Turner, G. I., 1957, Paleozoic stratigraphy of the Fort Worth basin, in W. C. Bell, ed.: Abilene and Fort Worth Geological Societies joint field trip guidebook, p. 57 – 77

Van Alstine, D., and Butterworth, J., 2002, Paleomagnetic Core-Orientation Helps Determine the Sedimentological, Paleostress, and Fluid-Migration History in the Maracaibo Basin, Venezuela. http://www.appliedpaleomagnetics.com.

Van der Voo, R., 1993, Paleomagnetism of the Atlantic, Tethys, and Iapetus Oceans: Cambridge University Press.

Walper, J.L., 1982, Plate tectonic evolution of the Fort Worth basin, in, Charlee A. Martin (ed.) Petroleum geology of the Fort Worth basin and Bend Arch area: Dallas Geological Society, pp. 237-241

Zhao, H., Givens, N.B., and Curtis, B. 2007, Thermal maturity of the Barnett Shale determined from well-log analysis: AAPG Bulletin, v. 91, (4), pp. 535

Chapter 2

Diagenesis and Paleomagnetism of the Mississippian Barnett Shale, Fort Worth Basin, Texas.

Abstract

The Mississippian Barnett Shale is the primary source rock and the major unconventional gas reservoir in the Fort Worth basin, Texas. Previous workers have hypothesized that orogenic hydrothermal fluids, originating from the nearby Ouachita thrust front, locally affected the thermal maturity of the organic-rich shale near fluid conduits. The extent of fluid alteration, as well as the timing and origin of the fluids are poorly understood. An integrated geochemical/petrographic/paleomagnetic/rock magnetic study was conducted to better understand the nature and timing of the hypothesized diagenetic alteration events. Samples from five scribe oriented conventional drill cores in the Barnett Shale were analyzed for their diagenetic and paleomagnetic properties. Thermal demagnetization of samples from reveals a low-temperature (< 200°C) steeply-downward viscous remanent magnetization (VRM) as well as several components that are removed at higher temperatures (200-540°C). The higher temperature components reside predominantly in magnetite and are interpreted as chemical remanent magnetizations (CRMs) based on low burial temperatures. The specimen directions are streaked from an easterly and shallow direction to a southerly and shallow direction. The modern VRM was used to orient the CRM data for one

of the wells and to test the scribe orienting method. The results confirm that the streak of directions is real and were not caused by rotation of the core.

Subdivision of the paleomagnetic data does not reveal an apparent control on the CRMs by lithofacies. Fracture orientation, however, appears to be correlated to the paleomagnetic directions. Fractures associated with bed-parallel stratiform mineralization contain a CRM interpreted to the mid-Pennsylvanian and the fracture fills are mostly non-radiogenic. Sub-vertical fractures with northeasterly azimuths are found in rock that contains a similar mid-late Pennsylvanian CRM and the fracture fills are non-radiogenic. Both bed-parallel and sub-vertical fractures are interpreted to have formed from early burial diagenetic fluids. Vertical northwesterly fractures are associated with rock that contains a late Pennsylvanian to early Permian CRM. These rocks are interpreted to have been altered primarily by internally derived fluids based on their relatively low levels of radiogenic strontium. The CRM is interpreted to have formed from burial diagenetic processes, such as clay transformations or hydrocarbon generation and migration. A set of vertical, northeasterly fractures contains a late Permian CRM. These fractures commonly display evidence of reactivation and are filled by multiple generations of calcite, silica, sulfides and sulfates, and may contain open vugs and incomplete cementation. The fluids that precipitated these late fracture fills were largely radiogenic. This late CRM is interpreted as related to gravity driven orogenic fluids sourced from the uplifted Ouachita front. The paleomagnetic data suggests the possibility of a counterclockwise block rotation of up to 20° in late Pennsylvanian time in the northern

half of the basin. Vertical magnetic susceptibility data shows similarities between some cores and suggests that MS data can be used to correlate the Barnett in some parts of the basin. The early and late diagenetic alteration of the Barnett resulted in the addition of some minerals (e.g., silica, sulfates, and authigenic albite) that could have changed the mechanical behavior of the mudstones by making them more or less rigid.

2.1 Introduction

Bowker et al. (2007) and Pollastro et al. (2007) suggest that orogenic fluids (e.g. Oliver, 1986, 1992) exerted a major control on the thermal maturity of the Mississippian Barnett Shale in the Fort Worth Basin, Texas. These studies hypothesized that warm fluids migrated away from the Ouachita thrust front during foreland basin formation, creating maturity variations in the shales that are independent of depth of burial. Evidence in support of this hypothesis includes elevated vitrinite reflectance values in some stratigraphic intervals as well as anomalous maturities near major through-going faults (Pollastro et al., 2007)(Figure 2-1).

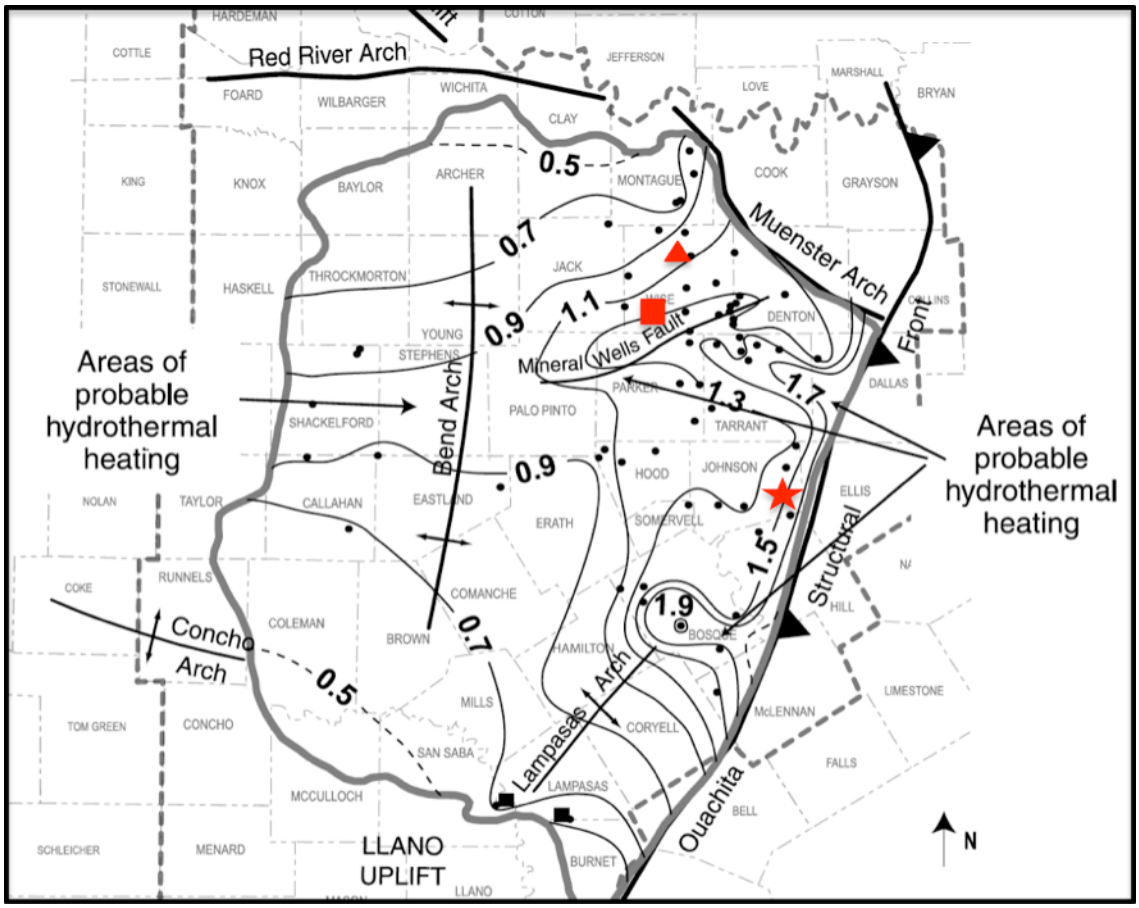

Figure 2-1. Lines of equal thermal maturity, as determined from a mean vitrinite isoreflectance (Ro) map for the Barnett Shale (based on data from Humble Geochemical Services, Humble, Texas). The map highlights areas speculated to have been areas of hydrothermal heating that created the anomalously high Ro values. Symbols represent the cores used in this study; the triangle is the Ernest Smith A 1, square is the Adams Southwest 7, and star shows the location of three cores in Johnson County: Freddy Lynn 1, Spencer Trussel 1, and Rose Children's Trust 1. Map modified from Pollastro et al., (2007).

Bowker (2007) and Pollastro et al., (2007) relate the variations in vitrinite reflectance around faults in the Barnett Shale to focused fluid flow. Faults have long been shown to be conduits for fluids in other studies (e.g. Smith and Davies, 2006). Fault history and character can influence the ability of faults to conduct orogenic fluids. For example, faults that may be good candidates for focusing orogenic fluids in foreland basins include those that are basement-linked, have large throw and heave, and which were active on multiple occasions.

Various studies (e.g., Neuzil, 1994; Best and Katsube, 1995; Ingram et al., 1997; Harrington and Horseman, 1999; Hildebrand and Urai, 2003; Loucks et al., 2009) suggest that shale and mudstone source rocks tend to be extremely tight to natural fluid movement, with permeabilities measured in the nanodarcy to microdarcy ranges. Unconventional resource plays in shale, therefore, require artificial fractures to be created by hydraulic stimulation in order to increase the rock's permeability and to make economic reservoirs of (Fisher, 2002; Pollastro, 2003). Like natural fluids, frac fluids may act as agents of diagenetic change by causing dissolution and cementation (scaling) as well as causing localized maturation of hydrocarbons, all of which can affect the final mechanical behavior of the mudrocks (Williamson, 1992; Best and Katsube, 1995). The natural and artificial diagenesis of the shales is of importance not

only to geologic prospectivity of the formation, but also producibility.

Recent studies by Gale et al. (2007) and Papazis (2005) have presented evidence of natural fluid alteration in cores. Complex veining and sub-vertical to vertical tectonic fracturing exists in the Barnett Shale. These often contain a complex record of fluid alteration with multiple generations of cementation. This suggests that multiple fluid events may have occurred in the Barnett Shale, as proposed by Bethke and Marshak (1990). These events may have been generated internally, during burial processes, or may have been sourced externally, from faults, fractures or the surrounding carbonates.

The objective of this study is to conduct an integrated diagenetic and paleomagnetic study of the Barnett Shale in order to further characterize the diagenetic features in the unit, investigate the origin and extent of any alteration by external fluids, as well as determine the timing of the events. The study specifically 1) tests the hypothesis that the Barnett Shale has been altered by externally derived fluids, and 2) determines the origin and timing of the fluid migration events. In addition, the diagenetic characteristics are evaluated in terms of their affect on the mineralogy and mechanical behavior of the shale.

Data for this study comes from five subsurface oriented cores in Wise and Johnson Counties, Texas. These cores contain evidence of fluid-related diagenetic processes as

well as fracturing. Petrographic and geochemical analysis ($^{87}Sr/^{86}Sr$ and C and O isotopes) were used to test for alteration by external or internal fluids, construct a general paragenesis for the cements, and determine the origin of the diagenetic features. Paleomagnetic and rock magnetic studies were used to identify chemical magnetizations and determine the absolute timing of the events.

2.2 Geologic Setting

The Barnett Shale was the first of now over thirty identified and potentially economically viable shale resource plays in the continental United States (Jarvie, 2009). Many of these are Mississippian or Devonian age rocks found in major foreland basins associated with the Appalachian-Ouachita orogenic belt (Thomas, 1993). The shale acts as both source and reservoir rock for production of natural gas. Since its first economic production as an unconventional target for natural gas drilling in the 1990's, the Newark East-Barnett Shale field has become the second largest natural gas field in the United States (EIA, 2008).

The Barnett Shale occurs in the subsurface of northern, central and western Texas, and in outcrop in the Llano Uplift region of central Texas. The productive shale gas play is centered near the city of Fort Worth in the Fort Worth Basin (Figure 2-2).

The Barnett Shale is Mississippian (Chesterian) in age and consists of silica- and carbonate-rich mudstones that first began forming in a pre-orogenic drowned platform basin in advance of the Ouachita orogenesis. The Barnett shale is thickest near the Muenster Arch (over 350m) and thins to less than 35m over the Bend Arch and at the Llano Uplift (Pollastro et al., 2003; Jarvie et al., 2007); (Figure 2-2). The shale is in the thermal maturity window for hydrocarbon generation in all or part of 14 counties, with the most prolific areas located along the basin's 320+ km frontage with the Ouachita fold-thrust system and the Muenster Arch tectonic uplift (Zhao et. al., 2007; Jarvie et al., 2007; Bowker, 2007).

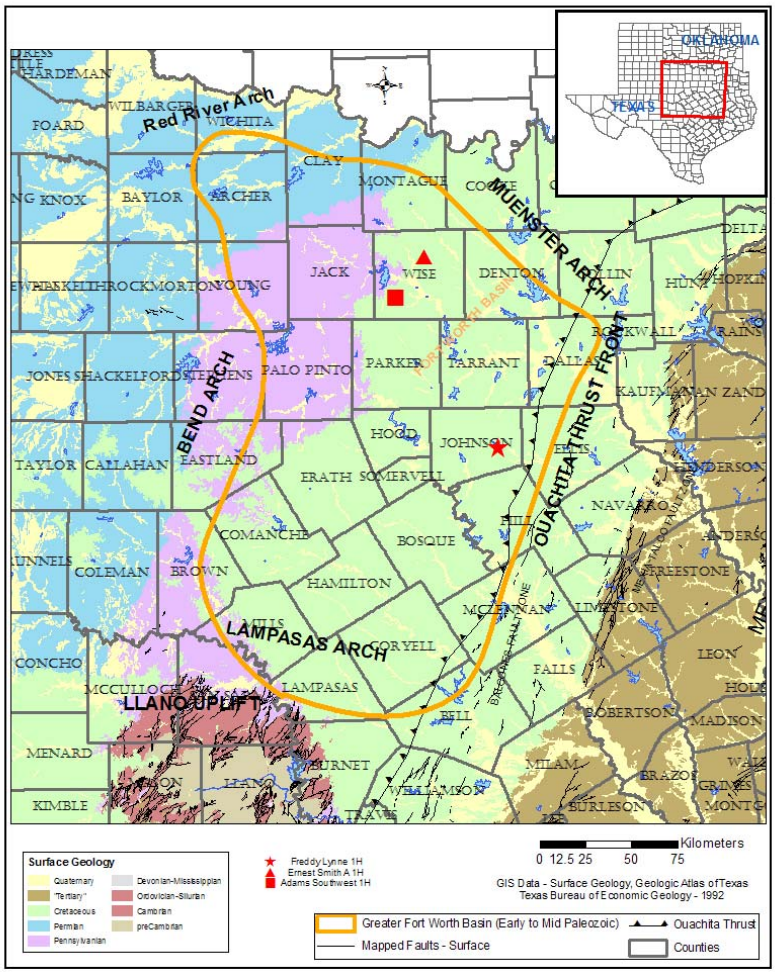

Figure 2-2. Well core locations in the Fort Worth Basin study area. Dark line shows the outline of the greater Fort Worth Basin. Inset map shows Texas counties and location of the Fort Worth Basin. The location of cored wells are shown by the symbols.

The modern Fort Worth Basin began forming in late Mississippian time prior to the initiation of deformation associated with the Ouachita fold-thrust belt (Meckel, 1992). The basin is constrained to the north by the pre-Ouachita Muenster Arch and Red River uplifts which are tectonically adjacent to the Southern Oklahoma aulacogen (Thomas, 1993). Paleozoic rocks of the southern Fort Worth Basin onlap the Bend arch to the west where they change to carbonates. The Barnett Shale thins over the Lampasas - Concho arches to the south (Turner, 1957).

The Muenster Arch appears to have exerted an important early control on the deposition of the Barnett Shale. The early Paleozoic uplift is located near the edge of the southeastern margin of the southern Oklahoma aulacogen. Major basement reverse faults (Flawn, 1961; Henry, 1982) associated with the aulacogen were reactivated as zones of weakness during the Ouachita orogeny. Some workers have suggested that reactivation of these old faults during early Mississippian time (Johnson et al., 1988; Hale-Erlich and Coleman, 1993; Erlich and Coleman, 2005) caused the creation of a northwesterly oriented sub-basin parallel to the Muenster Arch prior to development of the Ouachita fold-thrust belt. This was the Barnett Shale depositional basin.

Many regional faults in the basin have a northeasterly orientation, typically downthrown to the north and west, although some basement faults have a northwesterly

trend (downthrown to the north and east). With initiation of downdropping of the foreland basin along the Ouachita fold-thrust belt in the early to middle Pennsylvanian, subsidence occurred and deposition of the Pennsylvanian clastic molasse commenced. Changes in stress direction (anisotropy of horizontal stress) and rate of orogeny produced complex changes in fault and fracture (joint) character as the Ouachita front-evolved as suggested by Erlich and Coleman (2005) and Pollastro et al., (2007).

Stratigraphically, the region contains Pre-Cambrian to late Cretaceous rocks (Figure 2-3). Cambro-Ordovician rocks overlie Precambrian granite and diorite basement igneous rocks (Pollastro et al., 2007), and may incorporate meta-sedimentary complexes from the Ouachita thrust belt (Montgomery, 2005). The Cambrian Riley Formation sandstones and Wilburn (Hickory) Formation shales and carbonates unconformably cap the basement rocks. These formations underlie the thick Ellenburger Group dolomites, limestones and sandstones, which formed on a carbonate shelf during late Cambrian through early Ordovician time (Adams, 1954). A period of exposure and erosion in the mid-Ordovician created extensive karsting of the Ellenburger carbonates (Flippin, 1964).

Following this period of erosion, the mid-Ordovician Simpson Group and Late Ordovician Viola Group shales and limestones were deposited over the Ellenburger

unconformity. The Ordovician Simpson/ Viola Groups and the Silurian-Devonian deposits were truncated by a pre-Mississippian period of subaerial exposure. Today the Viola/Simpson is limited to subcrop in the eastern and northern portions of the Fort Worth Basin (Figure 2-4).

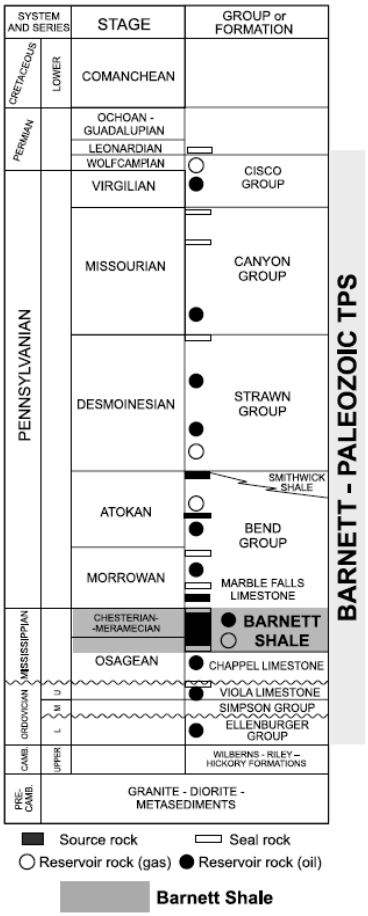

Figure 2-3. Generalized stratigraphic column for the Fort Worth Basin, from Pollastro (2003).

The Barnett Shale is informally subdivided into the upper and lower Barnett Shale within the Fort Worth Basin (Pollastro et al., 2007). The Forestburg Lime is a muddy limestone that serves to stratigraphically divide the Upper and Lower Barnett in northestern portions of the basin. The original productive area is the region where Viola Limestone subcrops beneath the Barnett Shale. Other intraformational carbonates or carbonate washes are found on the northern and northeastern portions of the basin, some of which may originate from the Muenster arch platform (Bowker, 2003). To the south of Fort Worth, the Barnett Shale is a carbonate-poor unit. Barnett-equivalent Chappel limestones (Mississippian Limes) occur in the shallower western portions of the basin (Pollastro, 2003; 2007; Bowker, 2003).

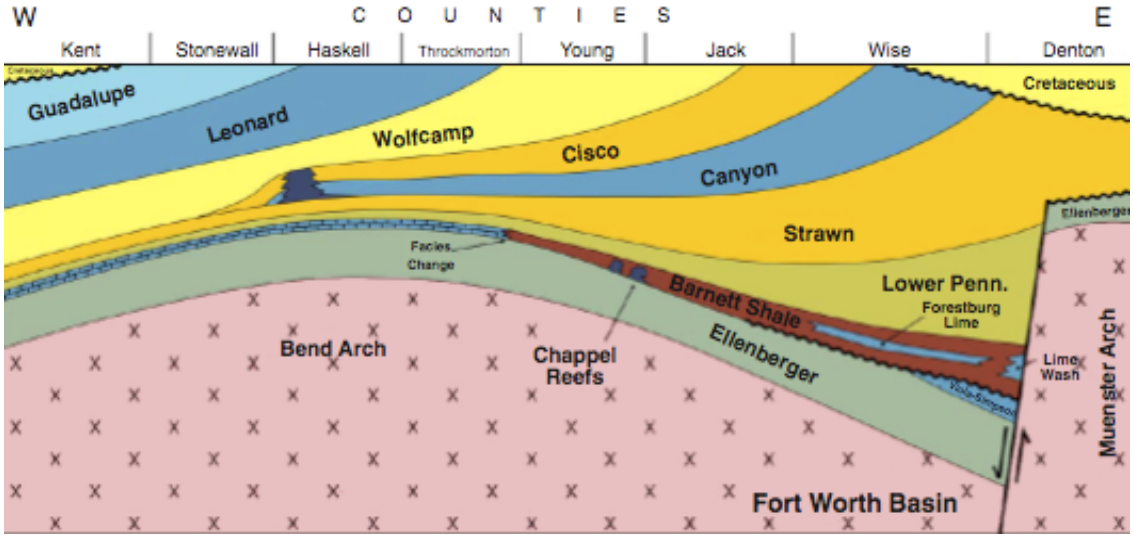

Figure 2-4. Idealized cross section from west to east across the Fort Worth Basin. From Jarvie (2004). Note the thickening of the Barnett toward the Muenster Arch, with the axis of deposition parallel to the arch and normal to the axis of Ouachita folding.

2.3 Previous Work

2.3.1 Barnett Shale Studies

The Barnett Shale is composed primarily of dark, organic- and silica- to carbonate-rich mudstones. The Barnett Shale has been the subject of intensive research in the last decade. Much of the work has been focused on lithofacies and characterization of the shale mineralogy, fabrics, and fracture behavior. Detailed descriptions of the lithofacies are provided by Jarvie et al.(2004, 2007), Papazis (2005), Montgomery at al. (2005), Hickey and Henk (2007), Loucks and Ruppel (2007, 2009), Milliken (2007), Singh et al. (2007), Hill et al. (2007), and Loucks et al. (2009). The formation is very heterogeneous despite its uniform appearance. Silica-rich organic (black) mudstone is commonly interbedded with carbonate-rich, pyritic, and phosphatic mudstone. Overall, the Barnett is variably argillaceous with 15-40% clay-sized minerals. Carbonate content is highly variable, and silica is abundant in some zones in the Barnett as both very fine quartz silt and as siliceous cements. Carbonate is derived

from depositional settings as well as diagenetic reworking. The silica is interpreted to be sourced from detrital and biogenic sources, with most silica volume derived from biological debris (Schieber et al., 2000; Papazis, 2005; Loucks and Ruppel, 2007; Milliken, 2007). Silica cements are widely distributed at very fine scales and in fracture cements suggesting that remobilization and re-precipitation of silica occurred during burial diagenesis. Silica diagenesis may have been a major factor in decreasing the porosity and permeability of the mudstones and siltstones during burial (Schieber et al., 2000). Petrophysical measurements of bulk shale mineralogy are presented by Karastathis (2007) and are related to petrophysical behaviors in Sagar (2009).

Most prior studies on the diagenesis of shales focused on relatively early diagenetic processes, e.g., the nature and source of silica cements, the nature and modification of rock fabrics, preservation of organics, and nature and origin of carbonate concretions. Few studies have addressed issues related to the extent and timing of internally and externally derived fluid alteration in the Barnett Shale.

Veins and vertical to sub-vertical fractures are present in the Barnett Shale (Papazis, 2005; Gale et al., 2007). Most fractures in the Barnett Shale are healed with multiple generations of calcite cement although silica, barite, sphalerite and pyrite have also been described (Papazis (2005). Several workers (Bowker, 2003; 2007; Pollastro et

al., 2007) discuss externally derived fluids as a potential source of Barnett shale variability in terms of maturity and productive behavior. Pollastro et al. (2007) provided the aforementioned synopsis of vitrinite reflectance data showing enhanced zones of thermal maturity near known fault systems, and in other parts of the basin (Figure 2-1). Such faults can be identified in the Fort Worth Basin from seismic data such as in (Figure 2-4). Pollastro et al. (2007) proposed that "hydrothermal" fluids, which were sourced from the basement and moved along faults and fractures, were the cause of this alteration.

Fractures have been shown by various studies to be potential conduits for fluids in shales with very low matrix permeability (e.g. Neuzil, 1994). Excess fluid pressures trapped by the low permeability shales can aid nucleation and growth of faults and fractures (Hubbert and Ruby, 1959), the orientation of which is driven by tectonic stress and compaction (Jones and Addis, 1984). Cyclic buildup and expulsion of fluids causes periods of time in which the shale's overall permeability to fluids increases and decreases (Bolton and Maltman, 1998). Bethke (1985) and Bethke and Marshak (1992) as well as others have made the case that external fluids, as well as internal fluids, would have been migrating through the basin during basin formation. Expulsion of internal fluids could potentially open up new permeable pathways for external fluids.

Externally derived fluids may have different chemistry and temperatures compared to internal fluids, and, therefore, result in geochemical imbalances, which resulted in dissolution and cementation of fractures and matrix in the shales (Hanor, 2001).

Regional fluid events that could apply to the Fort Worth Basin have been proposed in a number of tectonically derived basin flow models. Garvin (1995) proposed a gravity flow model in which meteoric recharge and gravity feed from highlands caused fluid migration events in paleoaquifers and through faults and fractures. An alternative hypothesis, proposed by Oliver (1986, 1992), is that tectonic thrusting causes the expulsion of fluids ('squeegee' model). These warm fluids, if charged with minerals, could alter rock, precipitate ore deposits (Oliver, 1986), cause potassium alteration (e.g., Hearn and Sutter, 1985; Hay et al., 1988), alters coal at high temperatures (Daniels et al., 1990), trap hot fluids in fluid inclusions (e.g., Leach and Rowan, 1986; Dorobek, 1989), and pool oil (Oliver, 1986).

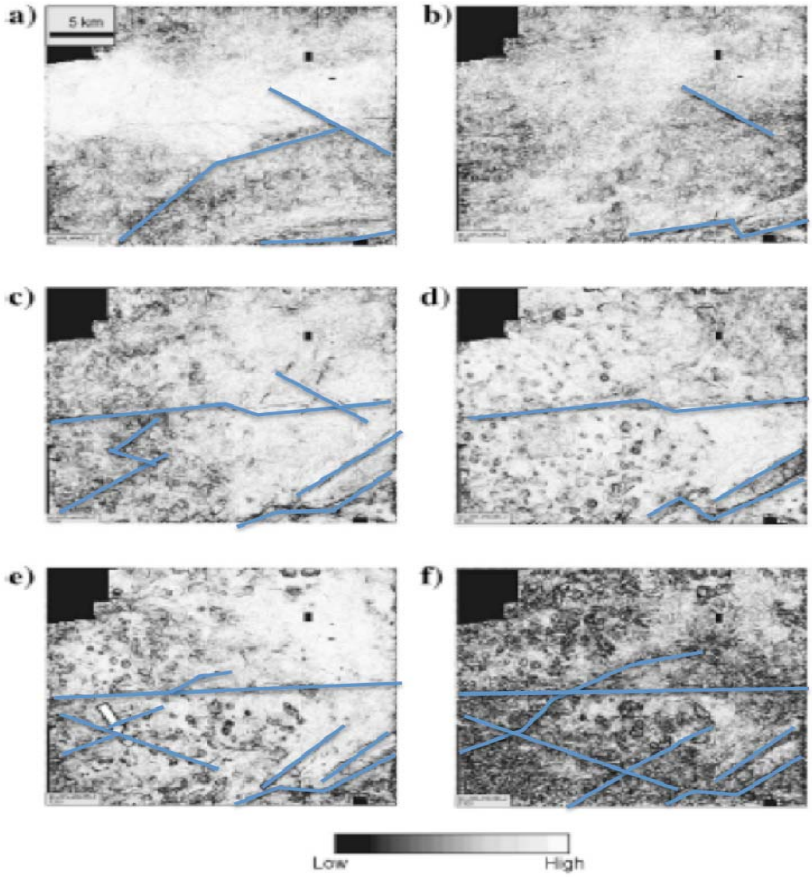

Figure 2-5. Time slice images through a 3D seismic coherency volume in southwestern Wise County. At a) 0.8 s, _b) 0.9 s(top Pennsylvanian-Atokan (Caddo lime), c) 1.0 s, d) 1.1 s (Pennsylvanian-Morrowan Marble Falls lime), e) 1.2 s (top Ellenburger), and f) 1.3 s(base Ellenburger). The analysis window is ±10 ms and 9 traces. White arrow in e) indicates location of the ASW core. Linear features are faults or tectonic structures; circular or semi-circular features are interpreted as paleokarsts or late paleokarst-related collapse structures. Modified from Sullivan et al. (2006). High-low refers to level of seismic coherence. Wrench fault present in SE corner of E), indicative of strike-slip and compressional fault motion.

2.3.2 Paleomagnetism of Related Units

There have been no previous paleomagnetic studies of the Barnett Shale. A regional paleomagnetic study was conducted on the underlying Ellenburger carbonate outcrops in central Texas and in the Franklin Mountains in west Texas (Haubold, 1999). Haubold (1999) determined that diagenetic alteration of the rocks during burial created authigenic magnetite. The study found a correlation between magnetization intensity, directions, and lithofacies suggesting a permeability control on remagnetization by migrating fluids (Haubold, 1999). The study also found that the amount of magnetization in the Ordovician rocks decreased with distance from the Ouachita thrust in a manner consistent with an orogenic fluid event (e.g., Bethke and Marshak, 1990) as the agent of remagnetization. Other studies have reported that rocks in Oklahoma and Texas were remagnetized during the Ouachita orogeny (e.g., Elmore et al., 1993, Elmore et al., 1993, Elmore et al., 1998; Elmore, 2001; Lu et al., 1990).

2.4 Methods

2.4.1 Core Selection

This study utilizes five conventional, oriented well cores retrieved by drill stem coring tools at modern reservoir pressure and temperature conditions. Cores were oriented by standard industry down-hole magnetic survey and scribe methods (Nelson et al., 1987). The core locations range from the northwestern portion of the basin (Wise County, TX) to the eastern portion of the basin (Johnson Co., TX) near to the Ouachita thrust (Figure 2-1). The Wise County cores were the Devon Adams Southwest 7 and Ernest Smith A 1. In Johnson County, cores from three wells, the Devon Freddy Lynn 1H, and Devon Spencer Trussel 1 were combined so a complete section of the Barnett Shale could be sampled. These cores will be referred to together as the South Core (SC).

The well cores in this study were chosen to represent a number of Barnett Shale tectonic, stratigraphic and structural characteristics. The Devon Adams Southwest #7 well (ASW) is roughly equidistant from the Muenster Arch and Ouachita thrust. It contains a 250' foot (92 m) Barnett section (upper and lower Barnett) over previously identified karst breccias and fractured dolomite in the Ellenburger carbonates (Papazis, 2005; Loucks and Ruppel, 2007). The core contains two Ordovician unconformities

(which merge elsewhere to form a regional Ordovician Unconformity) and a relict Viola Limestone (Loucks and Ruppel, 2007). Pollastro et al. (2007) identifies a nearby major through-going fault, the Mineral Wells Fault, to the 5km south of the well location.

A second well is the Devon Ernest Smith A #1 (ES) which is located in north central Wise County approximately 20 miles from the ASW. The Barnett Shale in ES is closer to the Muenster Arch than the ASW, and lacks significant evidence of nearby regional faulting or karsting prior to or during Barnett deposition.

The third 'core' is the Devon "South Core" (SC) which, as mentioned previously, consists of three partial cores within the a 1 km^2 area in Johnson County. These cores are located approximately 70 miles southeast of the ASW well. This location is proximal to the front of the Ouachita thrust belt and is distal to the Muenster arch. The core is also the most proximal to the Llano Uplift of all cores sampled.

The cores were analyzed with particular emphasis on recognizing diagenetic features. Previous descriptions of the ASW core (e.g., Loucks and Ruppel, 2007; Singh, 2008) provided a basis for lithofacies, and a reconnaissance investigation of the cores was conducted prior to sampling. Samples were chosen from each core to analyze the geochemical and petrographic characteristics of the Barnett Shale and associated

carbonate-rich intervals.

2.4.2 Petrographic and Geochemical Methods

Petrographic analysis was conducted on both small and large format thin sections produced from both paleomagnetic core specimens and from samples specially cut from well core. Care was taken to remove a minimal amount of rock and leave a small "footprint" on the core. A total of 134 thin sections were analyzed and an additional 75 thin sections were reviewed from a previous study by Singh et al. (2008). Transmitted light microscopy was conducted using a Zeiss Axio Imager.Z1 petrographic microscope in order to determine lithology and the diagenetic features. Some carbonate-rich samples were stained with alizarin red and ferrocyanide blue for calcite and iron rich phases. Cathodoluminescence microscopy was conducted using an Olympus BX50 system microscope with a CITL CCL 8800 MK4 stage.

An automated Cameca SX50 electron probe microanalyzer equipped with an integrated energy-dispersive x-ray analyzer was used to investigate the nature of diagenetic minerals in the Barnett matrix and fractures. Backscatter electron imaging (BSEI) was used to image the opaques while energy dispersive x-ray analysis (EDXA) was used for qualitative elemental analysis of the minerals. Scanning electron

microscopy was conducted on select specimens using the scanning electron microscope (ZEISS DSM-960A) operated by the Microbiology Department at the University of Oklahoma. Preparation for scanning electron microscopy consisted of sputter coating broken surfaces with a gold target.

Carbon and oxygen stable isotopes were determined using standardized procedures detailed in previous studies and individual specimens were processed in the stable isotope geochemistry laboratory at the Sarkeys Energy Center, University of Oklahoma. Strontium isotope analysis was performed on representative specimens at the University of Texas-Austin. Twenty samples were processed from carbonate shells and fracture fill in the Barnett Shale. Samples were treated with acetic acid for dolomitic in order to dissolve the dolomite per standard procedure. ASW specimens were processed with a NIST SRM 987 standard mean value of 0.710243 ± 0.000007 (2σ = 0.000019, n = 7). ES and FL specimens were processed at a later time with a NIST SRM 987 standard mean value of 0.710258 ± 0.000012 (2σ = 0.000006, n= 32). Strontium values were normalized relative to NBS 987 = 0.71014. The $^{87}Sr/^{86}Sr$ values were then plotted versus coeval seawater for the Mississippian-Pennsylvanian seawater curve (Denison et al.,1998).

2.4.3 Core Sampling for Paleomagnetic Analysis

Core samples for paleomagnetic and rock magnetic analysis were collected from the five multi-shot magnetic survey oriented and reference scribed 10.16 cm (4 inch) diameter conventional well cores (2/3rds "butt" section only) from the Upper Barnett, Forestburg, and Lower Barnett intervals. The 2.2 cm (0.86 inch) diameter cores were cut with a fixed, variable-speed and water-cooled drill press with a non-magnetic core bit located at the Oklahoma Petroleum Information Center Core Facility, Oklahoma Geological Survey, Norman, Oklahoma. The cores were collected every 1-15 feet. In addition, multiple cores were also collected from lithofacies and near mineralized fractures. Most cores were sampled normal to the corrected tool-face azimuth (corrected true north) as calculated from the reference and scribe data. Since measured wellbore inclinations are small (between one and three degrees from vertical) and beds are near horizontal, this mode of sampling appears to approximate a true "in situ" sample orientation in most intervals.

Orientation of the ES core was an issue because the core was slabbed to maximum bedding dip as opposed to the orientation scribes. Samples were drilled normal to the slab face as opposed to the orientation scribe lines. The cores were therefore reoriented after measurement based on the near term, modern (<780,000 yr)

viscous remanent magnetization (VRM) component as isolated by low temperature demagnetization. This was accomplished using a technique similar to that described in detail by Van Alstine and Butterworth (2002).

One hundred twenty-four specimens were collected from the Barnett Shale in the ASW core. Samples were taken from representative lithofacies and near bedding parallel to non-directional veins and in shelly zones. Cores were collected across, and near to, vertical to sub-vertical healed fractures as well as in unfractured zones. Samples were also collected from the Upper Barnett and Forestburg intervals. Ninety-eight specimens were collected in the ES core. Specimens were taken across a similar spectrum of facies and features as found in the ASW core. Additional specimens were recovered from around the upper Ordovician unconformity where black-light examination revealed an unusual orange-yellow luminescence in one thin layer of altered k-bentonite.

Thirty specimens were collected in the FL core and forty-nine specimens from the Spencer Trussel (ST) core. Thirty-two specimens from the Rose Children's Trust (RCT) core were also collected in the Pennsylvanian shales above the Barnett though this data is not included in paleomagnetic analysis on the Barnett Shale interval.

Data were gathered on fracture orientation from a number of sources, including physical core analysis, core reports, and FMI (formation micro-imager) data. Fracture cements were studied for selected depths via petrographic analysis.

2.4.4 Paleomagnetic Methodology

The core plugs were measured and cut to specimens of standardized length (approximately 2.2 cm) with an ASC Scientific dual blade saw. Specimens were measured to determine bulk and total mass magnetic susceptibilities using a Kappabridge mass magnetic susceptibility meter.

Natural Remanent Magnetizations (NRMs) were measured using a 2G-Enterprises cryogenic magnetometer with DC SQUIDs in the shielded paleomagnetic laboratory at the Sarkeys Energy Center, University of Oklahoma. After the initial measurement of the NRM, selected specimens were cooled in liquid nitrogen by submerging them twice for two hours and returning them to room temperature in a zero field, in order to test for and remove the unstable remanence residing in multi-domain (MD) grains (Dunlop and Argyle, 1991). The NRM was re-measured following each low temperature treatment.

The specimens were then subjected to stepwise thermal demagnetization in 22 steps from 100 to 580°C using an ASC Scientific Thermal Specimen Demagnetizer. Some specimens were initially heated to 680°C in 27 steps to test for remanence in hematite; however, the NRM was removed below 580°C in all specimens. In subsequent analysis the numbers of steps were decreased to 23. Additional steps were added at low temperatures on some runs to help delineate the VRM for sample orientation purposes.

Zijderveld diagrams (Zijderveld, 1967) were examined to determine principal components (Kirsvink, 1980) of the magnetization. Specimens with mean angles of deviation of values less than 15° were included in the calculation of the statistics (Fisher, 1953). In order to investigate the magnetic mineralogy of the samples, isothermal remanent magnetization (IRM) acquisition was performed first by AF demagnetizing samples at 120 mT using a 2G Automated Degaussing System. The specimens were subjected to a 26-step IRM acquisition up to 2500 mT using an ASC Scientific Impulse Magnetometer. The samples were then subjected again to AF demagnetization at 120 mT. LAP-GAP-SAP modeling was conducted on the IRM acquisition data using the IRM-CLG 1.0 software generated by Kruiver et al. (2000) to investigate the characteristics of the magnetic mineral coercivity spectrum.

2.5 Results and Interpretations

2.5.1 Paleomagnetism

The low temperature treatments resulted in the loss of between 0.9 and 19.7% of the NRM on the first cycle and 0 to 4% after the second cycle. Multi-domain magnetite does contribute some portion of the total NRM in some specimens but most of the remanence appears to reside in single domain or pseudo-single domain grains.

Magnetic components were defined from data collected during stepwise thermal demagnetization of the Barnett Shale specimens. Thermal demagnetization removed a component interpreted as a VRM at low temperatures (NRM to 280°C). The VRM resides in unstable grains that acquire the Earth's magnetic field as it changes over time (Tauxe, 2002). In most studies, the VRM is considered magnetic "noise" but in this study it is important because it was used to check the orientation of the core. The VRM preserves an average magnetic field orientation over the last tens to hundreds of thousands of years that is a good approximation of the modern magnetic direction. Multiple demagnetization steps below 300°C allow the VRM to be determined. Some data from specimens was not included in the analysis because the directions were spurious or the specimens had very low intensities (see Appendix).

The characteristic remanent magnetization (ChRM) or high stability component of the rock's magnetization has easterly to southerly declinations and shallow inclinations (Figure 2-6A, B and C). The magnetization decays to the origin by 450°C in most specimens (Figure 2-6A,C), although maximum unblocking temperatures extend up to 480°C in a few specimens. The fact that the ChRM decays below 580°C suggests that it resides in magnetite.

A)

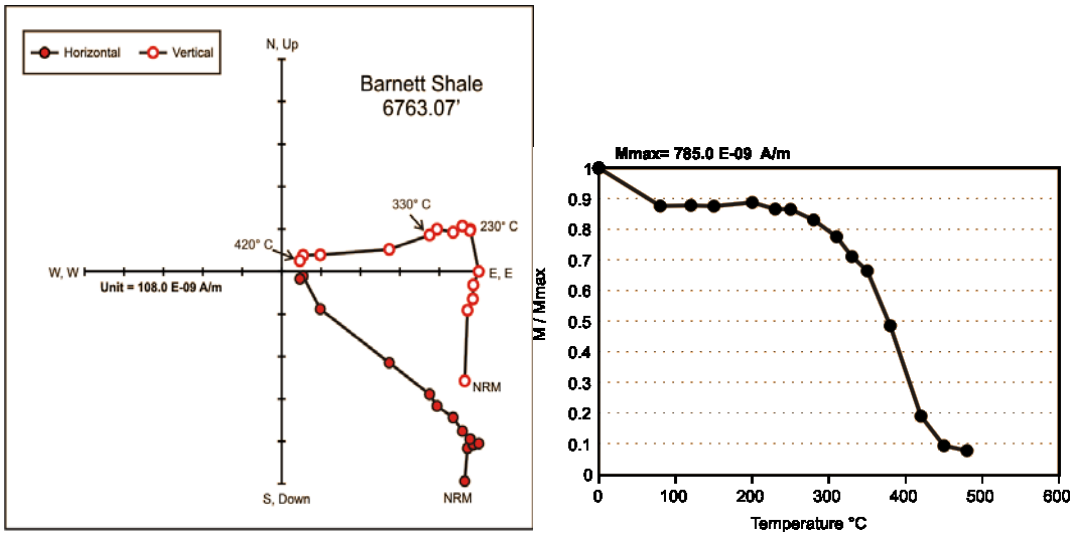

B)

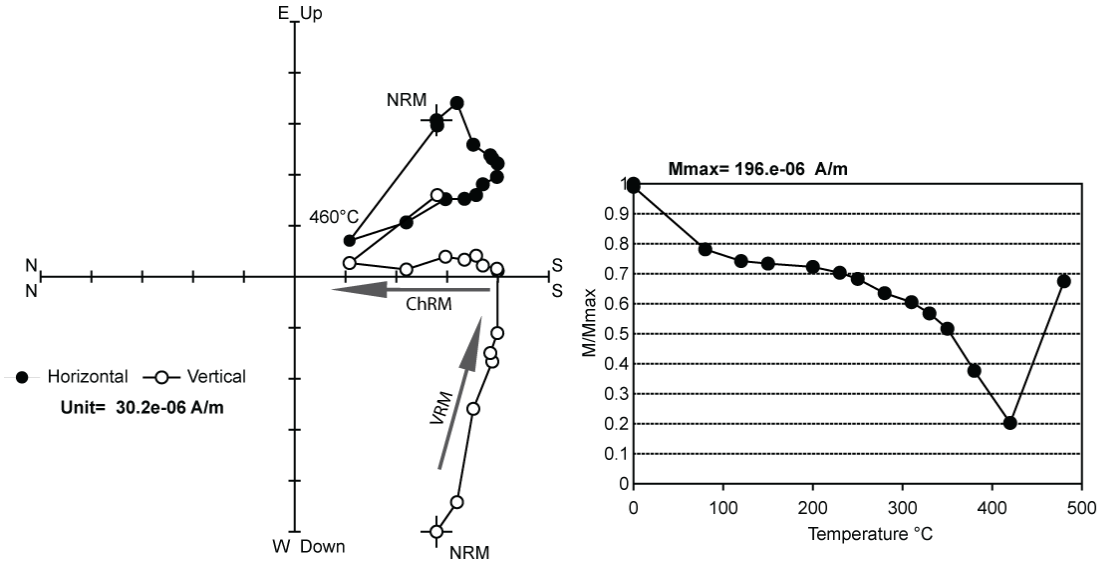

C)

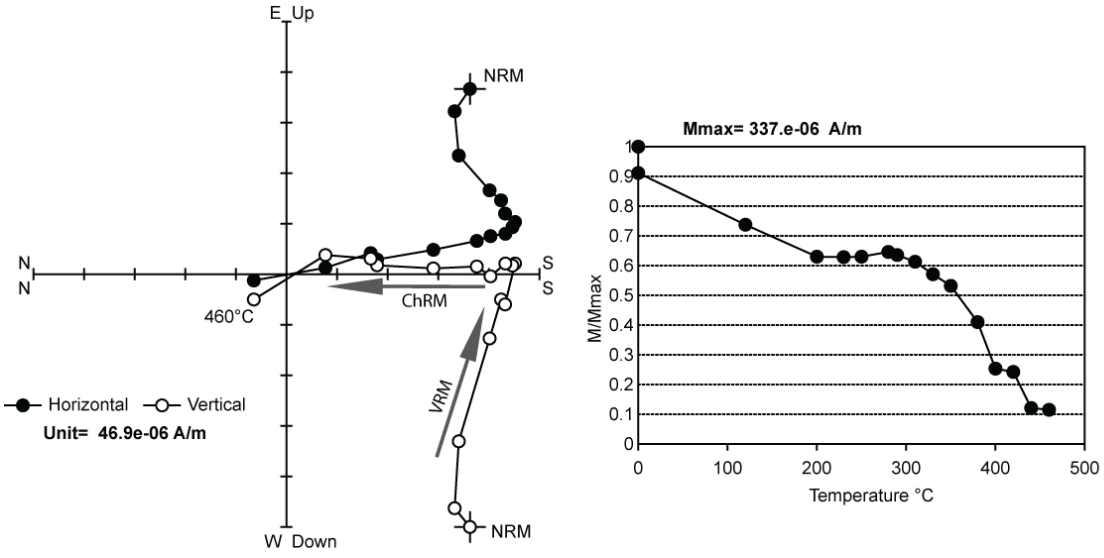

Figure 2-6A-C. Representative Zijderveld diagrams and normalized thermal decay curves for ASW (A,B) and South Core (C).

The ChRMs from the specimens in the ASW and SC cores were oriented using the scribe method and plot with southeasterly to southerly declinations and generally shallow-up inclinations (Figure 2-7A, B). For the ES core, the VRM was used to orient the core yielding similar results (Figure 2-8A, B). The VRM and ChRM were calculated for specimens in the ES core. The VRM declination was "corrected" back to the modern direction and ChRM was corrected based on the VRM correction. Based on this analysis, the paleomagnetic specimen directions from all cores are clearly streaked (Figure 2-7C).

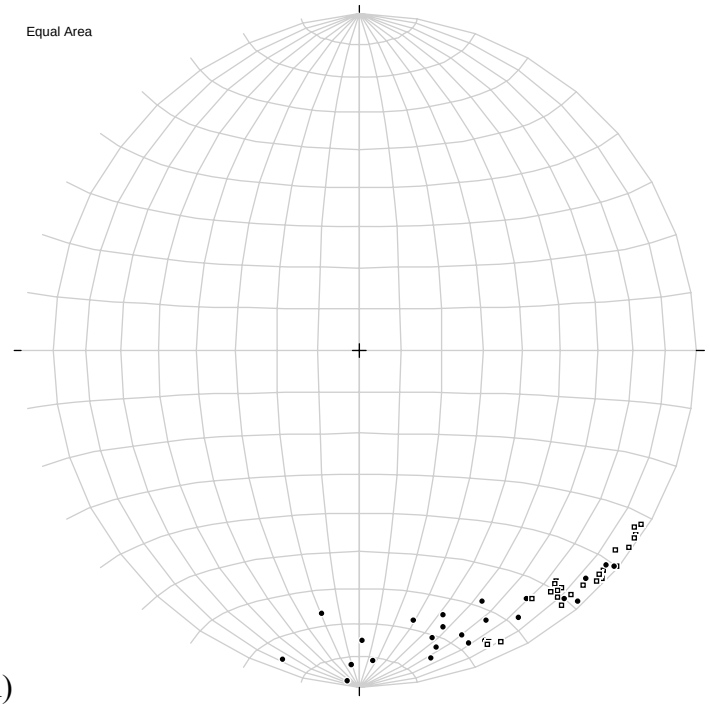

A)

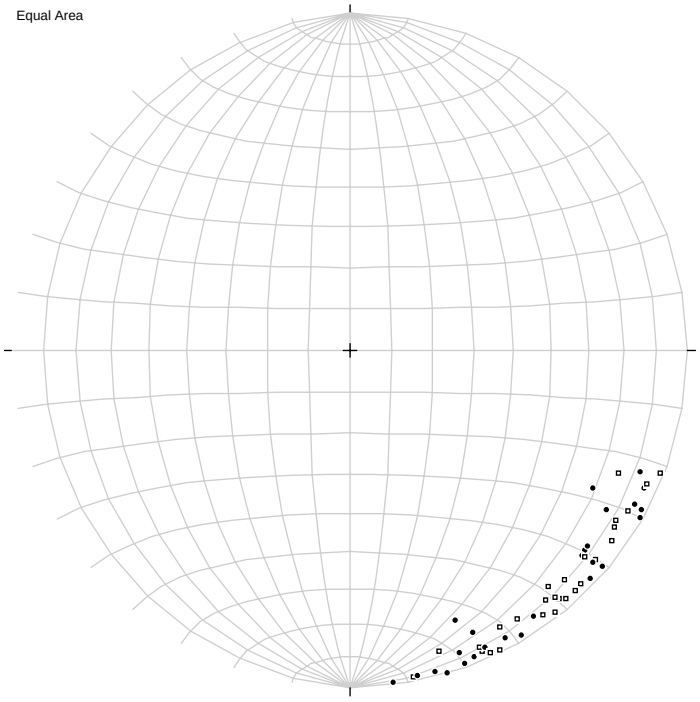

B)

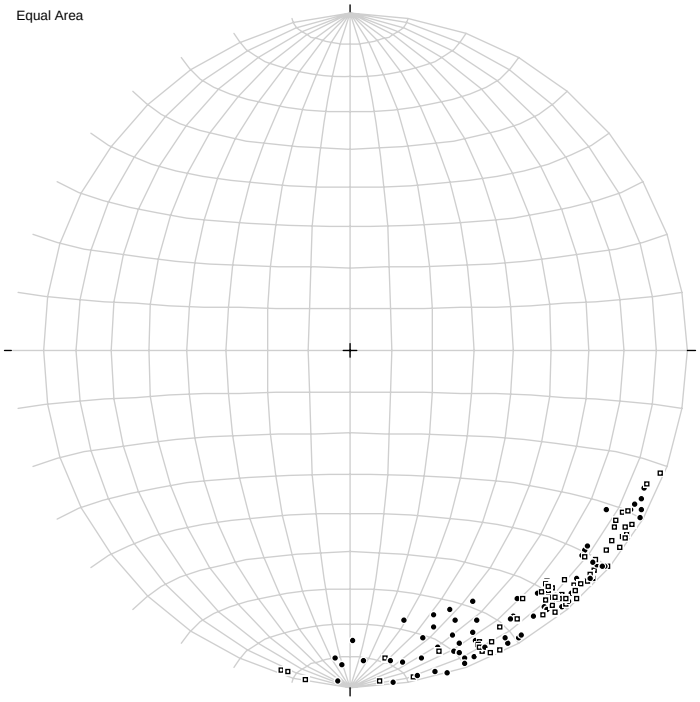

C)

Figure 2-7A-C. Equal area stereonet showing distribution of specimen directions data from the Barnett Shale in each sampled core. A) ASW B) SC C) All Wells. Closed symbols indicate down inclinations; open symbols; up inclinations. Some anomalous points were not used.

The ChRM data were analyzed by specimen directions (Appendix A; Figures 2-7A-C). The origin of the streak of specimen directions is a crucial issue. The streak could be caused by rotation of the cores during the acquisition process that would result in "false" directions. In order to test if the streak is a true representation of the data, the data from the FL core were oriented using the VRM method described for ES core (Figure 2-9A,B). The VRM was "corrected" back to the modern direction and ChRM was corrected based on the VRM correction (Figure 2-9B).

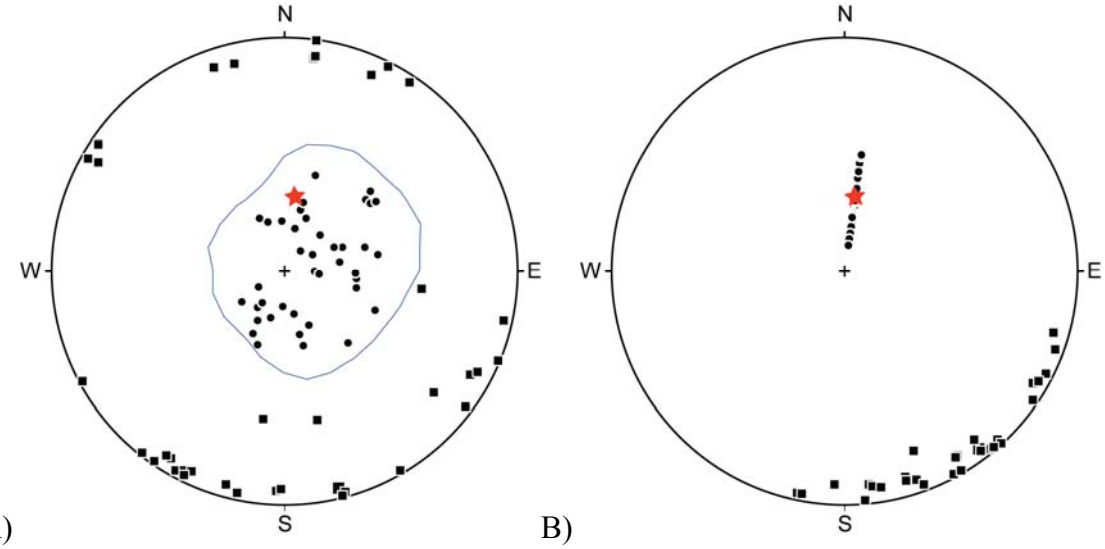

A) B)

Figure 2-8A,B. A) Unoriented, uncorrected specimens from the ES core, with the modern direction indicated by a red star. B) Declination-corrected VRM and ChRM (Black) directions. The line in VRM data shows the remaining variation in uncorrected inclination over the dataset.

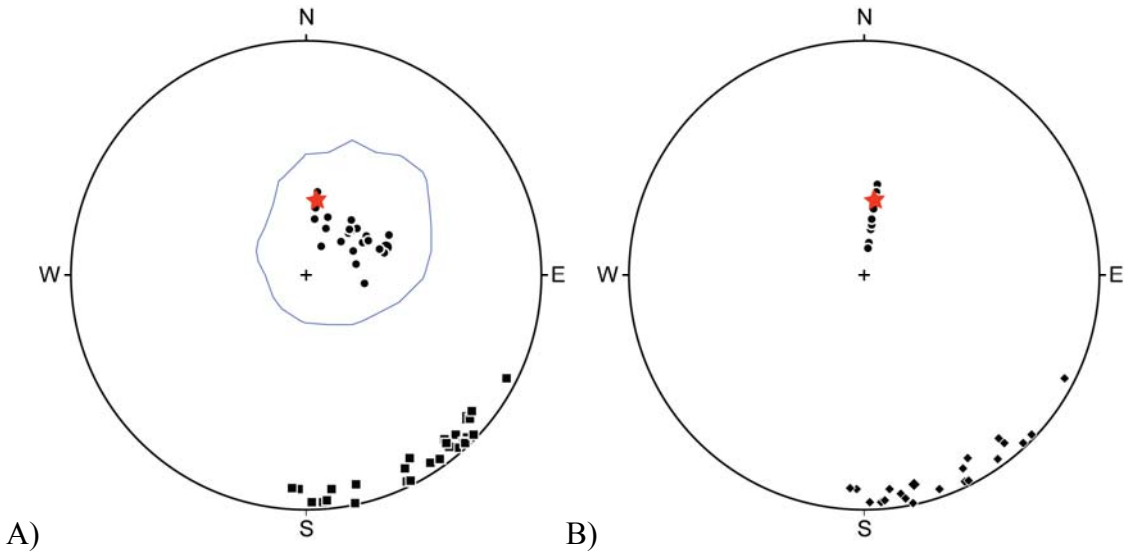

A) B)

Figure 2-9. Comparison of core orientation methods. A) FL data oriented by the scribe method. Red star shows modern magnetic direction. Circles show the Modern VRM. B) FL data oriented by the VRM method. Note rotation of declinations to near the modern direction.

The streak of directions that is produced is similar to the streak produced by orienting the core using the scribe method (Figure 2-9A, B). These results suggest that the streak represents real data and was not caused by core rotation.

The streak of directions, therefore, is interpreted to be real. There are several possible explanations for its origin. Overlapping components that are not resolved during demagnetization could cause a streak of directions but this unlikely because the ChRM displays linear decay on the orthogonal projections. The ChRM is composed,

therefore, of one component. Another possibility is that the streak could represent distinct groups of data that only appear streaked. Initially, as in the study of the Ellenburger carbonates (Dennie, 2010a, Chapter 1), an attempt was made to subdivide the ChRMs using depositional lithofacies and/or gamma ray parasequences (e.g., Singh et al., 2008). Upon subdivision by the facies in the Barnett Shale, the means were poorly grouped. As a result, the approach was abandoned with the interpretation that the thin Barnett lithofacies were too subtle to resolve with a paleomagnetic dataset. The ChRM directions were also compared with depths in the cores but no trends were apparent.

To further explore the streak of directions, the ChRM data in the ASW core was subdivided into groups starting with the easterly directions and moving in 10° declination increments toward the southerly direction (Figure 2-10 and Table 2-1). Each group consisted of 13-27 specimens (Table 2-1). The corresponding virtual geomagnetic pole (VGP) for each group of data was calculated and compared to the apparent polar wander path (APWP). The Barnett Shale poles from all wells plot on a great circle track that starts approximately 20° to the east of the APWP, and crosses the Permian part of the path (Figure 2-11).

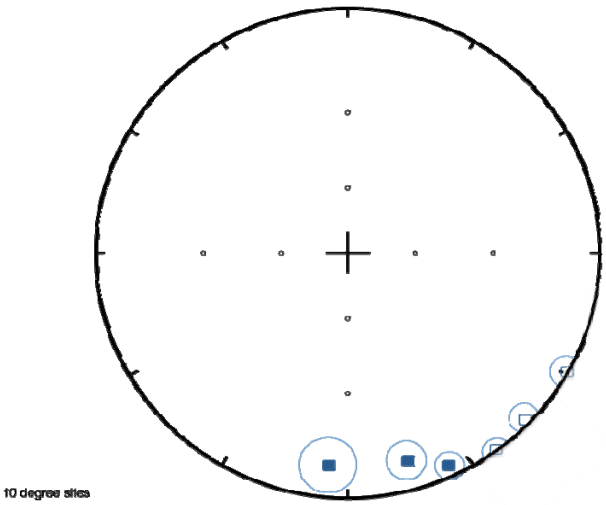

Figure 2-10. Statistical Site means per 10-degree increment, ASW well. Circles show the a95 (cone of 95% confidence) for the site mean directions.

	Site Mean ChRM Directions							Paleo poles		
Site	Dec °	Inc°	a95	k	N	Paleo Latitude	Paleo Longitude	dp	dm	AGE
					spec-imens					
-130	121.2	-0.3	2.5	144.5	23	25.8	154	1.3	2.5	OTP
130-140	135.1	-1.4	2.1	149.1	32	36.9	144.1	1.1	2.1	IP OTP
140-150	143.7	-0.6	3	106.2	22	42.7	135.8	1.5	3	IP-P
150-160	155.9	3.1	3.2	96.7	22	46.6	120.3	1.6	3.2	P
160-170	164.3	7.1	5.4	64.77	12	50.4	107.3	2	3.9	P-T
170-	183.3	7.3	5.4	157.7	6	55.2	81.3	2.7	5.4	T OTP

Table 2-1. 10-degree statistical unit means directional data. OTP = off the path between Pennsylvanian and Ordovician. IP=Pennsylvanian. Permian. T=Triassic.

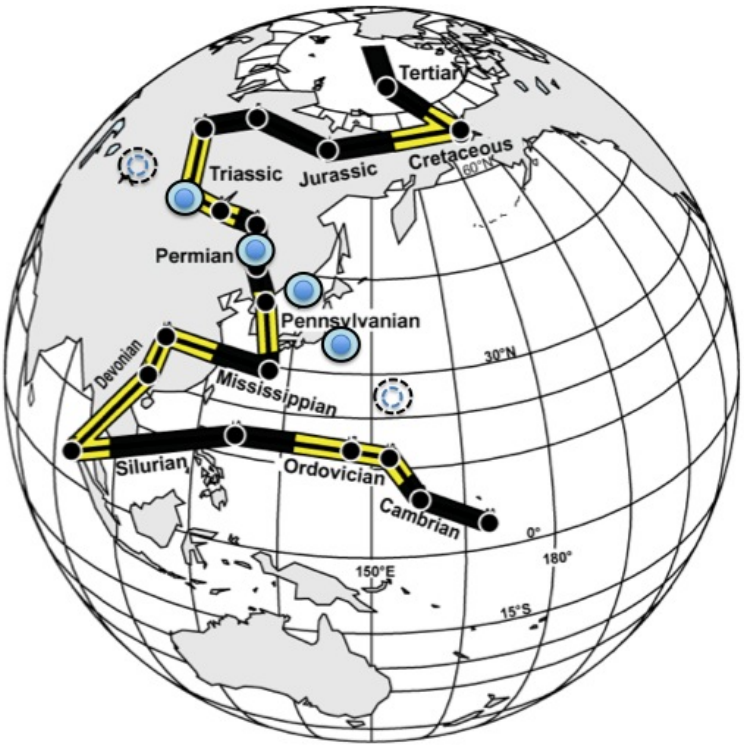

Figure 2-11. Barnett Shale virtual geomagnetic poles (VGP) from the streak of directions in the ASW core are plotted on the apparent polar wander path of Van der Voo (1993). Each pole corresponds to a separate 10-degree statistical site mean (Table 2-1). The two dashed end member groupings include greater than 10-degree statistical means, but are included for completeness.

The fact that the poles for the more easterly directions fall to the east of the path is problematic. The poles for the specimens with more southerly declinations plot on

the Permian-Triassic part of the APWP. A counterclockwise rotation of ~20° after the magnetization (Figure 2-12A) was acquired could account for the easterly pole positions (Figure 2-12B). If the rotation did occur, then the remagnetization would have been acquired in the late-Pennsylvanian to early Permian. This interpretation suggests that during the maximum rate of foreland burial of the basin, horizontal compressive stress may have been changing from a more Muenster Arch-involved stress (N,NE) to a more Ouachita thrust-involved stress (E,SE). The resultant shear may have been manifested via complex basement block motions and rotations today expressed in regional faults with both strike-slip and Compressional features (.

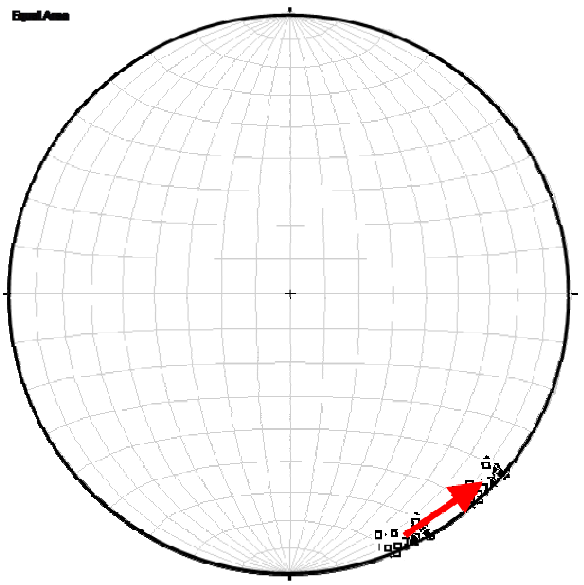

A)

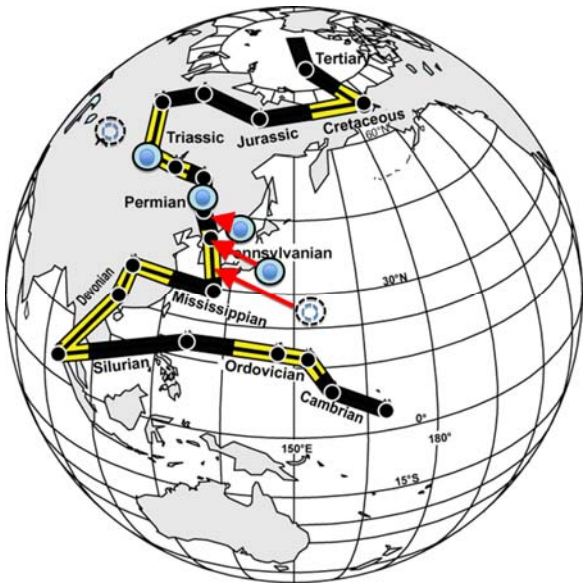

B)

Figure 2-12. Equal area plot (A) and pole plot (B) showing possible tectonic rotations from the streak of data, all wells. A) A counterclockwise rotation of 15-20 degrees results in rotation of the direction to the east. B) Correcting for this possible rotation moves the pole from off the path back to the mid-Pennsylvanian-early Permian part of the APWP.

Magnetic Mineralogy

Magnetic mineralogy can be estimated in part from plots of the acquisition of an imparted magnetic field at increasing applied field strengths. This property is known as the isothermal remanent magnetization (IRM). The maximum IRM (saturation magnetization) of a sample is the sum of the partial magnetic carriers saturation IRM (SIRM) contributions IRM acquisition curves for representative Barnett specimens

commonly reach saturation by about 300-500 mT suggesting the presence of a low coercivity magnetic mineral such as magnetite. A slight rise above 500 mT suggests the presence of a higher coercivity mineral such as hematite. The IRM acquisition curves can be further evaluated by modeling the curves using derivative curves, a process called linear/gradient/standardized acquisition (LAP-GAP-SAP) analysis (e.g., Kruiver et al., 2000).

The results of the LAP-GAP-SAP analysis of the Barnett suggest magnetite is the primary carrier of magnetization in most of the carbonates (Figure 2-13), with potential contributions by pyrrhotite in some samples (Table 2-2). If pyrrhotite does carry some remanence it would be in the same direction as the magnetite component because the Zijderveld diagrams for the specimens only show one component that decays from 280°C to 480°C. The hematite that is present in some specimens is not interpreted to carry a stable remanence.

Base Forestburg – Magnetite Base Lower Barnett – Magnetite/Pyrrhotite

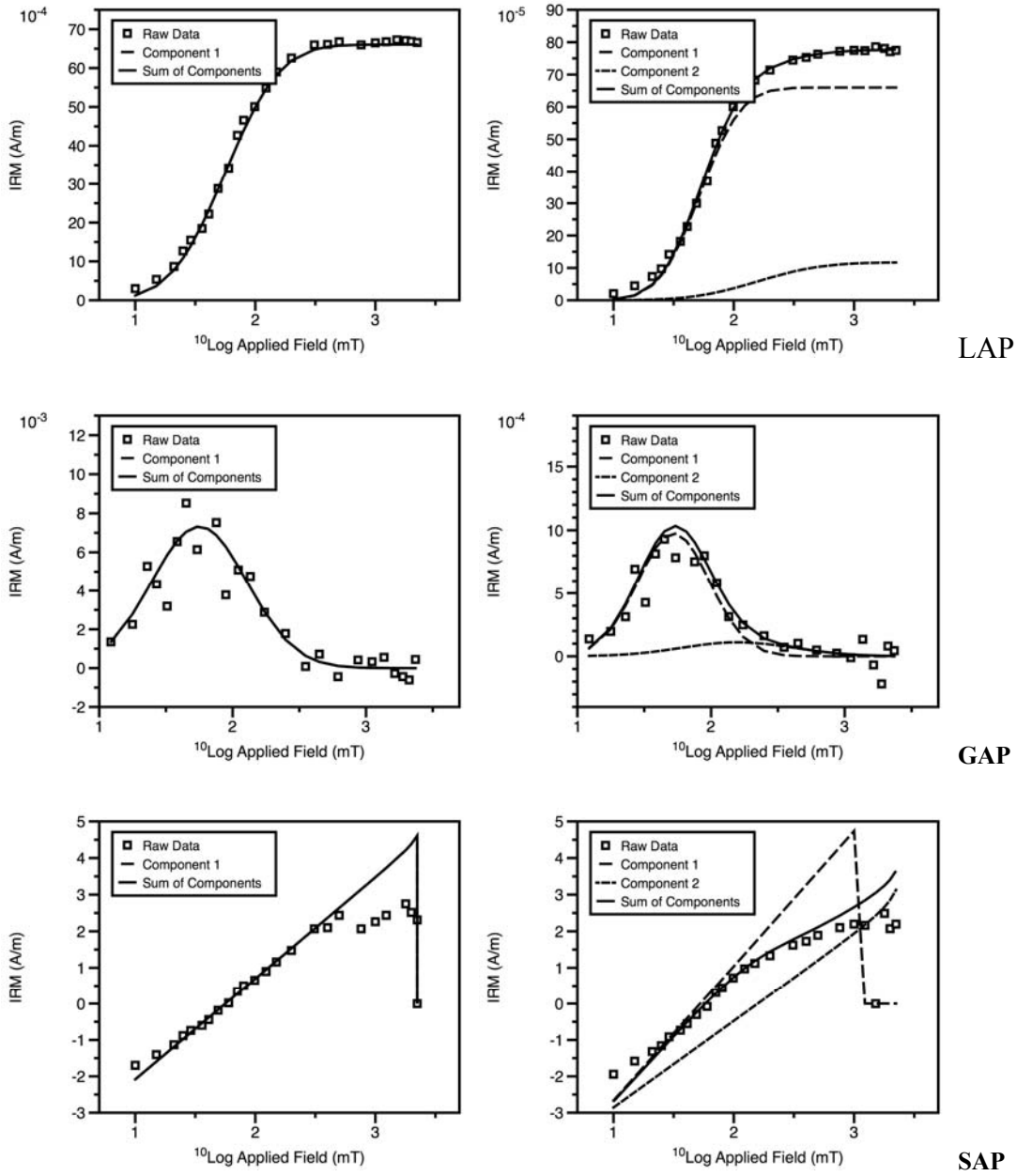

Figure 2- 13. LAP-GAP-SAP acquisition curves for magnetite in ASW .

Sample	Depth	Components	Contribution (Percent)	SIRM (A/M) 10-4	B1/2 (mT)	Magnetic Mineralogy
21802	6418.09	1	100.0	66.10	56.2	Magnetite
60612	6654.12	1	93.6	4.73	50.1	Magnetite
		2	6.4	0.33	398.1	Hematite
71011	6726.1	1	84.9	6.60	52.5	Magnetite
		2	15.1	1.17	158.5	Pyr-Tit-Heme
80922	6782.07	1	81.0	12.80	52.5	Magnetite
		2	19.0	3.01	162.6	Pyr-Tit-Heme

Table 2-2. Magnetic mineralogy from LAP-GAP-SAP analysis, ASW samples.

Bulk and total magnetic susceptibility (MS) data were collected on all three cores, and preliminary data are available from a fourth core (JP) located in Denton County, TX. Susceptibilities range from -5 to 250 (m^2/kg, x10-^{6}). A large peak in susceptibility is seen above a stratigraphic break near ASW 6512', and correlates with a similar increase in the ASW, ES and JP cores (Figure 2-14). The peak is not obvious in the SC core. Other spikes in MS may correlate with zones containing bedding parallel fractures, typically high gamma zones with elevated phosphates. Figure 2-14 compares gamma ray and TOC with MS. There appears to be an inverse relationship between TOC and MS, but a direct relationship with carbonate (low gamma ray).

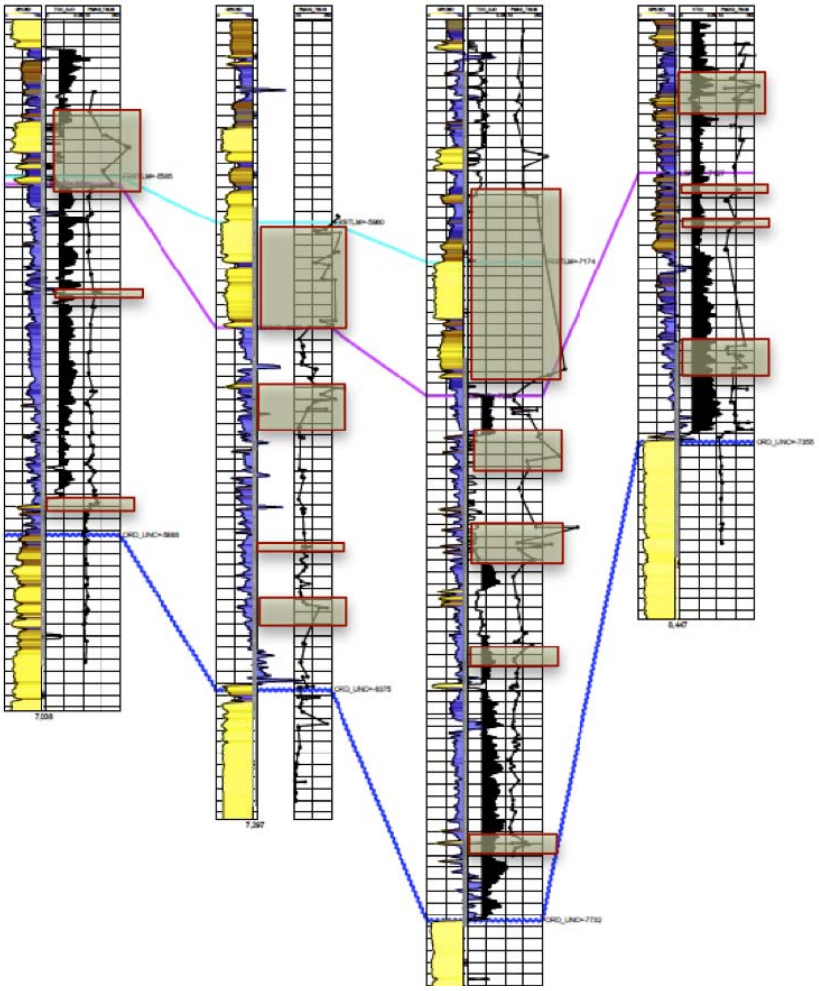

Figure 2-14. Magnetic susceptibility (m^3/kg) from core versus well log data. Gamma ray log with low API (<100)in yellow, high API (>100) values in blue. Total organic content is the center black filled curve. Purple line is base Forestburg Lime; blue line is Ordovician Unconformity. Tan boxes show spikes in magnetic susceptibility; note possible correlation with low TOC intervals. Additional (JP) well, Denton County, Tx. shown for comparison. Vertical scale = 1 tick is 10 feet.

2.5.2 Diagenetic Mineralogy of Barnett Shale

Evidence of post-depositional alteration in the Barnett shale is evident in authigenic minerals found both in the very fine-grained matrix and in cemented fractures. Carbonate minerals are the most common authigenic phases in the Barnett [e.g., Figure 2-15]. These commonly include authigenic calcite, dolomite, siderite and ankerite. Rhodochrosite was also identified in the South Core (SC = FL + ST) in one sample near the Ordovician Unconformity. These minerals are found in fracture fills in the Barnett, and also replace allochems and micrite in the matrix. Inversion and solution-reprecipitation of aragonite to calcite are both common processes observed in the Barnett Shale specimens.

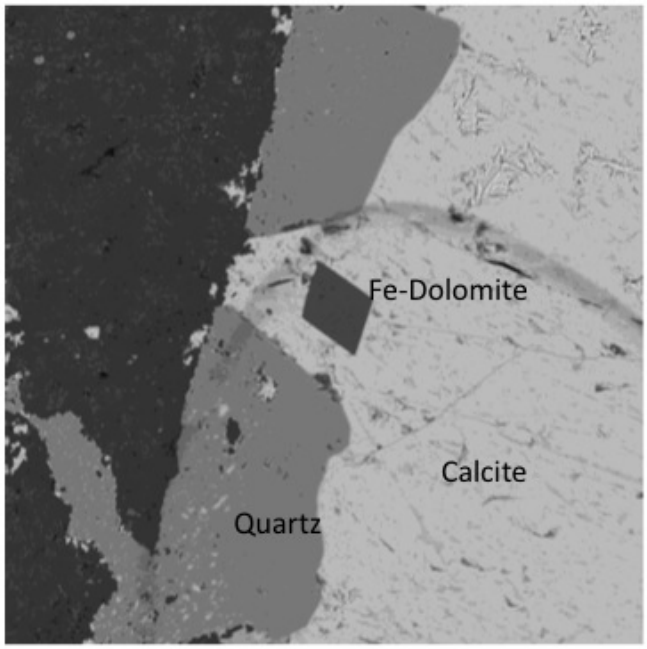

Figure 2-15. Fe-Dolomite rhomb and calcite fracture fill. Note slightly curved face on dolomite; some rhombs in veins display saddle dolomite-like textures. Vein fill is coarse calcite (light grey), quartz (dark grey), dolomite (center dark grey). Matrix is calcite, dolomite, pyrite, clay (mixed I/S, kaolinite) and kerogen.

Another common authigenic mineral in the Barnett Shale is silica. Silica is interpreted to be biologically-derived largely from radiolaria (Schieber, 2001; Milliken, 2005). Sponge spicules are also a source for silica in SC because they are abundant and partially replaced by barite and chlorite. Silica coats clay flakes but is also present as megascopic quartz and chalcedony cements in large aperture veins or fractures. Hydrocarbon inclusions are found in some silica cements [Figure 2-16].

Hydrocarbons occur as liquids, gas and solid residue (pyrobitumen) in the Barnett. This residue is found in the matrix around late fractures suggesting that the fractures were conduits for hydrocarbon-bearing fluids. Hydrocarbons are frequently present as coatings on shell fragments and diagenetic minerals [Figure 2-17].

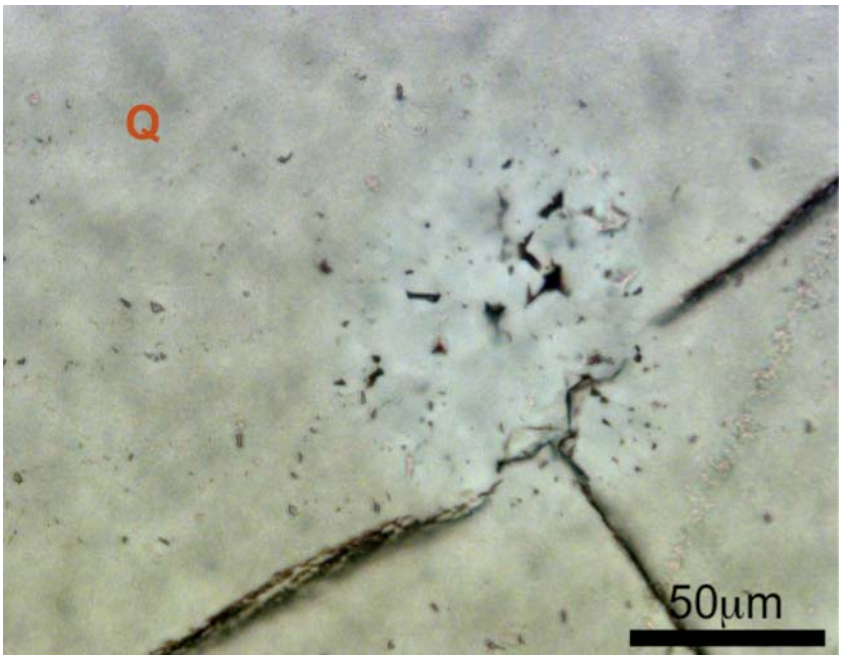

Figure 2-16. Hydrocarbons in fluid inclusions in late quartz cements near ASW 6700 suggest precipitation of the silica during the hydrocarbon generation-migration phase.

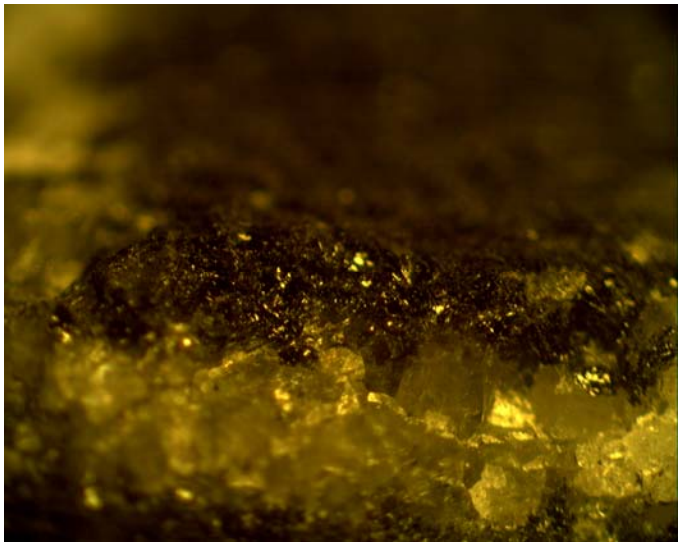

Figure 2-17. ASW 6727. Hand sample photograph of thick, solid pyrobitumen coat on quartz and calcite.

Sulfides are common in the Barnett Shale. Pyrite is by far the most common sulfide, and occurs as both framboidial pyrite, as well as bedded pyrite (Figure 2-18). Fracture- and vein-fill pyrite is euhedral and may have cubic or even trigonal forms. Marcasite is a common pseudomorph of pyrite in some intervals. Sphalerite (Figure 2-18) is the next most common sulfide and commonly occurs with barite in phosphatic intervals and intervals with a high gamma ray response. Trace amounts of chalcopyrite and galena have also been identified in the same intervals.

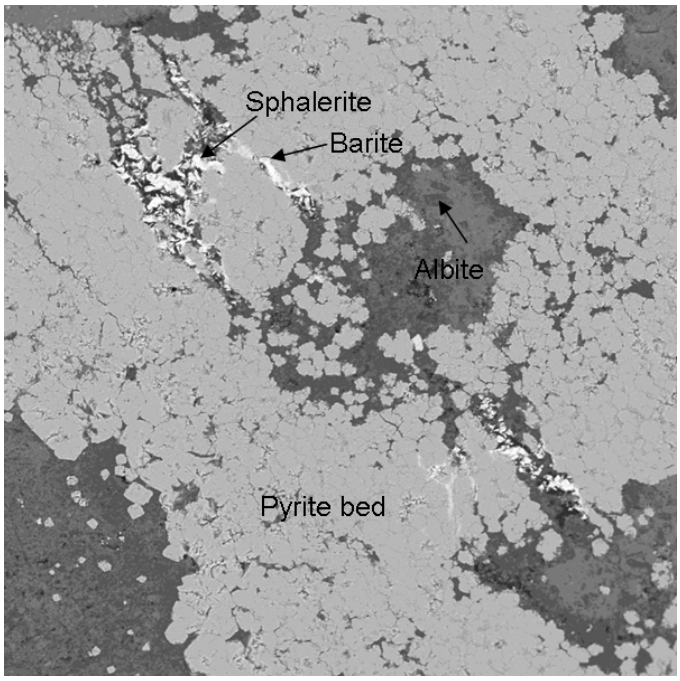

Figure 2-18. ASW 6603. Bedded pyrite with internal fracture, filled with sphalerite and lesser Pb-Cu sulfides, and barite. Dark grey mineral is albite (up to 20% of the rock volume). Image is 395µm x 395µm.

Sulfates are common in some veins and fractures in the Barnett Shale. Barite is the most common sulfate, followed by celestine and anhydrite/gypsum. Barite occurs as a matrix replacive cement and fracture fill, and does not appear to be a "scale" product of drilling. Barite-celestine is most common in sub-vertical or stratiform veins, where it is associated with albite, quartz, pyrite, sphalerite, and calcite. Minor quantities of sulfates are found in a few vertical fractures as well.

Anhydrite is found as a late fracture fill as well as matrix replacement. The anhydrite appears to be natural cement in all samples, although some prior studies have suggested the sulfate can be a product of drilling via oxidation of sulfides in carbonates (e.g., Dean and Ross, 1976). Evidence that the anhydrite is natural cement includes its location in the interior of the cores and that it is cut by younger pyrite and other cements unlikely to form as a scale.

Anhydrite is common near the top of the lower Barnett at the base of the Forestburg in northeasterly reactivated fractures. Anhydrite is commonly associated with a late phase of calcite, euhedral vein-fill pyrite and celestine (Figure 2-19).

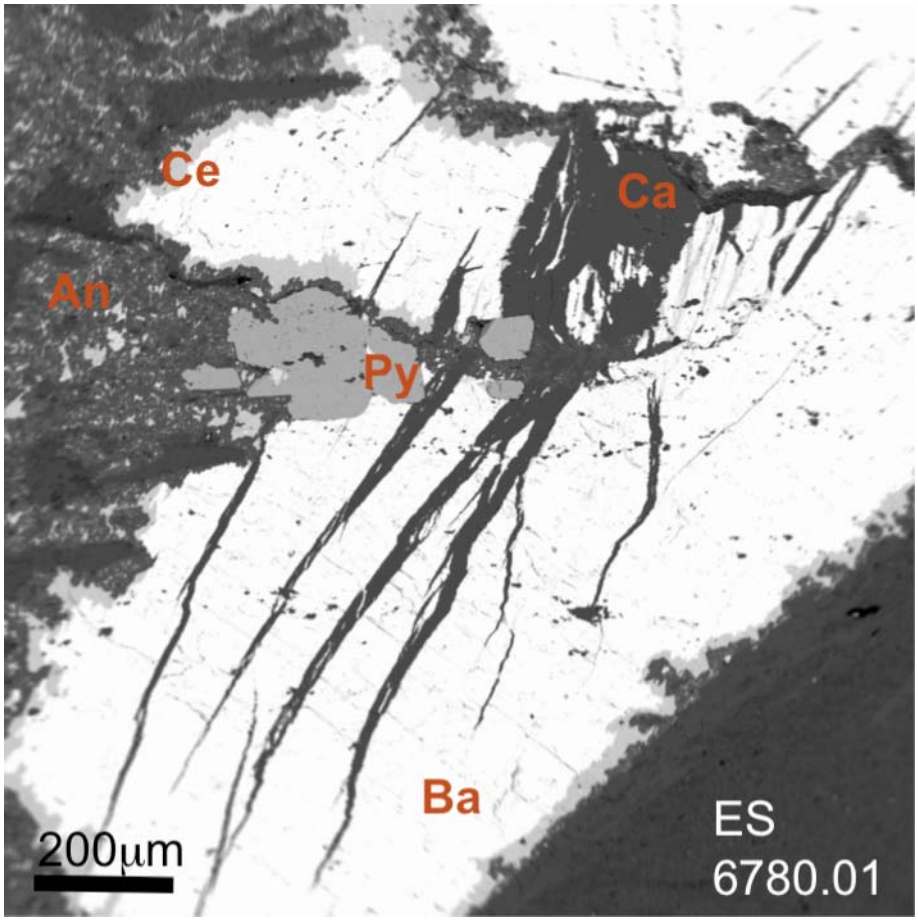

Figure 2-19. Refractured, multi-generational (multiple stage) fracture in the Forestburg Lime of the ES core. Celestine (outer rim) and barite make up the bulk of the vein. Late anhydrite and pyrite crosscut the vein. A late calcite cement "refractures" the barite, celestine and anhydrite along cleavage planes and between the barite and matrix.

Other authigenic minerals are present in carbonate- and phosphate rich intervals and suggest burial or fluid diagenesis of the shales. For example, rare earth element (REE)-enriched (cerium, thorium- and yttrium rich) monazite, as well as authigenic potassium feldspar, albite, titanite, and chromite are found in some localized zones.

Some zones contain abundant phosphate that appears to have been remobilized and precipitated into fractures (Figure 2-20).

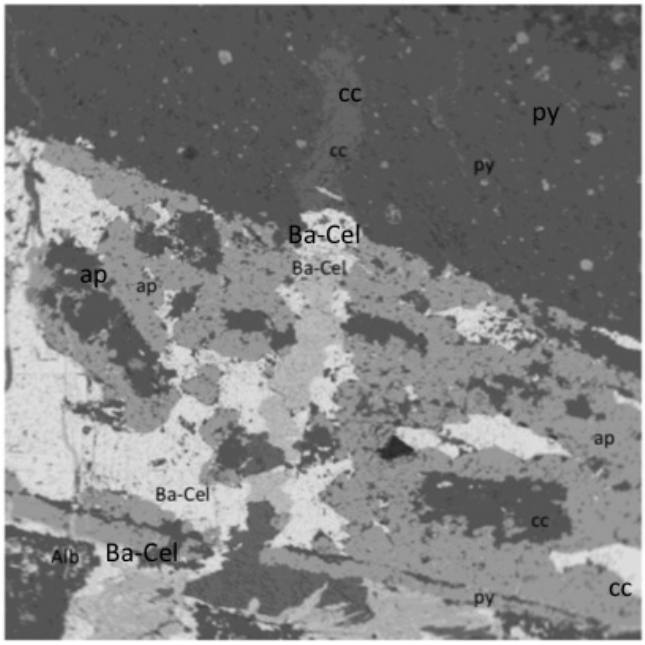

Figure 2-20. Two fractures, one late bearing calcite, barite and celestine with earlier fracture hosting remobilized phosphate. Apatite (ap) with calcite (cc), barite(ba) and celestine(cel). Albite (alb), pyrite (py) and sphalerite are also present. 1365 µm x 1365µm.

2.5.3 Geochemistry

Strontium ($^{87}Sr/^{86}Sr$) isotopic analysis

The $^{87}Sr/^{86}Sr$ ratios were compared to the coeval seawater curve (Denison et al.,1998) to determine if the fluid(s) that precipitated the carbonate and sulfate minerals had radiogenic sources of strontium. The results from multiple cements in fractures indicate a range from near coeval to highly radiogenic values for different parts of the Barnett shale (Figure 2-21). Calcite in the northeasterly sub-vertical fractures that contain low amounts of carbonate or phosphate and are high in TOC and silica contain generally low values (Table 2-3). Carbonate- or phosphate-rich matrix and cements, including those containing substantial sulfate cements, contain radiogenic values of $^{87}Sr/^{86}Sr$, which indicates the influence of externally derived fluids such as orogenic fluids or basement brines. Most barite contains intermediate radiogenic values that suggest it may be remobilized by externally derived fluids. The SC core, which is closest to the Ouachita thrust zone, contains the most elevated $^{87}Sr/^{86}Sr$ values (Table 2-3).

At the base of the Barnett, the (Ordovician) Viola Limestone and lower Barnett (ES71177, FL8140) also contain elevated radiogenic Sr levels in all wells, suggesting the Ordovician unconformity acted as regional fluid conduit for externally derived

fluids. In late refracturing cements such as in the vertical northeasterly fractures bearing calcite, pyrite and anhydrite, Sr is also radiogenic.

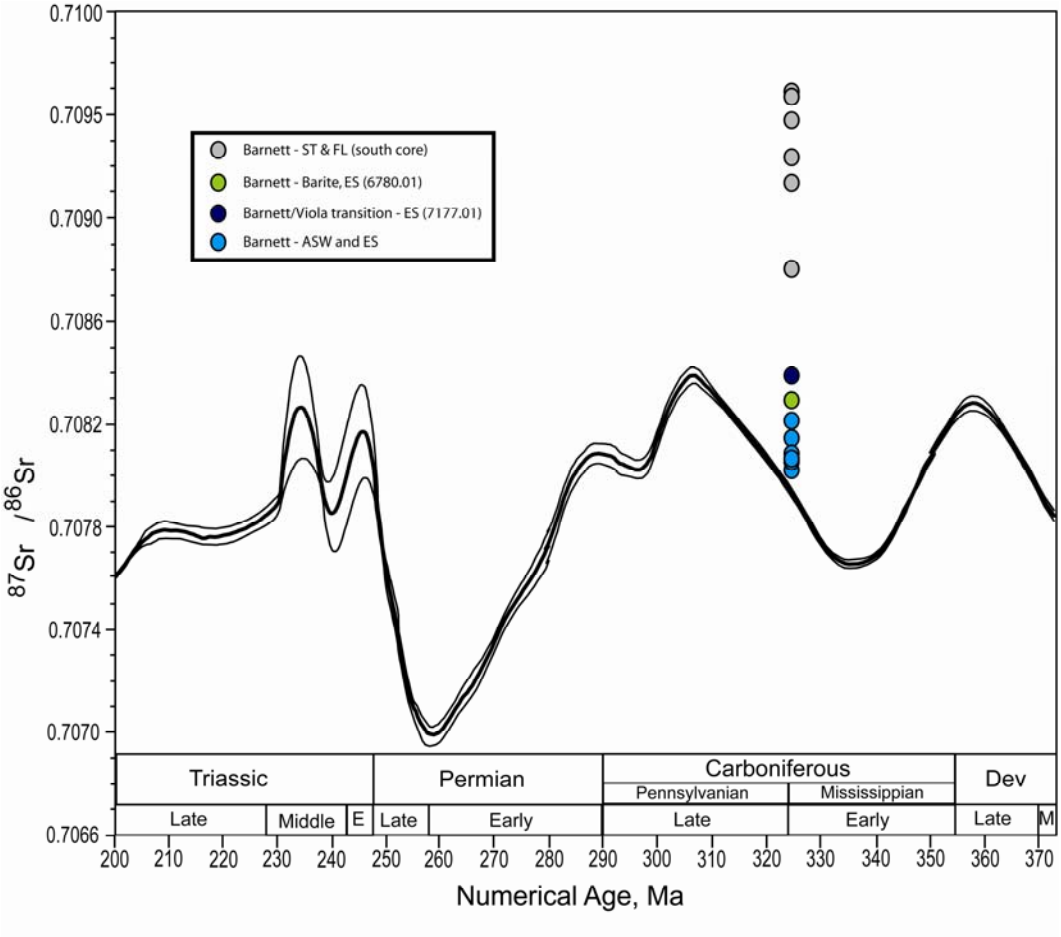

Figure 2-21. $^{87}Sr/^{86}Sr$ ratios for the Barnett shale calcite (Blue), Barite zone (Green), Viola Lime (Dark blue) and South Core (Mississippian and Pennsylvanian shales) (ST,FL, Grey).

Depth	Sr Ratio	N	Description	Radiogenic?	Min	Thrust?	Cement Fill
ASW 6700a-inner	0.70813	0.000006	Bed-parallel vein	Low	Calcite	NO	cc,si,hc
ASW 6700a-outer	0.70812	0.000005	Bed-parallel vein	Low	Calcite	NO	cc,si,hc
ASW 6700b	0.70812	0.000006	NE Sub-vertical Fracture	Low	Calcite	NO	cc,ba,cel
ES 7046.10 B	0.70805	0.000005	NE Sub-vertical Fracture	Low	Calcite	NO	cc,hc
ES 7177.01	0.70843	0.000005	Bed-parallel vein	High - Ord.Unc.	Calcite	NO	cc, monaz
ES 6780.00	0.70834	0.000006	NE Sub-vertical Fracture	Intermediate	Barite	NO	bar,cel,anh
ES 6780.01	0.70834	0.000006	NE Sub-vertical Fracture	Intermediate	Barite	NO	bar,cel,anh
FL 807906 bur	0.70809	0.00001	Bed-parallel vein	Intermediate	Calcite	YES	cc
FL 8138	0.70827	0.000006	NW Vertical	Intermediate	Calcite	YES	cc
FL 8140	0.70914	0.000005	NE Vertical Fracture	High - Ord. Unc.	Calcite	YES	cc
ES 6882.07	0.7081	0.000005	Bed-parallel vein	Low	Calcite	NO	cc
ES 6851.01	0.70809	0.000005	NW Vertical	Low	Calcite	NO	cc
ES 7156.05	0.70819	0.000007	NE Vertical Fracture	Intermediate	Calcite	NO	cc
ST 7766	0.70884	0.000004	Bed-parallel vein	High	Calcite	YES	cc
ST 7754.3	0.70926	0.000006	NE Vertical Fracture	High	Dolo	YES	dm
ST 7805.4	0.70994	0.000005	Matrix	High	Calcite	YES	cc
ST 7757	0.70961	0.000005	NE Sub-vertical Fracture	High	Calcite	YES	cc
Estimated analytical uncertainty (95% confidence):	+- 0.00012			Coeval values - 0.7079-0.7080 (Mc			

Table 2-3. $^{87}Sr/^{86}Sr$ data. Highly radiogenic values of Sr are derived from the cores closest to the Ouachita thrust. Note bed parallel veins generally contain lower values of strontium, and vertical fractures have higher values. (Cc= calcite, bar=barite, cel=celestine, anh=anhydrite, monaz=monazite, dm=dolomite, si=silica, hc=relict hydrocarbons.)

Carbon-Oxygen Stable isotopes

Most samples from the Barnett Shale yield slightly depleted values in both carbon and oxygen stable isotopes (Figure 2-22). In one set of calcite- and quartz-filled fractures near ASW 6700' (Figure 2-23), multiple generations of calcite can be clearly delineated. In the oldest outer vein, light values of $\delta^{13}C$ (-16 to -26 per mil (PDB) are found. The younger inner vein calcite contains less depleted values of $\delta^{13}C$ (+2 to -10 per mil (PDB)). The outer vein cement is interpreted to have incorporated some biogenically fractionated light carbon from organic matter into the calcite lattice. The inner vein cements are interpreted as younger cements unaffected by the early incorporation of organic material. Values for $\delta^{18}O$ observed in the Barnett Shale typically contain near coeval values (Veizer, 1983) to slightly depleted values between -2 and -10 per mil (PDB).

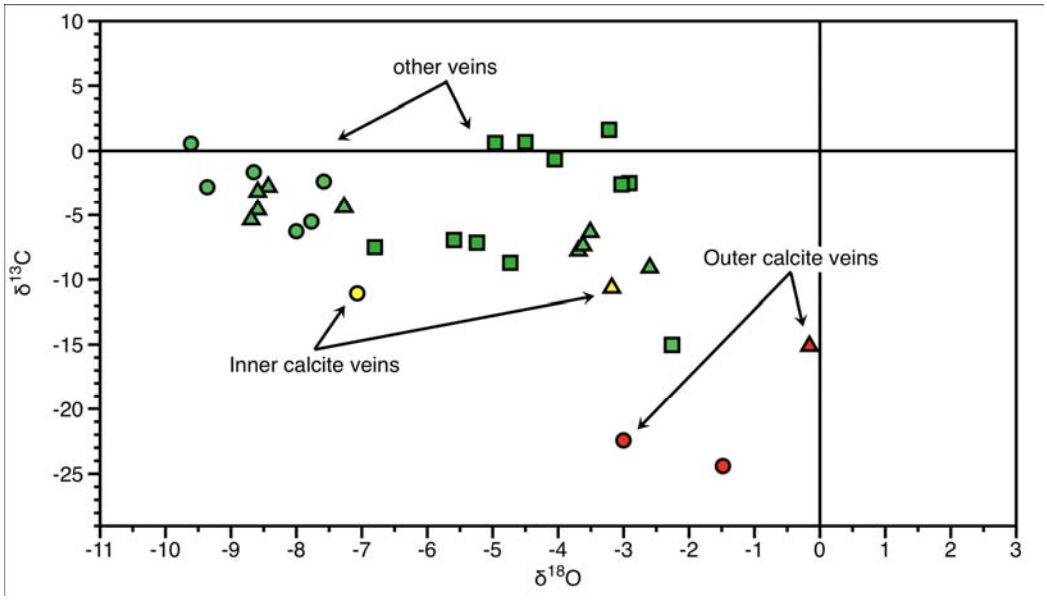

Figure 2-22. Carbon and Oxygen Stable Isotope Composition for the Barnett Shale. Most values are near normal for a buried marine carbonate (green). Outer vein calcites in tectonic fractures appear to be incorporating light C into its matrix (red).

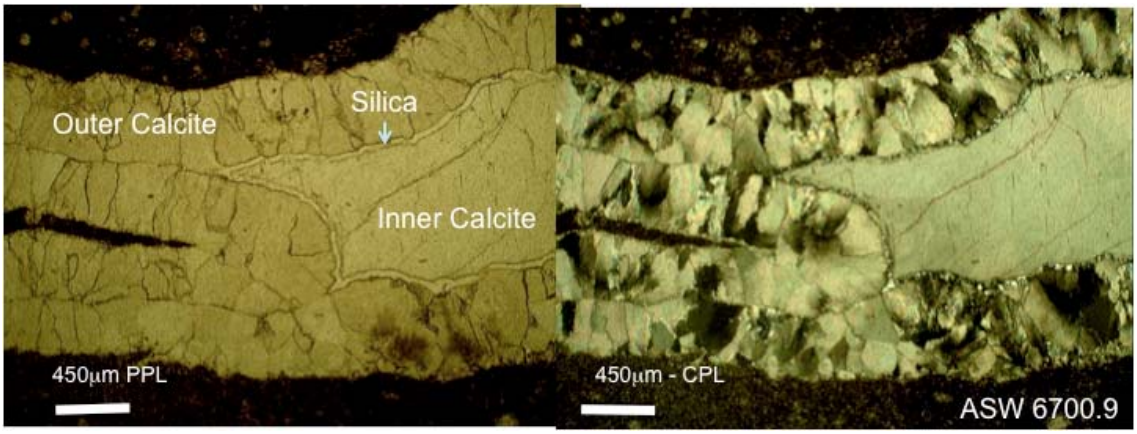

Figure 2-23. Outer and inner calcite veins containing one generations of light $\delta^{13}C$, a siliceous cement, then a less depleted $\delta^{13}C$ calcite in the vein interior.

2.5.4 Fracture Orientation and Fill: Geochemistry and Mineralogy

Natural fractures served as conduits for fluids within the Barnett Shale. Fractures of varying widths (aperture), orientation, and linearity are present. Barnett shale fractures are typically described as healed fractures although open fractures do exist and they can contain vugs and are mineralized [Figure 2-24]. Healed fractures contain a network of cements. Many fractures are stratigraphically confined within the shale, terminating at lithologic changes. Most are tensile (natural opening-mode; Gale et al., 2008) mode fractures although some northeasterly fractures show evidence of shear. Most fractures are vertical, tectonic, have very narrow azimuths, and are filled with mostly calcite or calcite-silica-minor barite. Some fractures and veins, especially near known faults, have large apertures >1 cm in diameter that can be open and conductive.

Figure 2-24. A large 2.5 cm aperture, northeasterly vein preserves a partially mineralized vug within the Barnett Shale. Several east-west fractures intersect the vein near this vug.

Barnett Shale fracture orientations were determined from formation microscanner/microimager (FMS/FMI) log data, and from oriented core (Table 2-4). Dip and dip azimuth orientation data, and to a lesser extent aperture, were used to classify fracture trends. Notes on the character of the fracture (open, partially open, or healed) as well as the fracture mode (shear, or non-shear) were also noted. The three cores were subdivided into two groups, ASW and ES representing Wise County of the Fort Worth Basin, and the SC representing Johnson County (Figure 2-25). The two areas are 110 kilometers apart and the influence of the Muenster Arch is presumed to have been different between the two areas. The fracture orientations between the two areas are different though internal angles between sets are simliar [Figure 2-25].

Set	Fracture Description	Azimuth Range	Dip	Cements (in order of abundance)			
1	Bed Parallel (minor)	NA	~0	Calcite	Barite-celestine	Albite-Apatite	Pyrite
2	Northeast (sub-vertical)	45-80	50-70	Calcite	Barite-celestine	Albite-Apatite	Pyrite
3	Northwest	315-350	80-90	Calcite	Silica	Dolomite	Hydrocarbons
4	Northeast (vertical)	5-40	~90	Calcite	Silica	Dolomite	Hydrocarbons
5	East-West (and Northeast?) (faults)	90-110	50-70	Calcite to Open	Hydrocarbons	-	-

Table 2-4. Major and minor fracture trends as described from ASW, ES and SC cores.

A)

WISE CO
ES and ASW

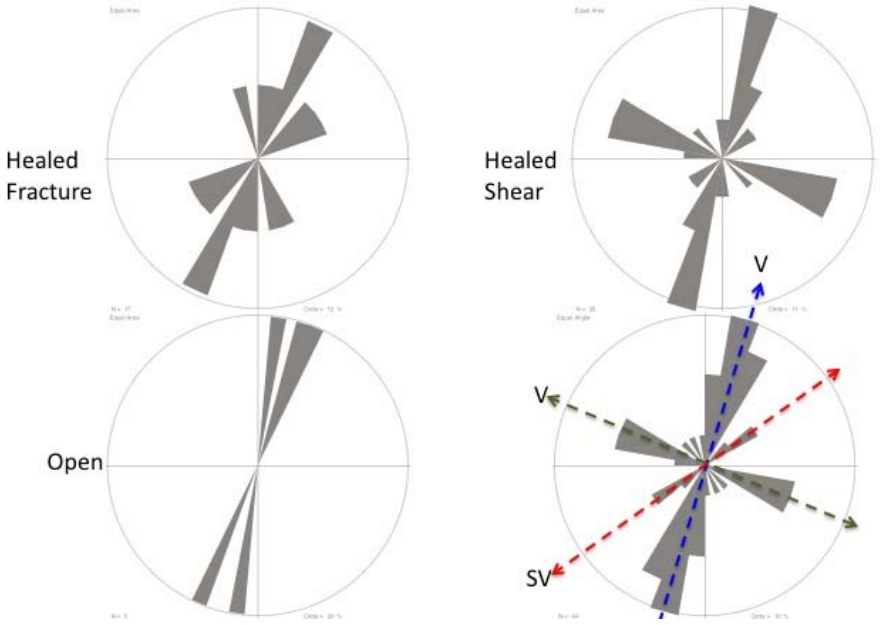

B)

JOHNSON CO
(South Cores)

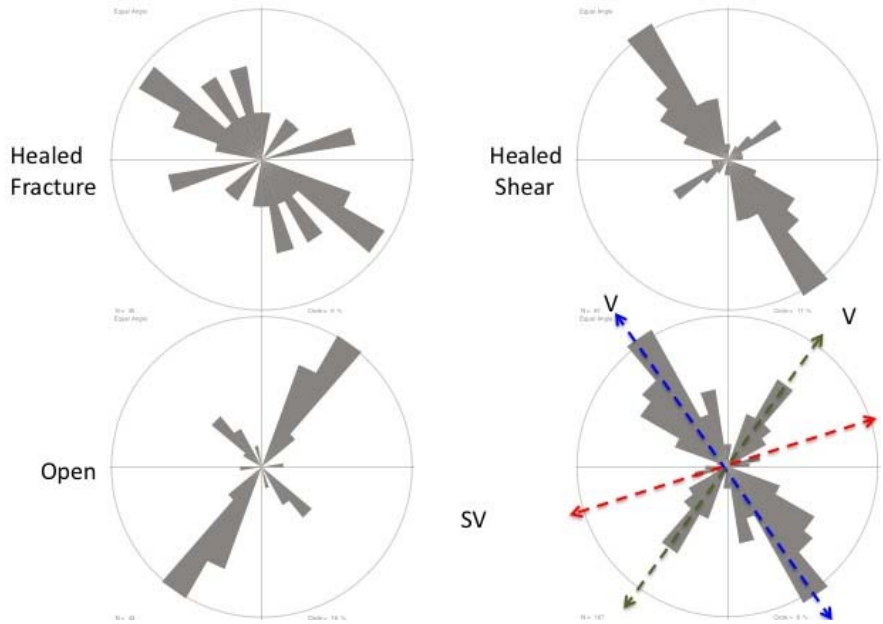

Figure 2-25 Rose diagrams showing major fracture trends in Wise County wells (A: ASW and ES) versus Johnson County (B: SC). The lower right rose diagram is a composite of all natural fractures in each area. Blue dashes trend are primary vertical fractures containing shear; green dashed trend are non-sheared healed fractures (near-vertical to vertical). Red dashed trend are non-vertical, non-tectonic veins and bed parallel fractures. Note the diagrams have similar overall angular relationships but the fracture orientations are approximately 40 degrees apart, except for the non-vertical fracture trends.

Five general fracture trends can be defined in the Barnett Shale.

1) Bedding parallel or stratiform fractures [Figure 2-26] are minor in terms of abundance but have distinctive mineral assemblages (Figures 2-27). These fractures may be related to fractures with a northeasterly, sub-vertical trend. The stratiform fractures contain a distinctive mineral assemblage with sulfate-rich cements (barite and celestine) as well as authigenic albite and pyrite [Figure 2-27]. These are often associated with phosphatic, pyritic intervals below dolomitic intervals, and they are associated with hot gamma ray signals on well logs that have been identified as parasequence boundaries and are interpreted as maximum flooding surfaces (Singh et al.,

2008). Most cements in this group of fractures have low radiogenic $^{87}Sr/^{86}Sr$ values (Table 2-3).

Figure 2-26. ASW 6623. bedding parallel or stratiform fractures. Discolored bed below contains bedded pyrite and phosphate. Note the transition to sub-vertical fracture (northeast azimuth) on the left side of the photo suggesting a possible genetic relationship between the two fracture types. Sample is 2.3cm wide.

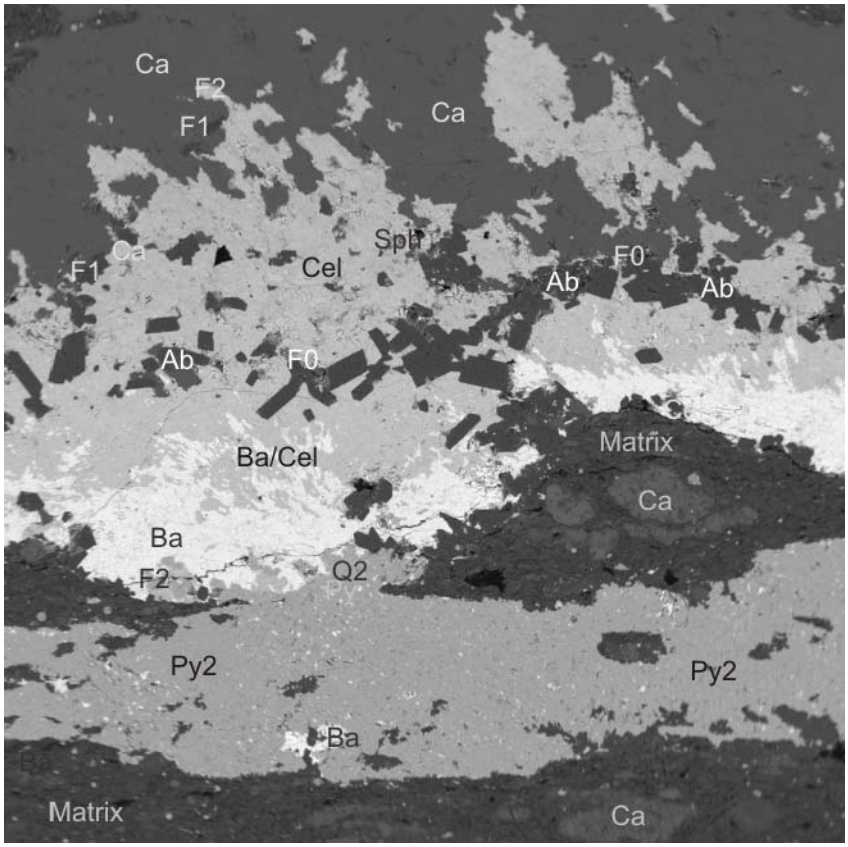

Figure 2-27. Interpreted SEM image of a stratiform fracture fill/deposit at ASW 6603. Zone is co-incides with a very high gamma ray spike, a pyritic and phosphatic shale interval. Barite-Celestine appears to replace calcite in the vein and matrix, which contain an early generation of quartz and authigenic albite. Barite and celestine show a solid solution relationship between Ba and Sr on SEM suggesting precipitation from a common fluid.

2) A second minor fracture set consists of northeasterly trending, sub-vertical veins (Figure 2-28). They contain sulfate that replaced earlier calcite. This is similar in overall mineralogy to the bedding parallel fractures. These veins are well developed in the more carbonate-rich intervals such as the Forestburg Limestone. Most cements contain low to intermediate radiogenic $^{87}Sr/^{86}Sr$ values. Northeast fractures in general contain more evidence of shear motion and evidence of reactivation. These fractures have the most complex healing history, largest apertures, and most heterogeneous mineralogy of the fracture sets identified in the cores. These fractures are healed by carbonate, sulfate and sulfide cements, in multiple episodes of cementation (Figure 2-28;2-29). Some cements ranges are luminescent and

others are not.

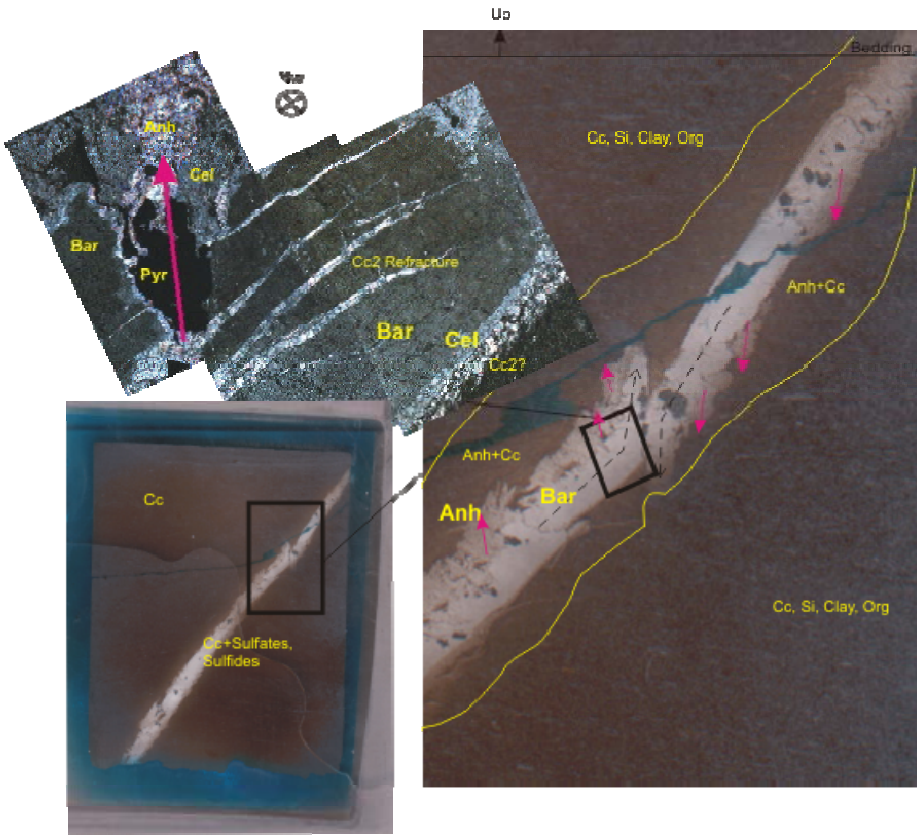

Figure 2-28. ES 6780. Two intersecting, complex northeasterly fractures in the carbonate-rich Forestburg Lime. Earliest fracture fill is barite and calcite. Late calcite is present in re-fracture exploiting early barite cleavage planes. Late calcite is accompanied or followed by anhydrite, celestine (strontium sulfate) and euhedral pyrite in later, more vertical northeasterly fractures. Red arrows show late refracturing fluid (cements) breaking out vertically away from the pre-existing fracture).

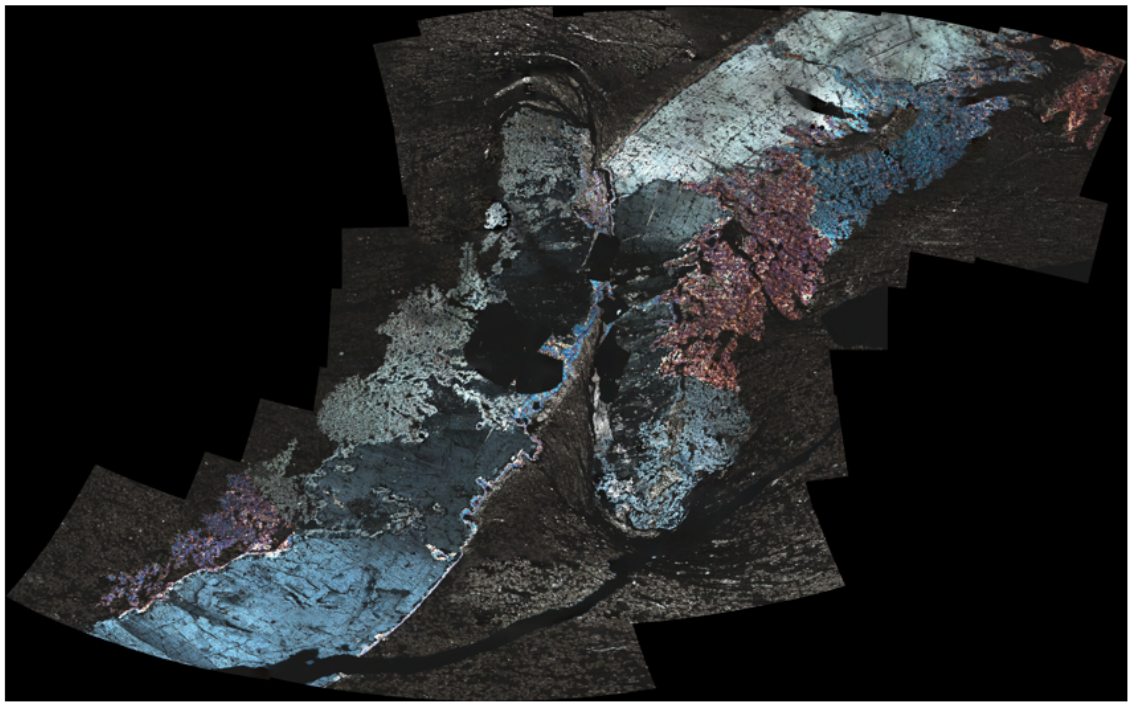

Figure 2-29. Panoramic mosaic of ES 6780 showing 170 10X magnification PPX photomicrographs showing the complex mineralogy and interaction of two northeasterly propagating fracture tips.. Note compressed laminae ahead of the fracture tips. Opaque minerals are pyrite; blue is barite; purple/pink is anhydrite, grey iscelestine.

3) Northwesterly fractures are narrow, vertical fractures filled with calcite and silica cements and only minor sulfate minerals. Hydrocarbons are found as inclusions within silica and also coating silica cements, suggesting this fracture set formed concurrently with hydrocarbon generation and migration. En echelon fracturing (Figure

2-30) and fracture tip interference is seen in this set and suggests a natural hydraulic fracturing mechanism during advanced burial diagenesis.

Many of these fractures comprise one or more generations of calcite and silica cements, with some minor sulfides and dolomite. In these fractures, the barite replaces earlier calcite cements and is associated with silica [Figure 2-31]. Although the data are limited, the fracture fill is moderately radiogenic (Table 2-3). Some of these fractures are incompletely cemented (Figure 2-32) which may result in a mechanically weak fracture planes. Finally, rate of fracture propogation may vary between lithofacies because fractures show refraction at bed interfaces (Figure 2-33).

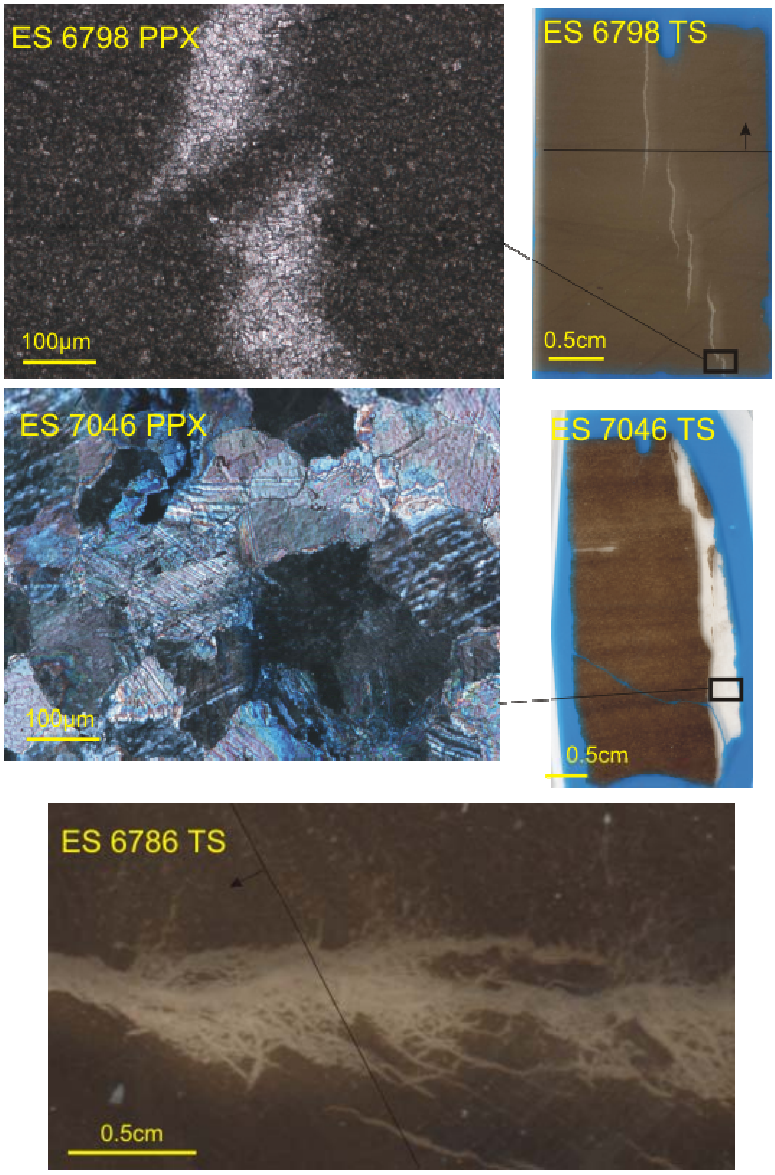

Figure 2-30. ES 6798. Fractures with northwesterly azimuths show en-echelon fracturing, with simple single generational calcite cement. ES 7046 shows larger aperture vertical fracturing with coarser calcite fill. ES 6786 shows highly complex microfractures "feeding" a sub-vertical central vein.

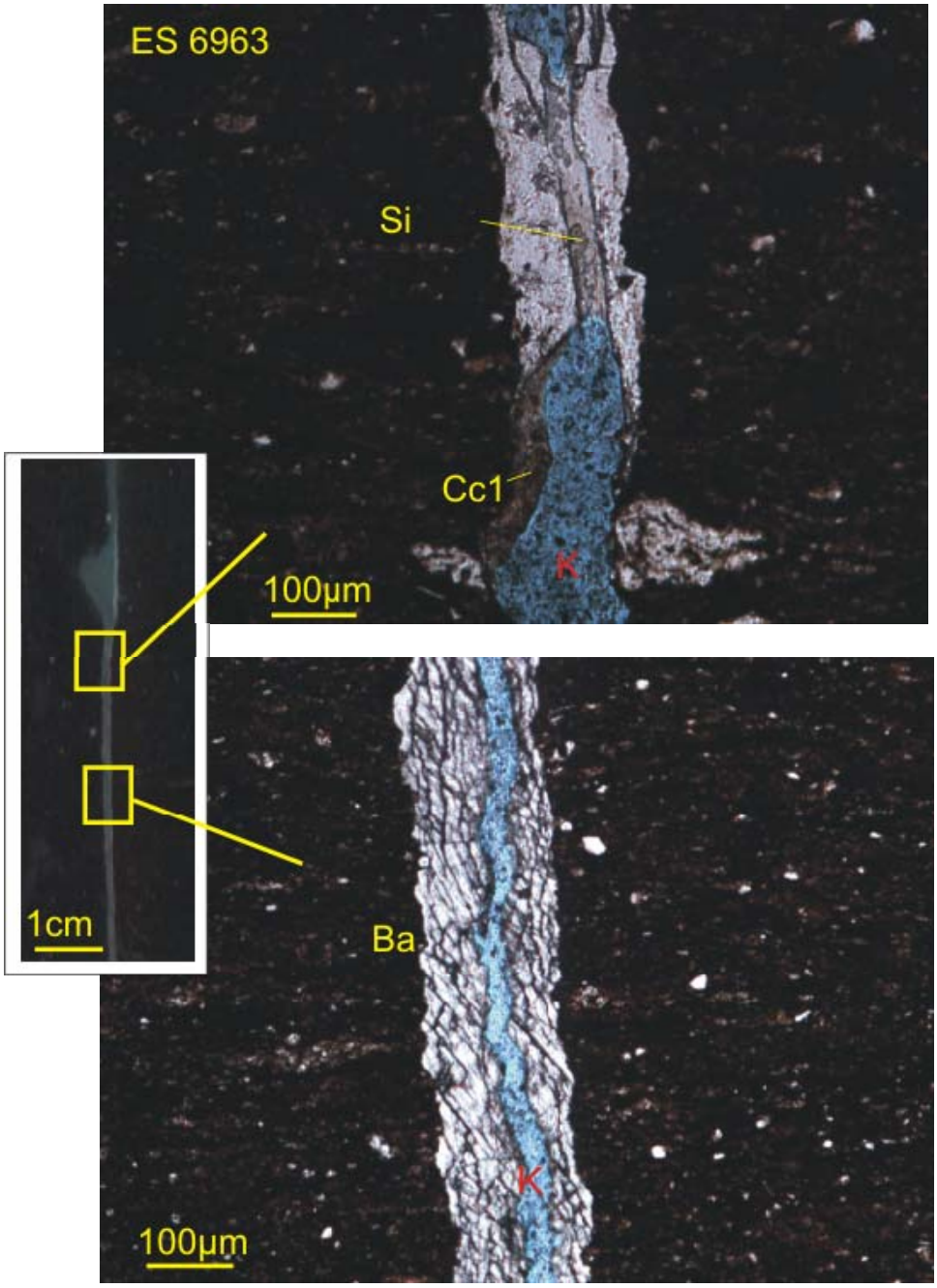

Figure 2-31. ES 6963. Thin section scan of a northwesterly and vertical partially healed fracture with characteristic narrow (<1mm) aperture. Upper right insert shows porosity in blue, with calcite, silica and lesser barite cements. B) Lower right inset shows a partially healed portion of same fracture with barite cement instead of calcite.

Figure 2-32. An exposed partially healed en echelon fracture, northwesterly, ES core. Note the fracture plane shows a incomplete distribution of cement. Core is 4" in diameter.

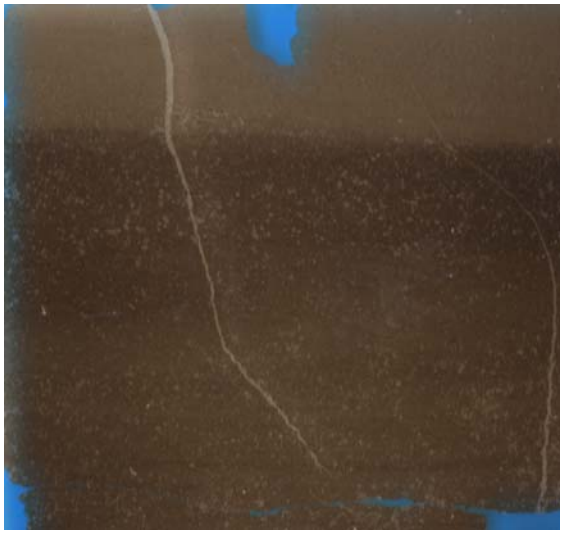

Figure 2-33. ES 6843. Refraction of a northwesterly fracture's dip, likely due to changes in rate of propogation through the different rock types. Thinly laminated heterogeneous beds attenuate and refract small fractures. Note fracture eventually dies out with depth and runs bedding parallel below thicker clay-rich laminae. Photo is 2.2cm wide.

4) A second vertical fracture set has narrow apertures and a northeasterly direction. Unlike northwesterly fractures, a significant amount of sulfate and shear motion are present in this set. Celestine appears to be possibly altered from barite in this fracture set, and late calcite and euhedral pyrite are common. The barite and calcite in these fractures are more highly radiogenic (Figure 2-21;Table 2-3) suggesting involvement of late external fluids.

5) Finally, a late E-W fracture set contains evidence of local shear displacement cutting both the northeasterly and northwesterly sets. This set is rare in the Barnett, has variable apertures and is either partially healed by coarse calcite or is open. Where this set intersects northeasterly sets, vugs and other macroporous zones may form (Figure 2-24).

2.6 Synthesis: Hypothetical fracture and basin stress controls on fluid remagnetization in mudrocks

As previously stated, there is no obvious connection between (Singh, 2008) lithofacies or depth and the ChRM directions. I hypothesize that paleomagnetic data can be categorized by fracture orientation (proximity of specimens to different fracture sets). To test this hypothesis, I compared fracture orientation and fracture-fill data with

the paleomagnetic data for the Wise County cores. All directions for the SC are Permian therefore no further subdivision of that data is possible. Fractures orientations were identified from FMI and oriented core. Paleomagnetic data from the nearest sites below and above each fracture were used to calculate a mean paleomagnetic direction. Fractures were grouped as a unit with a maximum ten foot window (5' above, 5' below the fracture) [Figure 2-34; Table 2-5].

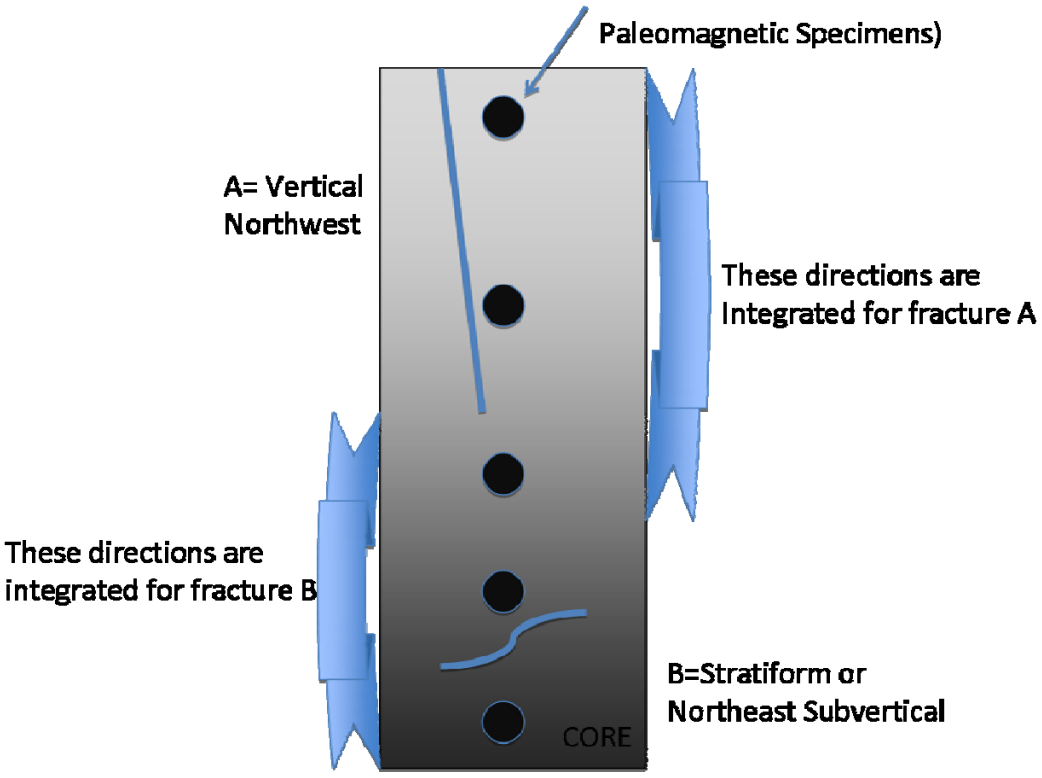

Figure 2-34. Schematic of the creation of the fracture unit mean. Up direction toward top of core.

Group	Core	Depth	Dec	Inc	a95	n	k	Cmt1	Cmt2	Cmt3
MT	ASW	6656	133	0.4	5.9	4	246.29	Matrix	Si	
MT	ASW	6727	162.8	17.3	7.5	2	1104.6	Matrix	CC C	
MT	ASW	6734	159.7	15	15.7	3	62.92	Matrix	Py	
NW	ASW	6723	158.2	14.5	14.2	3	76.7	Cc	Si	HC
NW	ASW	6745	140.9	-2.9	9.6	5	65.04	Cc		
NW	ASW	6771	140.6	-4.5	8	4	133.12	Cc		
BP	ES	6882	140.7	15.2	21.5	8	7.57	Cc		
BP	ES	7177_ou	125.9	6.4	15.6	4	35.46	Bent		
NE2	ASW	6582	129.3	1.7	20.1	2	129.97	Bar	Cel	Py
BP	ASW	6603	128.5	-1.6	3.5	7	295.5	Bar	Cel	Py
NE2	ASW	6651	133	0.4	5.9	4	246.29	Bar	Si	Dm
BP	ASW	6700a	125.9	-2.8	9.5	3	169.27	Bar	Cel	Cc
NE2	ASW	6745	140.9	-2.9	9.6	5	65.04	Cc		
NE2	ASW	6771	140.6	-4.5	8	4	133.12	Cc		
NE2	ASW	6784_ou	142.6	-1.6	14.6	5	28.52	Cc		
NW	ASW	6871	163.5	5.9	5.8	4	251.21	Cc		
NW	ES	7166	173.6	-0.7	13	10	14.82	Cc		
NE2	ES	6850	152.4	3.4	15.2	5	26.34	Cc		
NE1	ES	6727	168.3	13.3	19.4	4	17.81	Si	HC	Cc
NW	ASW	6522	179.2	10.5	8.2	6	68.02	Cc		
NE1	ASW	6700b	162.1	11.9	9.6	3	165.42	Cc	Si	Cc
NE1	ASW	6723	158.2	14.5	14.2	3	76.7	Cc	Si	HC
NE1	ASW	6744	156.5	-1.9	8.3	4	124	Cc	HC	

Table 2-5. Results of grouping paleomagnetic data into integrated fracture unit means. The mineralogy of the facture fill was also noted if thin sections were available. Dec=declination. Inc=inclination. A95=alpha 95% cone of confidence (error; low is good). K=grouping (high is good). Cmt1,2,3= major cements by volume.

The fracture unit directions for all the data from the Wise county cores are streaked (Figure 2-7c) but show a general correlation when grouped by fracture type.

The paleomagnetic data from the bedding parallel fractures (Figure 2-35A;Table 2-6) have southeasterly declinations and shallow inclinations. The mean (Figure 2-36) has a corresponding pole that falls off of the mid-Pennsylvanian part of the APWP (Figure 2-37). Because of the sparse data (Table 2-6), this mean should be treated with caution. Sub-vertical and northeasterly fractures (Figure 2-35B) contain a similar distribution of directions to the bedding parallel fractures and the paleopole is just off the late Pennsylvanian part of the path (Figure 2-27). The fill of fractures is dominated by calcite with lesser sulfates. Although there are few specimens and the grouping is relatively poor, matrix sites (figure 2-35C) with no fracturing yield south-southeasterly directions with a paleopole on the late Pennsylvanian to Permian part of the path (Figure 2-37). The fill in northwesterly, vertical fractures (Figure 2-35D) are dominated by calcite, silica , dolomite and hydrocarbon, and they contain more southerly directions, with a Permian to earliest Triassic paleopole (Figure 3-37). Finally, the vertical northeasterly fractures (Figure 2-35E) have complex cements and south-southeasterly directions with a late Permian to early Triassic paleopole (Figure 3-37).

All cores, north and south, contain late vertical northwesterly and northeasterly tectonic fractures, although the orientation of the fracture sets are more northerly in Wise County and easterly in Johnson county. Gale et al. (2007) proposed that the

northwesterly fracture set is the younger set, and the northeasterly is the older set. The paleomagnetic data suggest that the northwesterly vertical fracture trend is younger than the northeasterly sub-vertical fracture trend, though later reactivation of some northeasterly vertical fractures are found the same age as the northwesterly trend. As a general observation, more carbonate-rich intervals in tectonic fractures contain more southerly directions and younger remagnetizations.

The paleomagnetic data from some of the fractures are relatively sparse and the interpretations are preliminary. The inferred ages need to be tested by additional sampling and paleomagnetic analysis. One issue with the vein tests conducted here is that the samples are limited by the core. Other fractures could occur laterally and were not identified in the cores.

Site	Dec °	Inc°	a95	k	N	Paleo-latitude	Paleo-longitude	dp	dm	AGE
1 – Bed Parallel	130.2	4.3	12.4	55.74	4	31.3	145.5	6.2	12.4	mid-IP (OTP)
2 – NE Group 1	139.8	-0.6	7.1	89.36	6	40	139.6	3.6	7.1	late IP-early P
3 – Matrix Only	151.7	11.2	28.9	19.21	3	42.9	122.3	14.9	29.3	late IP - P
4 – NW Vert.	159.3	3.9	15.1	20.74	6	49.9	115.4	7.6	15.1	late P – early T

5 – NE Group 2	161.2	9.5	10.5	77.5	4	48.1	111	5.4	10.6	late P – early T

Table 2-6. Paleomagnetic site means for fracture intervals, Wise County cores. In left column, IP = Pennsylvanian Period, P = Permian Period, T=Triassic. OTP = off the APWP path.

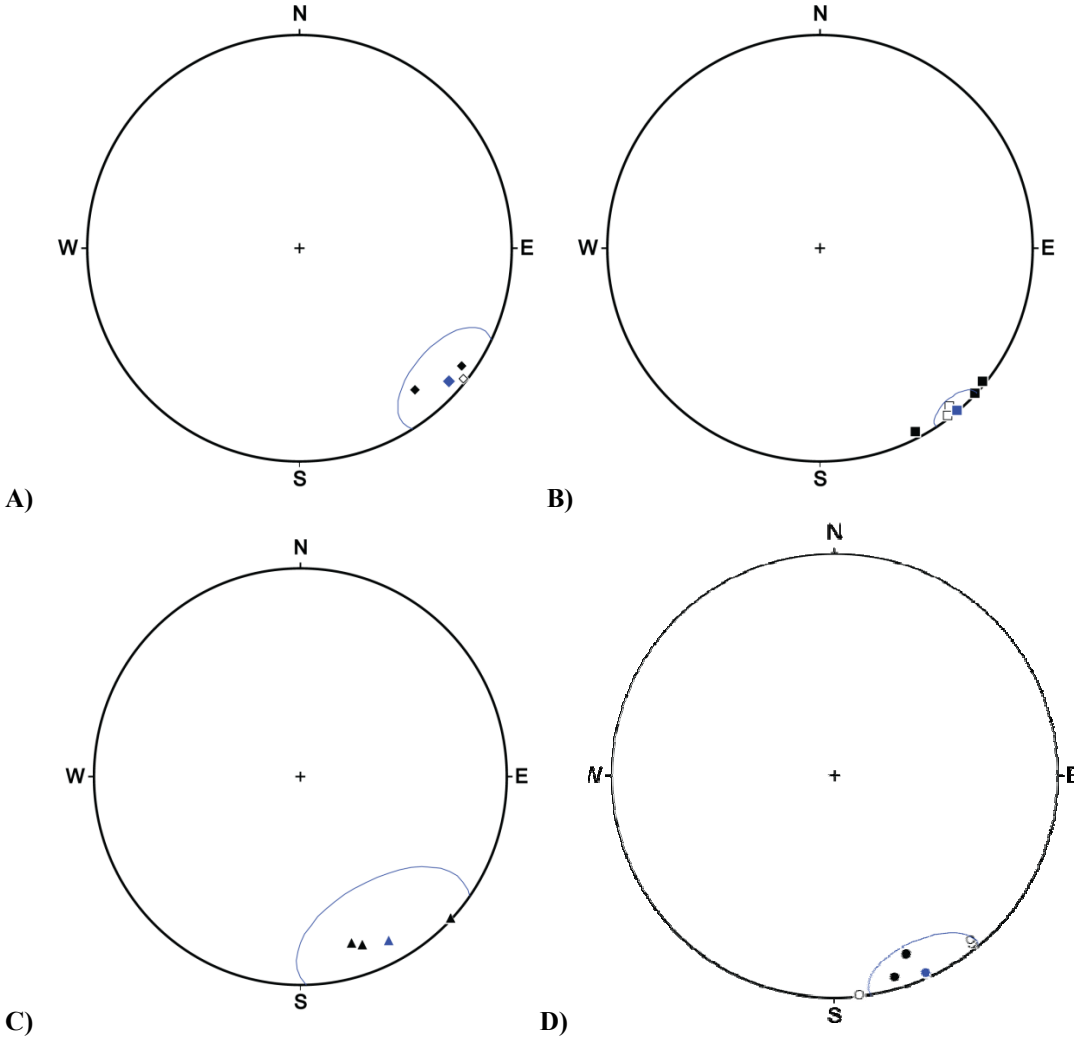

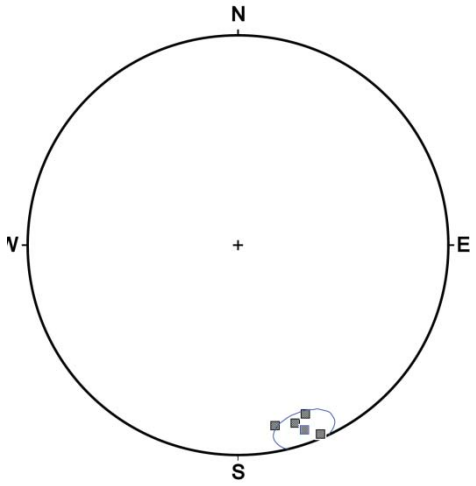

E)

Figure 2-35A-E. Paleomagnetic site means for the different fracture groupings. Wise County cores (ASW and ES). A) Diamonds are bedding parallel (stratiform) fractures; B) dark squares are northeasterly and sub-vertical fractures; C) triangles are matrix only; D) circles are vertical northwesterly tectonic fractures; and E) light squares are sub-vertical to vertical and northeasterly shear fractures. The plots show the variation in fracture mean direction, and therefore paleopoles (ages), between fracture subsets.

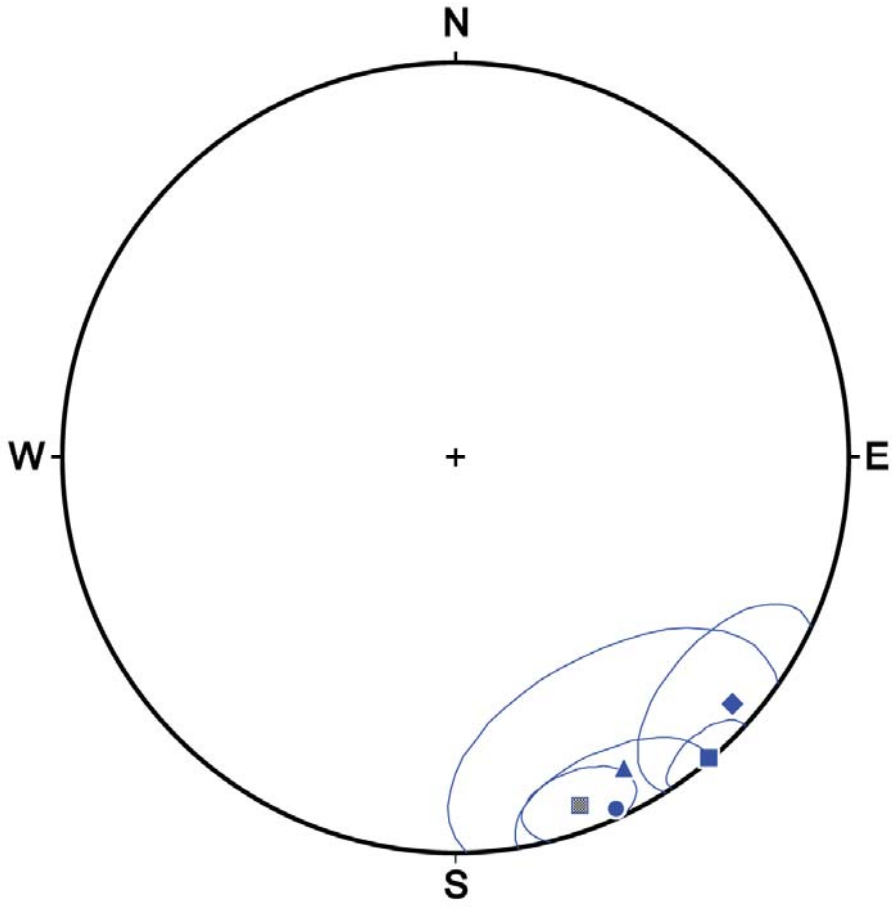

Figure 2-36. Fracture orientation "unit means." Diamond is bedding parallel (stratiform) deposits; dark square are northeasterly and sub-vertical fractures; triangle is matrix only; circle is vertical, northwesterly tectonic fractures; light square are vertical and northeasterly fractures.

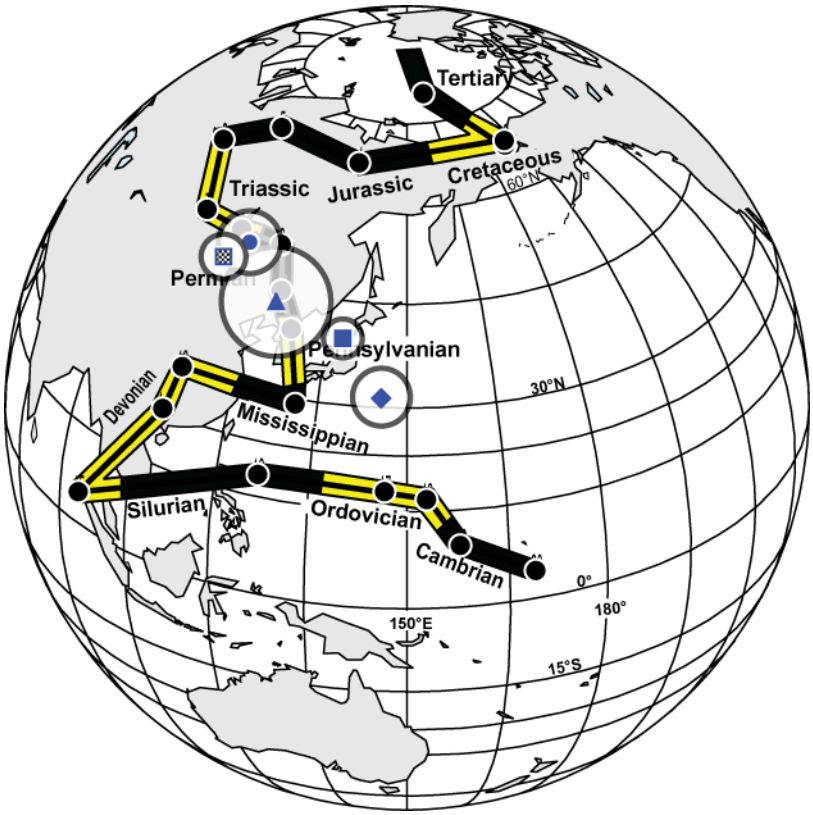

Figure 2-37. APWP paleopoles for data from the Wise County cores. Diamond is bedding parallel (stratiform) deposits; dark square is northeasterly and sub-vertical fractures; triangle is matrix only; circle is vertical, northwesterly tectonic fractures; light square is vertical and northeasterly fractures. Vertical fractures are interpreted as containing younger diagenetic remagnetizations than matrix, which have larger errors. Stratiform and sub-vertical fractures appear to preserve older remagnetizations.

2.7 Discussion

I interpret that the ChRMs within the Barnett Shale reside in magnetite based on unblocking temperatures below 580°C, the Curie temperature for magnetite, and LAP-GAP-SAP rock magnetic data. Paleotemperatures for the basin are estimated between 100°C and 180°C by Jarvie et al., (2009) based on rock pyrolysis and vitrinite reflectance data (e.g., Pollastro, 2003; Pollastro et al., 2003, 2004; Zhao, et al. 2007; Jarvie et al., 2007). Based on comparisons with the unblocking temperature-relaxation time curves (e.g., Dunlop et al., 1999) the maximum unblocking temperature of 480˚C is too high for the ChRMs to be thermoviscous remenant magnetizations (TVRM). Therefore, the ChRMs are interpreted as chemical remenant magnetizations (CRMs) residing primarily in magnetite. The rock magnetic data also suggest minor contributions from the mineral pyrrhotite although it is not clear it carries a remanence.

Total magnetic susceptibility data collected from all wells suggest that genetically similar zones can be correlated across the basin. Magnetic susceptibility, therefore, might be useful as a correlation tool in the Barnett Shale. A high susceptibility spike occurs with a glauconitic hardground near the top of the Lower Barnett, and remains high through the Forestburg Lime interval, suggesting a possible change in the environment of deposition (e.g., increase in detrital magnetite flux,

changes in seawater chemistry) or may reflect the more permeable nature of this unit to late fluid alteration.

The paleomagnetic directions fall on a streak from N120°E to 190°. The result of the VRM test indicates that this distribution of directions is real. There are several possible explanations for the origin of the data distribution. It could represent discrete CRMs with overlapping data distributions. If this were the case the CRMs were acquired between the Pennsylvanian and Triassic (Figure 2-11). Alternatively, one CRM could have been acquired over time between the Pennsylvanian and Triassic. This is considered unlikely because one diagenetic event would have to have occurred for a period of over 70 Ma.

The poles from the more easterly part of the streak fall off the APWP to the east. In contrast, the poles for the more southeasterly and southerly directions fall on the Permian or younger parts of the path. There are several possible reasons for this. For example, an early Pennsylvanian CRM could have been acquired in a relatively short period of time that did not average out secular variation and the resultant pole could fall off the path. Another possibility is that the basin was tectonically rotated. A 15-20° counterclockwise rotation would account for the offset of the direction and the pole (Figure 2-12). If the direction is rotated back to account for the counterclockwise

offset, the corresponding pole falls on the late Pennsylvanian to early Permian part of the APWP. This hypothesis is consistent with the findings in Chapter 1 for the Ellenburger Group rocks below the Barnett (Dennie, 2010a). Detailed structural analysis of Fort Worth Basin, however, is needed to test this hypothesized rotation.

Several sets of poles can be defined using fracture data as a discriminator for the paleomagnetic data. A set of northeasterly sub-vertical, and bedding parallel veins have a mid- to late-Pennsylvanian pole, after the hypothesized rotation is corrected. This set contains sulfates, albite and sulfides such as sphalerite. They are interpreted as forming during burial diagenesis and remobilization of early syndepositional cements that formed on a sediment starved, stagnant maximum flooding surface seafloor. The timing roughly corresponds to the early burial window (Figure 2-18) for methanogenesis and decarboxylization.

A second set of fractures is northwesterly and vertical, contain largely calcite, silica and liquid and solid hydrocarbons. The cements are slightly-radiogenic and they are interpreted as forming from either internally- or eternally derived fluids. The presence of hydrocarbons in inclusions suggests the cements were precipitated after the onset of hydrocarbon maturation. Paleopoles for this grouping fall in the mid- to late-Permian. This set of fractures is therefore interpreted as being formed in the oil window.

A third set of fractures is northeasterly and vertical, and is found in all cores. This set also contains shear offset and reactivation/refracturing of preexisting northeasterly fractures. The veins have a mixture of remobilized cements, and contain anhydrite (gypsum), late barite-celestine, late calcite, dolomite and pyrite. Paleopoles for this fracture set place the CRM in the late Permian to early Triassic. Replacive barite and calcite are highly radiogenic suggesting externally derived fluids altered the rocks. The fluids may have moved by gravity-driven flow (e.g. model proposed by Garven, 1985) from the uplifted Ouachita highlands immediately to the east.

Paleopoles from the Wise County cores showing the progression of older northeasterly veins, to younger northwesterly tectonic fractures, with a final remagnetization of some northeasterly veins by late fluids. Comparison of the paleopoles from the fracture synthesis to the burial history curves for Tarrant County (halfway between Wise and Johnson) allows a comparison of the dates to the geologic history of the basin [Figure 2-38].

A)

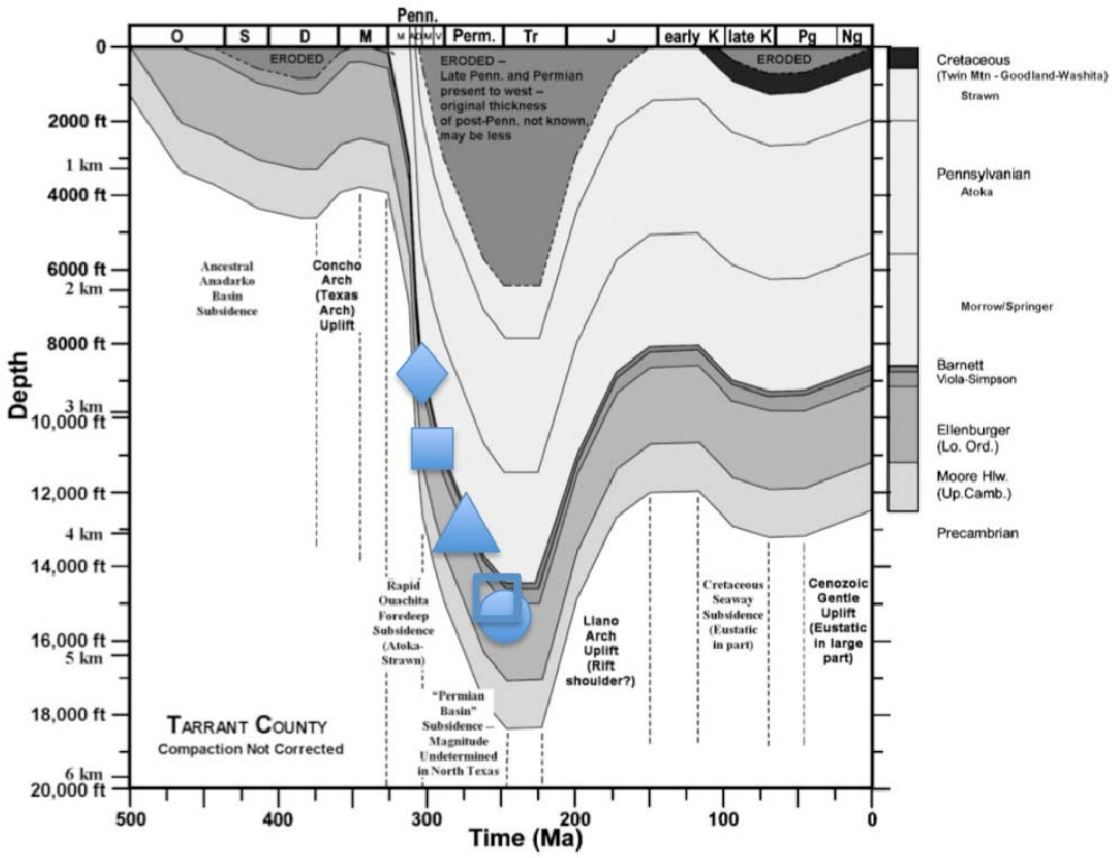

Figure 2-38. Age of remagnetizations versus burial history and thermal maturation chart for Tarrant County, between Wise and Johnson counties. Fracture timing is shown by symbols; Diamond is bedding parallel (stratiform) deposits; closed square are northeasterly and sub-vertical fractures; triangle is matrix only; circle is vertical, northwesterly tectonic fractures; open square are vertical and northeasterly fractures. Burial curve modified from Ewing, (2006).

The nature of the remagnetizations can be inferred from the geologic data (Figure 2-38). The mid Pennsylvanian CRM is suggested as forming from burial diagenetic fluids along poorly consolidated lineaments. Beginning in late Pennsylvanian to early Permian the northwesterly fractures formed during relatively deep burial of the Barnett Shale, as fluids probably generated internally formed hydraulic fractures and escaped out of the section. As the Ouachita orogeny reached its maximum and highlands were established, the late Permian-early Triassic CRM is interpreted to have precipitated from fluid off the Ouachita highlands. Alternatively, deep basement brines at the beginning of uplift of the Llano Uplift region to the south may have been an agent of remagnetization. The presence of anhydrite zones in Permian-aged rocks (Cheney, 1940) suggests a possible source of anhydrite, as gravity-driven flow percolated down through Permian sediments and into open Barnett fractures.

These findings fit the regional tectonic history of a basin that formed through oblique continent-continent collision that began in the northeast corner of the basin and progressed to the south and west (Figure 2-39A). This may explain the origin of possible block rotation, as a natural counterclockwise “torque” on the basement blocks would be exerted as the orogenic front swung past the end of the Muenster Arch (Oklahoma aulacogen). If the Barnett rocks were compressed in a NE-SW plane,

northeasterly fractures will be dialated and able take on fluids. Indeed we see older fluid CRMs in these fractures.

As the the orogeny progressed southward (Figure 2-39B) and shifted into a more west- to northwest compression, the northwesterly fractures responded by exhibiting opening mode behavior. This fits with the current understanding of the axis of maximum burial along the Ouachita front during the Pennsylvanian to early Permian. Finally, the late remagnetization in the latest Permian fits with post-orogenic basin relaxation and extension, coupled with Garven-type highland flow, during uplift of the Llano region to the south (Figure 2-39C).

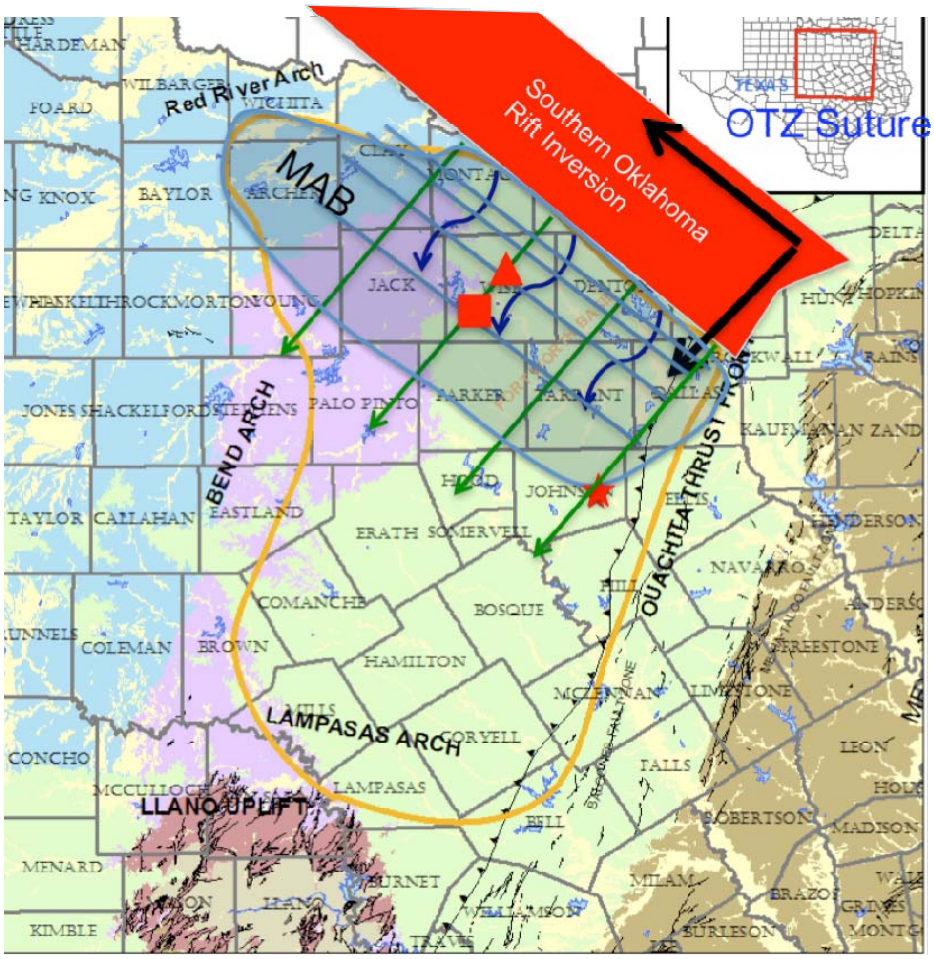

Figure 2-39A. Barnett Shale is first deposited along a basin subparallel to the Muenster Arch in a NW elongated basin (MAB). NE fractures (green arrows) accept internal fluids into the early-Pennsylvanian. Blue arrows are lineaments under compression. Black arrows show major directions of compression and shear motion. Otz=Ouachita thrust zone.

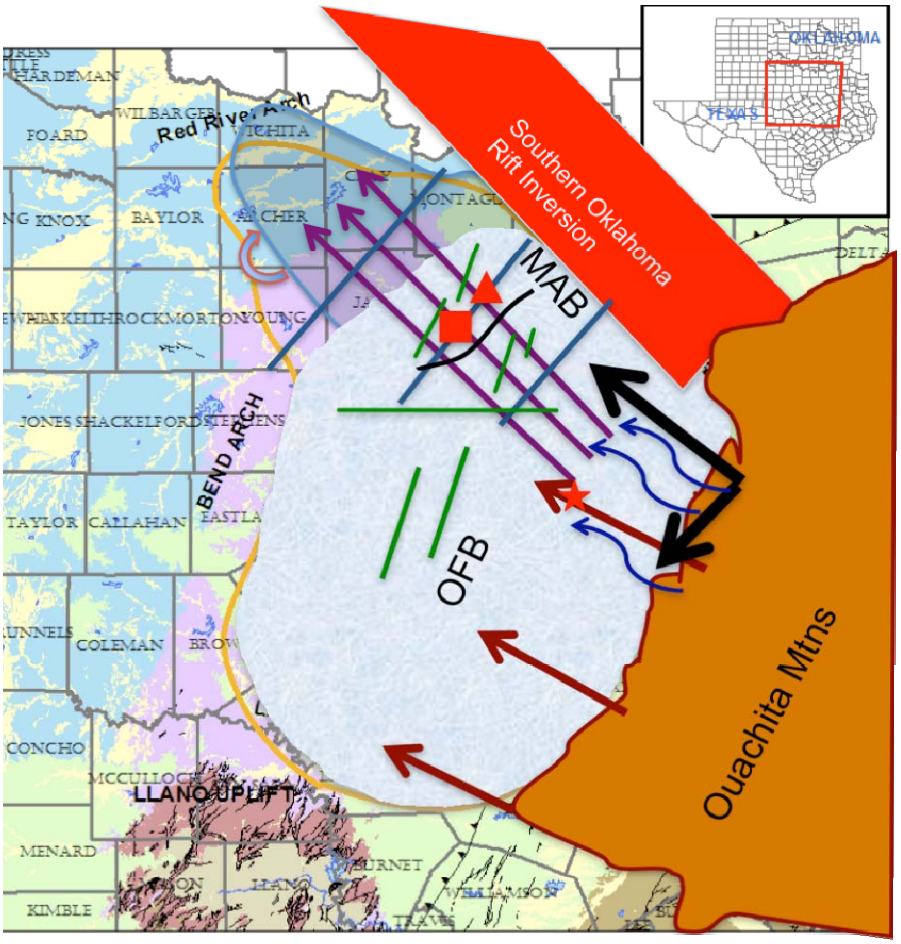

Figure 2-39B. Pennsylvanian to early Permian. Main thrust of Ouachita orogeny approaches from the northeast and east, and begins forming the Fort Worth (Ouachita) foreland basin (OFB) superimposed on the earlier MAB basin. Northwest fractures (purple) are activated during burial and receive internal and external fluids (near thrust). Basin rotation might have occurred as the thrust shifts from a southwesterly compressive direction to a more northwesterly compressive direction. (Black (and red) arrows show main directions of compression and shear.) Green lineaments are major faults of the time. Blue lines are earlier NE lineaments.

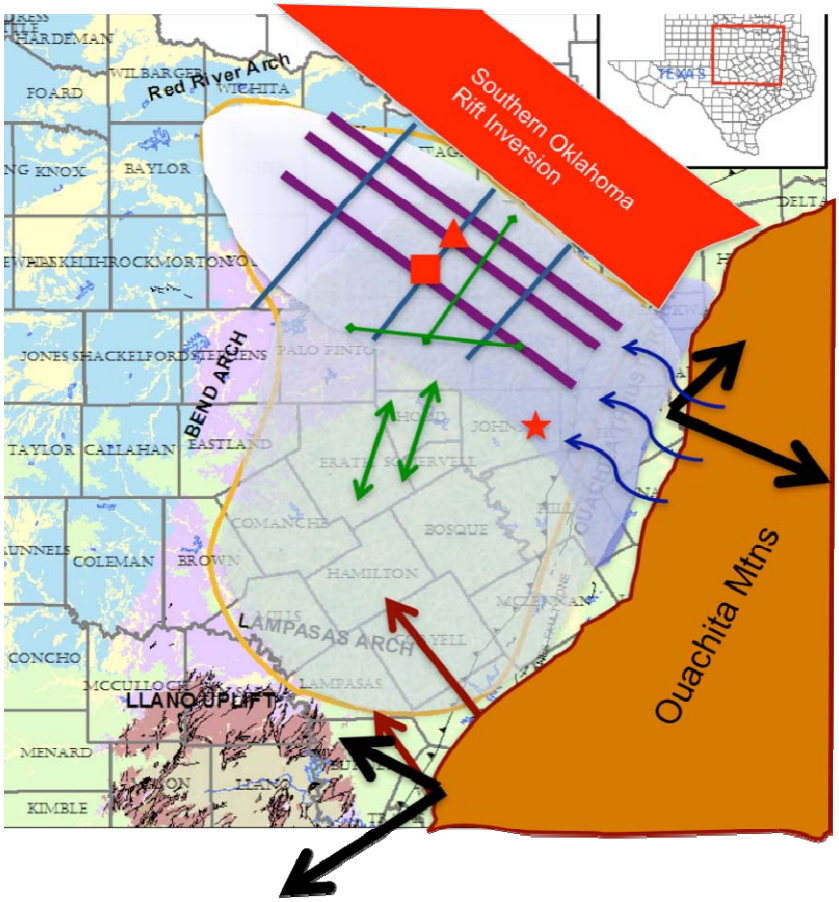

Figure 2-39C. End Permian. Orogeny is completed, and fluids from highlands (blue wavy lines), and basement fault fluids (green arrows) continue to affect the shale. Slight extension (black arrows) develop during uplift of the Llano, dialating late active faults particularly east-west and northeast azimuths (green) allowing later orogenic fluids to infiltrate these fractures and faults. NW fractures are largely healed and unaffected by relaxation.

Understanding the effects of internal fluids activated during burial, as well as hydrothermal or orogenic fluids, are important for future gas shale exploration. There is

substantial evidence that burial diagenetic and late diagenesis by fluids affected both maturation and migration of hydrocarbons and the final mechanical behavior of the shale. Post hydrocarbon maturation fluids may have adversely affected the hydrocarbon content of stratigraphic intervals. This may affect the placement of wells to avoid depleted zones in section. External fluids could locally influence shale maturity and gas in place, both of which are sensitive to elevated heat flow regimes. Fluid movement along faults may have caused increased heat flow into the rocks surrounding the fault, which could have caused secondary cracking to gas. This would have resulted in zones of enhanced production near to these faults and fractures. The same faults, however, could have associated macroporosity in the form of open fractures and vugs. These fractures and vugs could be sinks for frac fluids and impair gas production by limiting the effectiveness of the fracturing of new rock.

Diagenetic alteration also affects the distribution of some minerals (e.g., silica and plagioclase feldspars) throughout the final mudstone. These redistributions and additions of authigenic minerals likely will change the overall mechanical behavior of the shales by making them more rigid or brittle which may affect the propogation of fractures in these intervals. This is an important consideration in the prediction of fracture behavior during modern artificial stimulation of these rocks. If a unit has not

undergone a diagenetic history favorable to the redistribution or creation of these minerals, a rock may not behave as would otherwise be predicted. In addition to fracture behavior, some other minerals identified herein, namely anhydrite, celestine, may be unstable when in contact with freshwater fluids such as those in modern completions techniques. These minerals, when remobilized, could cause problems with hydraulic stimulation due to their ability to crystallize and plug off pore throats in newly created fractures. Minerals such as anhydrite may also remobilize in the wellbore as scale during drilling and production.

2.8 Conclusions

1) The Barnett Shale has undergone multiple remagnetization events beginning in the mid-Pennsylvanian and continuing into the late Permian. The magnetizations reside in magnetite and are interpreted to be CRMs.

2) The observed specimen directions are streaked from a southeasterly and shallow direction to a southerly and shallow direction. The modern VRM was used to orient the CRM data for one of the wells and to test the core scribe orienting method. The results confirm the streak of directions is real and not caused by core rotations.

3) Subdivision of the paleomagnetic data does not reveal obvious control on the CRMs by lithofacies. Fracture orientation, however, does appear to be correlated to the paleomagnetic data.

Fractures with northeasterly azimuths are found in rock that contains a Pennsylvanian and a late Permian CRM. These fractures are filled by calcite, and sulfates. The earlier fluids precipitated fracture fills that were not highly-radiogenic, and the later fluids precipitated radiogenic cements. The early CRM is interpreted to have formed during burial diagenesis, and the latter from gravity-driven orogenic fluids derived from the uplifted Ouachita highlands.

Northwesterly fractures are associated with rock that contains a late Pennsylvanian to early Permian CRM. These are filled with calcite, quartz and contain relict hydrocarbons. The CRMs are interpreted to have formed from deep burial diagenetic processes. A final E-W fracture set is rare, and is typically open to partially healed where found, and appears to be the youngest set though it does not contain a associated CRM.

4) The paleomagnetic data suggests the possibility of a counterclockwise block rotation of up to 20° beginning in late Pennsylvanian time. This fits the current understanding of

the mechanism of tectonic closure of the Llano uplift portion of the Ouachita thrust behavior described by Erlich and Coleman (2005 in which the Llano behaved as a series of rotated basement blocks.

5) Vertical magnetic susceptibility data show similarities between some cores. It is possible that magnetic susceptibility data can be used to correlate Barnett intervals in some parts of the basin.

6) The diagenetic alteration of the Barnett resulted in the addition of some minerals (e.g., silica and plagioclase feldspars). This changed the mechanical behavior of the shales by making them more rigid or brittle which may affect the propogation of fractures in these intervals.

7) Some other minerals (anhydrite, celestine) are labile and could cause problems with hydraulic stimulation. Minerals such as anhydrite may remobilize to create loss of permeability or scaling during drilling and production.

8) The radiogenic strontium data suggest an orogenic fluid contribution sourced from the Ouachita thrust invaded and altered the Barnett Shale, with its effect becoming less pronounced as you approach the western portions of the basin.

2.9 Future Work

1 Further understand the source and nature of the sulfate and sulfide fracture fill phases and their relationship to fracture azimuths, by performing a sulfur isotope (^{34}S) study to determine biological versus hydrothermal sources for the sulfides and sulfates.

2 Further investigate the source and role of bedding-parallel or stratiform mineral deposits in the Barnett and other gas shales and determine if they are related to sedimentary exhalative systems such as is found in some Mississippi Valley type-ore deposits.

3 Further work on cores to extend understanding of the mineralogy related to orogenic fluids and typing those fluids to basement rocks or thrust related rocks.

4 REE analysis of the shale to determine auto-cyclical patterns in salinity and temperature, which may be related to early deposition of barite and celestine.

5 Appropriate fluid inclusions are rare in the Barnett Shale and further study may yield usable primary inclusions. These could be important to better understand the thermal history of the fluids affecting the formation.

6 Understand how non-quartz silicates, such as plagioclase (albite) feldspars, affect the ultimate fracturability of the unit and overall mechanical behavior of shales. Compare paleomagnetic data to FTIR elemental distributions.

7 Structural analysis to determine the extent and nature of hypothetical basin rotation and late extension, within the Fort Worth Basin, and its relationship to Barnett shale productivity.

8 Compare paleomagnetic timing of Barnett Shale rocks to that of overlying beds, including Pennsylvanian and Permian aged units.

2.10 References for Chapter 2

Adams, J.E., 1954, Mid-Paleozoic Paleogeography of Central Texas: Shale Shaker v.4, no.6, p.4-9.

Aktepe, S., Marfurt, K., Perez, R., 2008. Attribute expression of basement faulting - Time versus depth migration. The Leading Edge.

Amthor, J. E., and G. M. Friedman, 1991, Dolomite-rock textures and secondary porosity development in Ellenburger Group carbonates (Lower Ordovician) west Texas and southern New Mexico: Sedimentology, v. 38, p. 343 – 362.

Barnes, V. E., P. E. Cloud, L. P. Dixon, R. L. Folk, E. C. Jonas, A. R. Palmer, and E. J. Tynan, 1959, Stratigraphy of the pre-Simpson Paleozoic subsurface rocks of Texas and southeast New Mexico: University of Texas at Austin, Bureau of Economic Geology publication no. 5924, 837 p.

Best and Katsube. Shale permeability and its significance in hydrocarbon exploration. The Leading Edge (1995) vol. 14 (3) pp. 165-170.

Bethke, C. M. 1985. A numerical model of compaction-driven groundwater flow and heat transfer and its application to the paleohydrology of intracratonic sedimentary basins. J. Geophys. Res. 80: 6817-28.

Bethke, C.M. and Marshak, S., 1990. Brine migrations across North America-the plate tectonics of groundwater. Annual Review of Earth and Planetary Sciences. v. 18, pp. 287-315.

Bartram, J., Imbt, W., and Shea, E. 1950. Oil and gas in Arbuckle and Ellenburger formations, Mid-Continent region: Am. Assoc. Petroleum Geologists Bulletin, v. 34, pp. 682-700

Blumstein, A., Elmore, R.D., and Engel, M., 2004, Paleomagnetic dating of burial diagenesis in Mississippian carbonates, Utah: J. Geophys. Res., v. 109, no. B4, B04101, 10.1029/2003JB002698

Bolton, A., and Maltman, A., 1998. Fluid-flow pathways in actively deforming sediments: the role of pore fluid pressures and volume change. Marine and Petroleum Geology, vol. 15, (4), pp. 281-297

Bowker, K.A., 2003. Recent developments of the Barnett Shale play, Fort Worth Basin: West Texas Geological Society Bulletin, v. 42, no. 6, p. 4-11

Bowker, K.A., 2007. Barnett shale gas production, Fort Worth basin: issues and discussion. AAPG bulletin, vol. 91 (4) pp. 523

Bleakly, D. C., Van Alstine, D. R., and Packer, D. R., 1985a, Core Orientation 1: Controlling errors minimizes risk and cost in core orientation, Oil and Gas Journal, v. 83, no. 48, p. 103-109.
Bleakly, D. C., Van Alstine, D. R., and Packer, D. R., 1985b,Core Orientation 2: How to evaluate orientation data, quality control, Oil and Gas Journal, v. 83, no. 49, p. 46-54.

Bradfield, 1964.. The Ellenburger Group of North Central Texas. Tulsa Geological Society Digest,vol. 32, pp. 112-118.

Burgess, W.J., 1976. Geologic evolution of the Mid-Continent and Gulf Coast areas - A plate tectonics view: Trans. Gulf Coast Assoc, of Geol. Soc, v. 26, pp.132-143.

CER Corporation, 1992, Geological, petrophysical and engineering analysis of the Barnett Shale in the Mitchell Energy Corporation T.P. Sims No. 2, Wise County, Texas: Gas Research Institute Contract Report No. 5091-212-2242, 83 p..

Cloud, P.E., Jr., and Barnes, V.E, 1948. The Ellenburger Group of central Texas: University of Texas, Publ. 4621, 473 p.

Combs, D. M., Loucks, R.G., and Ruppel, S.C., 2003. Lower Ordovician Ellenburger Group collapsed paleocave facies and associated pore network in the Barnhart field, Texas, in T. J. Hunt and P. H. Luftholm, eds., The Permian Basin: Back to basics: West Texas Geological Society Symposium: Proceedings, West Texas Geological Society Publication 03-112, p. 397 – 418.

Daniels, E.J., Altaner, S.P., Marshak, S., and Eggleston, J.R., 1990, Hydrothermal alteration of anthracite from eastern Pennsylvania: Implications for mechanisms of anthracite formation: Geology, v. 18, p. 247-250.

Dean, R. S., and G. J. Ross, 1976, Anomalous gypsum in clays and shales: Clays and Clay Minerals, v. 24, p. 103–104.

Denison, R.E., Koepnick, R.B., Burke, W.H., and Hetherington, E.A., 1994 Construction of the Cambrian and Ordovician seawater 87Sr/86Sr curve. Chemical Geology (1998) vol. 152 (3-4) pp. 325-340.

Dewhurst, D. N, Y. Yang, and A. C. Aplin, 1999, Permeability and flow in natural mudstones: in A. C. Aplin, A. C. Fleet, and J. MacQuaker, eds. Muds and Mudstones-Physical and Fluid Flow Properties: Special Publication 38, Geological Society London, p. 23-43.

Dorobek, S.L., 1989, Migration of orogenic fluids through the Siluro-Devonian Helderberg Group during late Paleozoic deformation: Constraints on fluid sources and implications for thermal histories of sedimentary basins: Tectonophysics, v. 159, p. 25-45.

Dunlop, D. J., and Argyle, K.S., 1991. Separating Multidomain and Single-Domain-Like Remanences in Pseudo-Single-Domain Magnetites (215–540 nm) by Low-Temperature Demagnetization, J. Geophys. Res., 96(B2), 2007–2017.

EIA (ENERGY INFORMATION ADMINISTRATION), 2008 U.S. crude oil, natural gas, and natural gas liquids reserves 2008 annual report: EIA: http://www.eia.doe.gov/pub/oil_gas/natural_gas/data_publications/crude_oil_natural_ga

s_reserves/current/pdf/table09.pdf (accessed March 2010).

Elmore, R. D., 2001, A Review of Paleomagnetic Data on the Timing and Origin of Multiple Fluid-Flow Events in the Arbuckle Mountains, Southern Oklahoma, Petroleum Geoscience, 7, 223-229.

Elmore, R. D., Banerjee, S., Campbell, T., and Bixler, G., 1998, Paleomagnetic dating of ancient fluid-flow events and paleoplumbing in the Arbuckle Mountains, Southern Oklahoma: In: Parnell, J., ed., Dating and Duration of Fluid Flow Events and Rock-Fluid Interaction. Geological Society, London, Special Publications, 144, 9-25.

Elmore, R.D., and McCabe, C., 1991, The occurrence and origin of remagnetization in the sedimentary rocks of North America, in Contributions in Geomagnetism and Paleomagnetism, U.S. National Report 1987-1990, Rev. Geophys. Supplement, 377-383.

Elmore, R.D., London, D., Bagley, D., and Gao, G., 1993, Remagnetization by basinal Fluids: Testing the hypothesis in the Viola Limestone, southern Oklahoma: J. Geophys. Res., v. 98, p. 6237-6254.

Elmore, R.D., Kelley, J., Evans, M., and Lewchuk, M.T., 2001, Remagnetization and orogenic fluids: Testing the hypothesis in the central Appalachians: Geophysical Journal International, v. 144, p. 568-576.

Erlich, R., and Coleman, J., 2005. Drowning of the Upper Marble Falls carbonate platform (Pennsylvanian). Sedimentary Geology, 175, p. 479-499

Ewing, T. E., 2006, Mississippian Barnett Shale, Fort Worth Basin: North-central Texas: Gas-shale play with multi-tcf potential: Discussion: AAPG Bulletin, v. 90, p. 963 – 966.

Fisher, R.A., 1953. Dispersion on a sphere: Geophysical Journal of the Royal Astronomical Society, v. 217, p. 295–305.

Fisher, M.K., Wright, C.A., Davidson, B.M., Fielder, E.O., Buckler, W.S., Steinsberger, N.P., 2002. Integrating fracture-mapping technologies to optimize stimulations in the Barnett Shale. SPE Annual Technical Conference and Exhibition. SPE 77441.

Flawn, P. T., A. Goldstein, Jr., P. B. King, and C. E. Weaver, 1961.
The Ouachita system: University of Texas, Bureau of Economic Geology, Report 6120, 401 p., 6 sheets.

Flippin, J. W., 1982. The stratigraphy, structure, and economic aspects of the Paleozoic strata in Erath County, north-central Texas, in C. A. Martin, ed., Petroleum geology of the Fort Worth Basin and Bend arch area: Dallas Geological Society,, p. 129 – 155.

Gale,J.F., Reed, R.M., and Holder, J. 2007. Natural fractures in the Barnett Shale and their importance for hydraulic fracture treatments. AAPG Bulletin vol. 91 (4) pp. 603

Garven, G., 1995, Continental-scale groundwater flow and geological processes: Annual Review of Earth and Planetary Sciences, v. 24, p. 89-117.

Hale-Erlich, W.S., and Coleman, J.L., 1993. Ouachita–Appalachian juncture: a Paleozoic transpressional zone in the southeastern USA. AAPG Bulletin, vol.77, pp.552 – 68.

Hanor, JS (2001) Reactive transport involving rock-buffered fluids of varying salinity. Geochim Cosmochim Acta, 65, pp.3721–3732

Harrington, J. F., & Horseman, S. T. (1999). Gas transport properties of clays and mudrocks. In A. C. Aplin, A. J. Fleet, & J. H. S. Macquaker (Eds.), (158) (pp. 107 – 124). Muds and mudrocks: Physical and fluid-flow properties, London: Geological Society, Special Publications. hydrogeological, geochemical and geotechnical experiments performed in 1996 and 1997. Swiss National Hydrological and Geological Survey (Bern), (p. 191).

Haubold, H., 1999. Alteration of magnetic properties of Palaeozoic platform carbonate rocks during burial diagenesis (Lower Ordovician sequence, Texas, USA) Geological Society, London, Special Publications; 1999; v. 151; p. 181-203.

Hay, R.L., Lee, M., Kolata, D.R., Matthews, J.C., and Morton, J.P., 1988, Episodic potassic diagenesis of Ordovician tuffs in the Mississippi Valley area: Geology, 16, 743-747.

Hearn, P.P. and Sutter, J.F., 1985, Authigenic potassium feldspar in Cambrian carbonates: evidence of Alleghenian brine migration: Science, 228, 1529-1531.

Henry, J. D., 1982. Stratigraphy of the Barnett Shale (Mississippian) and associated reefs in the northern Fort Worth basin, in C. A. Martin, ed., Petroleum geology of the Fort Worth basin and Bend arch area: Dallas Geological Society, p. 157 – 178.

Hickey and Henk. 2007, Lithofacies summary of the Mississippian Barnett Shale, Mitchell 2 TP Sims well, Wise County, Texas. AAPG bulletin, vol. 91 (4) pp. 437.

Hildenbrand and Urai, 2003. Investigation of the morphology of pore space in mudstones — first results. Marine and Petroleum Geology, vol. 20 (10) pp. 1185-1200.

Hill, RJ, Jarvie, DM, Zumberge, J.,Henry, M., and Pollastro, R.M., 2007. Oil and gas geochemistry and petroleum systems of the Fort Worth Basin. AAPG Bulletin,v. 91 (4) pp. 445.

Hoak, T.E., Sundberg, K.S., Ortoleva, P. and Shebl, M., 1998. Fracture Characterization and Discrimination Criteria for Karst and Tectonic Fractures in the Ellenburger Group, West Texas.: Implications for Reservoir and Exploration Models. DOE-OSTI Technical Report. DOE/PC/91008--23-Pt.6. 63p.

Horseman, S. T., Higgo, J. J. W., Alexander, J., & Harrington, J. F., 1996. Water, gas and solute movement through argillaceous mediaexperiments on gas migration in repository host rocks. The NEA (Nuclear Energy Agency) Working Group on Measurement and Physical Understanding of Groundwater Flow Through Argillaceous Media (‘Clay Club’), a subgroup of the NEA Co-ordinating Group on Site Evaluation and Design of Experiments for Radioactive Waste Disposal (SEDE), Report 96/1 OECD, Paris, (p. 290).

Hubbert. M. K.. and Ruby, W.W., 1959. The role of fluid pressure in mechanics of overthrust faulting. Gcological Society of America. Bulletin, 70, p15- 66.

Ingram, G. M., J. L. Urai, and M. A. Naylor 1997, Sealing processes and top seal assessment: in P. Moller-Peterson and A. G. Koestler, eds., Hydrocarbon Seals-Importance for Exploration and Production: Norwegian Petro-leum Society Special Publication 7, p. 165-174.

Jarvie, D., 2010. Characteristics of economically-successful shale resource plays, DGGS Talk, Grapevine,TX May 5 2009. Worldwide Geochemistry. http://www.wwgeochem.com/resources/Jarvie+DGGS+May+5$2C+2009.pdf

Jarvie, D., 2004, Evaluation of hydrocarbon generation and storage in the Barnett Shale, Ft. Worth Basin, Texas: Special BEG / PTTC Presentation, 116 p.: http://www.humble-inc.com.

Jarvie,D.M., Hill,R.J., Ruble,T.E., and Pollastro, R.M. 2007. Unconventional shale-gas systems: The Mississippian Barnett Shale of north-central Texas as one model for thermogenic shale-gas assessment. AAPG bulletin (2007) vol. 91 (4) pp. 475.

Johnson, K.S., Amsden, T.W., Denison, R.E., Dutton, S.P., Goldstein, A.G., Rascoe Jr, B., 1988, Southern midcontinent region. Chapter 12, In: Sloss LL, editor. Sedimentary Cover—North American Craton. The Geology of North America, vol. D-2. Geological Society of America; p. 307 – 59.

Jones. M. E., and Addis. M. A., 1986. The application of stress path and critical state analysis to sediment deformation. I. Structural Geology, 8, p.575-580.

Karastathis, A., 2007. Petropysical Measurements on Tight Gas Shales. Masters thesis, Oklahoma U., Norman, Oklahoma.

Kirschvink, J.L., 1980, The least-squares line and plane and the analysis of paleomagnetic data: Geophys. J. R. Astr. Soc., v. 62, p. 699-718.

Kruiver, P.P., Dekkers, M.J., and Langereis, C.G., 2000, Secular variation in Permian red beds from Dome de Barrot, SE France: Earth Planet. Sci. Lett., v. 179, p. 205-217.

Leach, D.L., and Rowan, E.L., 1986, Genetic link between Ouachita foldbelt tectonism and the Mississippi Valley-type lead-zinc deposits of the Ozarks: Geology, 14, 931-935.

Loucks, R.G. and Ruppel, S.C., 2007. Mississippian Barnett Shale: Lithofacies and depositional setting of a deep-water shale-gas succession in the Fort Worth Basin, Texas. AAPG Bulletin. vol. 91 (4) pp. 579.

Loucks et al. Morphology, Genesis, and Distribution of Nanometer-Scale Pores in Siliceous Mudstones of the Mississippian Barnett Shale. Journal of Sedimentary Research (2009) vol. 79 (12) pp. 848-861.

Lowrie, W.,1990. Identification of ferromagnetic minerals by coercivity and unblocking temperature properties:. Geophysical Research Letters, v.17, p.159–162.

Lu, G., C. McCabe, J.S. Haner, and Ferrell, R.E., 1991, A genetic link between remagnetization and potassic metasomatism in the Devonian Onondaga formation, northern Appalachian basin: Geophys. Res. Lett., v. 18, pp. 2047-2050.

Meckel Jr, L.D., Smith, D., and Wells,L., 1992. Ouachita foredeep basins: regional paleogeography and habitat of hydrocarbons. Foreland Basins and Fold Belts. Tulsa, American Association of Petroleum Geologists, Memoir vol. 55 pp. 427□444.

Milliken, K., Choh,S., Papazis, P., and Schieber, J. 2007. "Cherty" stringers in the Barnett Shale are agglutinated foraminifera. Sedimentary Geology (2007) vol. 198 (3-4) pp. 221-232

Montgomery, S. L., D. M. Jarvie, K. A. Bowker, and R. M. Pollastro, 2005. Mississippian Barnett Shale, Fort Worth Basin, north- central Texas: Gas-shale play with multi-trillion cubic foot potential: AAPG Bulletin, v. 89, p. 155 – 175.

Nelson, R. A., Lenox, L. C., and Ward, B. J., Jr., 1987, Oriented core: Its use, error, and uncertainty: AAPG Bulletin, v. 71, p. 357-367.

Neuzil, C. E. (1994). How permeable are clays and shales? Water

Resources Research, 30(2), 145 – 150.

Oliver, J., 1992, The spots and stains of plate tectonics: Earth Sci. Rev., v. 32, p. 77-106.

Oliver, R., 1986, Fluids expelled tectonically from orogenic belts: their role in hydrocarbon migration and other geologic phenomena: Geology, v. 14, p. 99-102.

Schieber, J., 2001, A role for organic petrology in integrated studies of mudrocks: examples from Devonian black shales of the eastern US. International Journal of Coal Geology.

Sullivan, E.C., Marfurt,KJ., Lacazette, A., and Ammerman, M. 2006. Application of new seismic attributes to collapse chimneys in the Fort Worth Basin. Geophysics (2006) vol. 71 pp. B111-B119.

Papazis, P.K., 2005. Petrographic characterization of the Barnett Shale, Fort Worth Basin, Texas. Master of Science Thesis, The University of Texas at Austin, Austin, 142 pp.

Pollastro, R.M., Hill,R.J., Jarvie, D.M., Henry, M., 2003. Assessing undiscovered resources of the Barnett–Paleozoic total petroleum system, Bend Arch–Fort Worth Basin province, Texas. American Association of Petroleum Geologists Convention, Fort Worth, Texas, American Association of Petroleum Geologists/Datapages,vol. 18.

Pollastro, R.M., Jarvie, D.M., Hill, R.J., and Adams, C.W., 2007. Geologic framework of the Mississippian Barnett Shale,Barnett-Paleozoic total petroleum system, Bend arch–Fort Worth Basin, Texas. AAPG Bulletin. vol. 91 (4) pp. 405-436.

Sagar, K. 2009. Petrophysical characteristics of the Barnett Shale Play. Masters Thesis. Oklahoma U. Norman, Oklahoma.

Slatt et al., 2007. RESERVOIR CHARACTERIZATION OF UNCONVENTIONAL GAS SHALE RESERVOIRS: EXAMPLE FROM THE BARNETT SHALE, TEXAS, U.S.A. . 2007 GSA Denver Annual Meeting (2007).

Singh, 2008, LITHOFACIES AND SEQUENCE STRATIGRAPHIC FRAMEWORK OF THE BARNETT SHALE, NORTHEAST TEXAS. OU PHD THESIS pp. 1-198 .

Smith Jr,L.B., and Davies, G.R., 2006. Structurally controlled hydrothermal alteration of carbonate reservoirs: Introduction. AAPG Bulletin. vol. 90 (11) pp. 1635.

Stamatkos, J., Hirt, A., Lowrie, W. 1996. The age and timing of folding in the central Appalachians from paleomagnetic results. Geological Society of America Bulletin., 108, 815-829.

Tauxe, L., 2002. Paleomagnetic principles and practice: Boston, Kluwer Academic Publishers, v., p. 299.

Tauxe, L., 2005, Lectures in Paleomagnetism: http://earthref.org/MAGIC/books/Tauxe/2005/.

Thomas, 1993. Low-angle detachment geometry of the late Precambrian-Cambrian Appalachian-Ouachita rifted margin of southeastern North America. Geology. vol. 21 (10) pp. 921-924.

Van Alstine, D., and Butterworth, J., 2002. Paleomagnetic Core-Orientation Helps Determine the Sedimentological, Paleostress, and Fluid-Migration History in the Maracaibo Basin, Venezuela. Avaiable at web: http://www.appliedpaleomagnetics.com.

Turner, G. I., 1957, Paleozoic stratigraphy of the Fort Worth basin, in W. C. Bell, ed., Abilene and Fort Worth Geological Societies joint field trip guidebook, p. 57 – 77.

Van Alstine, D. R., and Butterworth, J. E., 2002,Paleomagnetic core orientation helps determine the sedimentological, paleostress, and fluid-migration history in the Maracaibo Basin, Venezuela, Core Workshop for I Congreso Virtual de Sedimentología, 11 de Febrero al 08 de Marzo de 2002.

Van der Voo, R., 1993. Paleogmagnetism of the Atlantic, Tethys, and Iapetus Oceans. Cambridge University Press.

Walper, J.L., 1982. Plate tectonic evolution of the Fort Worth basin, in Charlee A. Martin (ed.>. Petroleum geology of the Forth Worth basin and Bend Arch area: Dallas Geological Society, pp. 237-241.

Williamson, M.A.,1992, The subsidence, compaction, thermal and maturation history of the Egret Member source rock, Jeanne D'Arc Basin, offshore Newfoundland. Bulletin of Canadian Petroleum Geology, 40, 136-150.

Zhao, H.,Givens, N.B., and Curtis, B. 2007.. Thermal maturity of the Barnett Shale determined from well-log analysis. AAPG Bulletin vol. 91 (4) pp. 535.

Zijderveld, J.D.A., 1967, A.C. demagnetization of rocks: analysis of results, in Methods in Paleomagnetism, Nato Advanced Study Institute on Paleomagnetic Methods: University of Newcastle Upon Tyne, p. 254-286.

SUMMARY

Chapter 1 identified a complex paragenetic history in the uppermost Ellenburger Group of the Fort Worth Basin, which compares well with published studies on the paragenesis of Ellenburger in west and central Texas. The unit contains multiple magnetizations that reside in magnetite and are interpreted to be CRMs. Karst breccias in core contain a late Ordovician to Silurian CRM are interpreted as related to early diagenetic processes, perhaps associated with Ordovician-Silurian dolomitization. Breccia clasts were uniformly magnetized after karsting occurred suggesting that karsting was an early phenomenon.

Fractured limestone intervals in the overlying Viola-Simpson Group contain a Pennsylvanian CRM, interpreted as resulting from burial maturation of organic matter or the smectite-to-illite conversion. This Pennsylvanian pole is off of the APWP. One possible interpretation for this is a regional counterclockwise tectonic rotation of between 15-20°. Mottled carbonates, crystalline dolomites and fractured intervals contain a late Permian-Triassic CRM. The rocks with this CRM are enriched in radiogenic strontium and are interpreted as forming from externally derived fluids that may have migrated from the Ouachita thrust zone. The interval also contains evidence of warm fluid alteration, such as mineralized vugs with fluid inclusions yielding highly saline, 100°C+ fluids.

One group of mineralized sites contain a late Triassic to Jurassic CRM, interpreted as a late fluid event, as the unit is associated with dissolution and precipitation textures. This fluid migration event may be related to fluids activated by late extension during the uplift of the Llano and breakup of Pangaea. The question of

whether or not these late fluids infiltrated the tight shale of the Barnett is the subject of Chapter 2.

Chapter 2 presented evidence that the Barnett Shale has experienced multiple remagnetizing events beginning in the mid-Pennsylvanian and continuing into the late Permian. The unit contains magnetizations that reside in magnetite and are interpreted to be CRMs. The specimen directions are streaked from a southeasterly and shallow direction to a southerly and shallow direction. The modern VRM was used to orient the CRM data for one of the wells and to test the core scribe orienting method. The results confirm the streak of directions is real and reproducible, and not caused by core rotations.

Subdivision of the paleomagnetic data does not reveal an apparent control on the CRMs by lithofacies. There appears to be a correlation between fracture orientation and the paleomagnetic data. The evidence suggests that perhaps like a traffic light, when one set of fractures is in a favorable stress regime it is open to fluids whereas the other sets are not. When there was a change in basin stress direction, the preferential fluid filling fracture orientation also changed and was recorded by a CRM.

Bed parallel fractures, or stratiform mineral deposits, are rich in sulfates, sulfides, phosphates, albite, calcite and quartz, and contain a Pennsylvanian CRM. These minerals are interpreted as sourced during very early diagenesis related to stagnant maximum flooding surface marine conditions on a sediment-starved surface. The sulfates and phosphates were then remobilized during early burial into fractures.

Northeasterly sub-vertical fractures contain a mid-Pennsylvanian age CRM and are associated with cements similar in nature to the stratiform deposits. Calcite is the

dominant mineral fill and multiple generations of calcite are present. Barite and celestine form significant secondary cements in these fractures. The fluids that precipitated the fracture fills were radiogenic. They are interpreted to have formed from early burial diagenesis.

Vertical fractures with northwesterly azimuths include stress interference at fracture tips and narrow vertical apertures. En echelon fracturing is common in this group. These fractures are associated with an early Permian CRM. The fractures are largely filled with calcite, silica, dolomite, and only minor barite. These fractures contain hydrocarbon inclusions in silica as well, suggesting they formed in the hydrocarbon maturation window during burial and may have been precipitated from internally derived fluids. The unfractured siliceous Barnett shale matrix contains a similar Permian CRM.

A final CRM occurs in vertical and northeasterly fractures. These fractures show evidence of refracturing by late fluids, and contain late pyrite, calcite, anhydrite and celestine. The celestine appears to be altered by fluids from pre-existing barite. Highly radiogenic strontium values are found in these cements and therefore the cements are interpreted as result of late, externally-derived orogenic fluids originating from the Ouachita highlands to the east.

No CRM is associated with a rare late set of near east-west fractures although they contain evidence of shear motion suggesting these were reactivated during late regional uplift of the Llano region to the south.

Vertical total magnetic susceptibility (MS) data shows similarities among some cores. There is an apparent relationship with gamma ray log data in that younger

magnetizations and higher susceptibilities are associated with more carbonaceous intervals. Likewise, younger CRM ages also tend to favor these intervals. It is possible that MS data can be used to correlate the Barnett in some parts of the basin. This will require further investigation and testing.

The Ellenburger and Barnett have both experienced remagnetizing fluid alteration events during their histories, and connections can be made in some cases between the two units. Both units were remagnetized in the early-mid Pennsyvanian period, suggesting that the burial of the section into the range of decarboxylization and the thermal maturity windows for hydrocarbon generation remagnetized portions of both units. Both units also contain a widespread Permian to early Triassic aged set of remagnetizations, which correspond to maximum burial of the unit. Both units contain highly radiogenic strontium values in these zones suggesting a possible mixture of externally-derived radiogenic fluids perhaps from the Ouachita thrust (as supported by the highly radiogenic values of the SC core) or from deep basement brines. It is assumed that also internal burial fluids were present and played a role in these alterations.

The Ellenburger, unlike the Barnett also contains two events which are not recorded in Barnett CRMs; a late Ordovician-Silurian remagnetization which predates deposition of the Barnett, and a late Triassic to Jurassic CRM. It may be speculated that this late fluid could not infiltrate the tighter Barnett shale unit due to its low permeability after cementation during the Pennsylvanian and Permian periods. This cementation of the Barnett was likely one major factor why the rock exhibits such low permeabilities in the modern day.

Appendix

Paleomagnetic Data Tables (red directions are considered anomalous and are not considered in the analysis)

ES: 33.1N, -97.7W

Specimen	Depth (feet)	Weight (gm)	TSusceptibility (X 10^{-6})	NRM mA/m	ChRM Directions Dec °	Inc °	a95
ES 6777-11	6777.11	26.6	290.4	4.75	174.8	-2	3.1
ES 6778-02	6778.02	28.7	306.2	5.67	191	-3.3	3.4
ES 6778-07	6778.11	29	309.7	4.88	173.6	-8.9	3.3
ES 6789-09	6789.09	29.3	210.3	2.14	142.8	5	3.4
ES 6790-02	6790.02	24.9	137.8	1.69	124.4	-2.5	4.4
ES 6792-00	6792	25.9	149.8	1.75	120.7	-6.8	3.9
ES 6792-03	6792.03	25.1	161.5	1.69	129.3	-3.5	4.4
ES 6792-07	6792.07	23.6	315.8	4.09	95.7	-7.5	4.4
ES 6808-02	6808.02	25.3	268.2	4.09	163.7	3.4	3.2
ES 6808-05	6808.05	27.9	302.4	4.19	182.7	9.5	3.6
ES 6808-09	6808.09	25.8	290.1	4.98	148.4	8.4	6.3
ES6817-08	6817.08	21.5	133.6	1.81	117	3.3	4.9
ES 6817-10	6817.1	24.6	150.3	1.86	142.8	3.8	7.1
ES 6819-01	6819.01	24.6	234.7	2.31	137.6	3.1	4.6
ES 6831-01	6831.1	29.4	183.6	1.61	137.7	-0.3	6.1
ES 6832-00	6832	25.3	199.5	2.2	163.5	8.9	4.4
ES 6832-02	6832.02	29.3	274.1	2.59	172.5	8	4.7
ES 6866-07	6866.07	27.2	277.3	2.92	139.5	-1.4	4.1
ES 6866-11	6866.11	27.3	175.6	2.03	149.5	1.3	4.7
ES 6867-01	6867.01	27.6	189.2	2.14	116.9	3.3	4.6
ES 6870-06	6870.06	29.3	258.3	1.91	119.6	5	5
ES 6871-09	6871.09	28.9	255.8	2.13	160.9	6.2	1.5
ES 6872-05	6872.05	28.2	220.2	2.43	159.5	3.2	5
ES 6872-08	6872.08	28.1	227.6	2.5	163.5	7.1	3
ES 6872-10A	6872.1	27.6	99.29	2.35	170.3	7.1	3.7
ES 6882-07	6882.07	24.8	28.46	0.41	14.2	0.9	3.7
ES 6888-01	6888.01	24.6	57.8	0.1		no good data	
ES 6888-05	6888.05	23.4	47.58	0.1		no good data	
ES 6894-01	6894.01	24.7	58.78	0.12		no good data	
ES 6894-04	6894.04	24.9	49.15	0.16		no good data	
ES 6894-06	6894.06	22.4	44.32	0.13	106.5	7.2	11.9
ES 6897-09	6897.09	25.7	56.21	0.11	43.5	40.4	13.5
ES 6897-11	6897.11	26	61.76	0.09	158.9	18.7	1.6
ES 6901-03	6901.03	22.9	47.17	0.09	140.4	1.7	14.7
ES 6903-02	6903.02	25.4	41.77	0.05	89.7	0.7	2.7
ES 6903-06	6903.06	25.7	46.7	0.07		no good data	

ES 6907-06	6907.06	26.8	135.5	0.21	142.2	9.9	5.4
ES 6907-11	6907.11	26.3	148.4	0.45	110.4	4.1	5.1
ES 6915-02	6915.02	24.7	115.3	0.28	128.2	36.4	10.6
ES 6915-04	6915.04	23.3	93.31	0.26	154.3	35.2	10.5
ES 6921-03	6921.03	23.2	132.7	1.28	187.8	-1.6	1.7
ES 6924-01	6924.01	29.2	344	2.09			
ES 6924-04	6924.04	28.2	265.7	2.11			
ES 6929-01	6929.01	22.7	179.2	1.4			
ES 6929-03	6929.03	22	180.6	1.43			
ES 6933-10	6933.1	26.4	277.7	1.86			
ES 6935-05	6935.05	25.4	138.5	0.96			
ES 6941-02	6941.02	24.8	83.93	0.16			
ES6941-07	6941.07	26.9	217	0.5			
ES 6941-09	6941.09	25.1	87.83	0.09	149.2	8	9.8
ES 6998-02	6998.02	22.9	46.02	0.08	86.5	-6.1	2.3
ES 6999-00	6999	26.8	44.97	0.08		no good data	
ES 6999-02	6999.02	26.8	61.52	0.11	151.7	1.4	3.6
ES 7156-01	7156.01	25.5	42.12	0.09	175.6	11.4	7.7
ES 7156-05	7156.05	27.3	33.01	0.13	140.3	11.7	4.7
ES 7168-04	7168.04	27.1	84.97	0.18	156.8	3.3	13.2
ES 7168-08	7168.08	21.2	50.23	0.09	197.2	-9.5	15.5
ES 7176-02	7176.02	27.4	81.08	0.15	152.4	-1.1	2
ES 7174-04	7176.04			0.28		no good data	
ES 7176-07	7176.07	25.9	124.2	0.07		no good data	
ES 7177-02	7177.02	26.8	37.62	1.16	190.1	-4.5	8
ES 7177-06	7177.06	26	22.07	0.09	153.1	-13.7	7.9
ES 7177-09	7177.09	26.5	37.16	0.26	178.7	-25.9	4.1
ES 7184-08	7184.08	29.4	38.57	0.08	179.2	19.7	14
ES 7184-11	7184.11	28.6	19.2	0.1	130.3	21.5	9.4
ES 7185-02	7185.02	29.8	20.86	0.1	153.1	18.1	12.2
ES 7185-08	7185.08	28.7	161	0.24	187.5	0.5	7.3
ES 7187-02	7187.02	34.1	74.71	0.12	181.1	-5.3	10.9
ES 7187-06	7187.06	31.8	50.35	0.21	164.2	3.5	4.5
ES 7191-08	7191.08	27	42.36	0.13	195.4	2	9.4
ES 7194-03	7194.03	27.2	32.72	0.21	112.9	5.1	4.3
ES 7194-05	7194.05	27.8	29.97	0.25	127.9	-0.1	4.6
ES 7194-09	7194.09	28.2	29.66	0.26	132.5	-0.9	9
ES 7198-05	7198.05	27.5	47.56	0.39	180.4	0.3	3.2
ES 7198-07	7198.07	27.5	52.51	0.36	170.6	0.9	3.8
ES 7198-10	7198.1	27.7	50.67	0.38	178.5	1.7	3.5
ES 7208-00	7208	27.1	219.9				
ES 7210-11	7210.11	28	20.72	0.13	218.8	-4.1	7
ES 7211-02	7211.02	29	27.93	0.07	261.3	26.1	8.4
ES 7211-04	7211.04	29.3	20.25	0.06	134.4	27	7.4
ES 7227-12	7227.12	27.8	32.89	1.55	177.8	-7	1.5
ES 7234-01	7234.01	28.4	17.81	0.8	43.2	-8.3	2.8
ES 7234-05	7234.05	27.6	17.16	0.74	124.6	-2.3	4.2
ES 7241-11	7241.11	27.5	9.96	0.2		no good data	

ES 7242-02	7242.02			0.18	156.7	-13.8	10
ES 7242-05	7242.05			0.19	150.8	-0.4	6.4
ES 7244-10	7244.1	28.1	8.49	0.16		no good data	
ES 7245-02	7245.02	27.5	5.05	0.03	201.2		
ES 7245-05	7245.05	27.6	5.52	0.17		no good data	
ES 7251-07	7251.07	28.9	3.39	0.21	147.1	-8.9	6.6
ES 7251-10	7251.1	29.2	3.41	0.2	123.2	-0.3	3.3
ES 7252-02	7252.02	29.3	0.01	0.16	167	0.1	5.1
ES 7256-09	7256.09	29.5	-3.16	0.16		no good data	
ES 7257-01	7257.01	30.3	-1.73	0.16	121.5	-12.4	7.5
ES 7257-08	7257.08	29.7	68.56	0.16	144.8	-6.6	13.2
ES 7258-00	7258	29.3	-1.38	0.16	134.1	6.4	8.4
ES 7266-01	7266.01	35.2	3.55	0.15	157.6	14.4	10.3
ES 7266-04	7266.04	27.7	2.01	0.17	136.8	-0.1	4.7
ES 7266-08	7266.08	29.3	-1.76	0.11		no good data	
ES 7266-10	7266.1	28.9	-0.67	0.13	159.7	6.8	5
ES 7267-00	7267	28.1	0.11	0.13	151.8	8.5	2.6
ES 7267-02	7267.02	28.1	0.9	0.13	152.9	10.1	6.2
ES 7267-04	7267.04	27.3	-0.97	0.11	154.2	9	9.6
ES 7272-08	7272.08	29	1.09	0.16		no good data	
ES 7272-11	7272.11	29.6	1.49	0.16	113.3	27.9	11.4
ES 7273-01	7273.01	27.2	3.53	0.16		no good data	

ASW 33.07N; -97.81W

Specimen	Depth (feet)	Weight (gm)	Susceptibility ($X\ 10^{-6}$)	NRM mA/m	ChRM Directions Dec °	Inc °	a95	Demag type
02021a	6434.04	26.4	75.92					
02021b	6434.04	25.3	69.99		167.5	40.2	7.2	TH
02181a	6481.07	27.7	303.4		160.2	11.4	7.5	TH
3081	6512.01	29.6	202.5		182.2	2.2	4.5	TH
3091	6513.01	29.2	190.9		181.5	7.7	5	TH
03092a	6514.01	25.2	51.98		167	7.1	14.6	TH
3093	6515.03	26.9	58.19		177.4	8.6	9.8	TH
3094	6515.05	27.1	58.4		179.6	15.1	7.9	TH
31701	6539.25	34.4	21	0.09	159.3	-10.5	1.4	**TH**
04032b	6556	26.7	32.68		133.3	-1.4	0	TH
40801	6570.02	31	26	0.05	125.3	4.7	3.2	TH
42011	6603.09	27.3	61.86	0.14	126.1	-1.2	10.6	**TH**
42012	6603.09	25.6	57.63	0.23	132.1	-2.8	3.9	**TH**
42021	6603.11	28.5	90.62	0.64	123.6	-2	4.1	**TH**

42022	6603.11	25.5	79.32	0.62	127.9	-4.4	3.1	**TH**
42031	6604	29.3	120.05	1.02	124.3	-1.6	4.4	**TH**
42032	6604	28.7	114.33	3.27		no measurments		
42101	6605.09	31.8	76	0.11	131	3.2	11.6	TH
05031a	6616.01	26.6	53.38		134.3	-2.1	11.9	TH
60611	6654.12	29.4	44.6	0.12	130.1	-0.4	6.9	**TH**
60612	6654.12	27.3	38.62	0.1	135.2	5.4	4.9	**AF**
60621	6655.01	21.2	30.76	0.12	130.4	1.1	3.8	**TH**
60631	6655.03	26.7	32.5	0.09	136.3	-4.4	2.1	**TH**
62211	6698.09	24.1	7.33	0.04	165.5	10.1	7.3	**AF**
62212	6698.09	23.8	4.08	0.07	133	-2.9	5.8	**TH**
62221	6698.12	22.4	18.3	0.14	122.8	-3.4	8.3	**TH**
62231	6699.01	26.4	22.46	0.44	121.8	-2	5.6	**TH**
70101	6700.09	34.4	27	1.63	154.9	12.5	2.2	**TH**
7031	6706.02	27.4	47.34		165.9	13.1	7.3	**TH**
7092	6724.02	25.7	54.33		149.3	8.6	13.1	**TH**
71011	6726.1	28.7	32.33	0.19	162.5	19	3.2	**AF**
71021	6726.12	29.9	35.25	0.12	163.1	15.6	12.4	**TH**
7132	6734.11	25.2	60.96		153.9	18.4	13.4	**TH**
7133	6735.02	26.7	60.88		194.1	6.4	8.2	**TH**
71603	6742.06	28.2	57	0.12	168.6	19.5	12.5	**TH**
71602	6744.03	32.2	43	0.17	156.7	6.9	7.6	**TH**
71811	6749.08	28.7	11.56	0.22	156	-6.2	7.6	**TH**
71812	6749.08	21.4	10.03	0.21	154	-4.5	5.3	**TH**
71821	6749.11	30.2	13.98	0.2	156.4	-5.2	10.6	**TH**
71822	6749.11	23.3	9.43	0.17	159.6	8.4	3.3	**AF**
7191	6752.04	27	41.12		146.1	12.1	5.9	**TH**
80211	6763.07	33.1	37.38	0.79	140.4	-8.3	3.6	**TH**
80221	6763.09	33.6	38.12	0.73	139.5	-11.1	2	**TH**
80231	6763.1	32.1	39.45	0.73	139.6	-8.4	3.3	**TH**
80232	6763.1	26.1	29.59	2.4	138.9	1.5	3.4	**AF**
80711	6776.1	33	77.19	0.32	139.9	-10.6	4.1	**TH**
80712	6776.1	32.6	76.56	0.76	23.1	41.1	7.2	**TH**
80721	6776.11	32.3	74.95	0.27	140.4	-8.6	5.3	**TH**
80731	6777.05	29.1	71.77	0.27	141.6	-3.8	2.1	**TH**
80732	6777.05	25.5	60.19	0.33	140.4	5.1	6.1	**AF**
80911	6782.05	34.8	100.58	0.29	141.2	-6.6	4.7	**TH**
80912	6782.05	29.6	84.05	0.25	141.5	-9.5	10.6	**TH**
80921	6782.07	30.8	85.03	0.27	145.2	-11.3	5.1	**TH**
80922	6782.07	29.3	80.09	0.24	146.2	25	5.9	**AF**
80931	6782.08	33.5	93.85	0.24	139.1	-4.1	11.2	**TH**
81011	6784.07	32.5	45.06	0.29	131.8	3.7	10.6	**TH**
81021	6784.08	31.4	39.44	0.26	134.2	0.4	8.4	**TH**
81031	6784.09	31.2	41.19	0.21	133.9	-5.3	7.8	**TH**
08104a	6786	28.1	39.23		127.6	10.9	10.5	**TH**
08105a	6786.11	28	40.3		*130.3*	*25.7*	*8.9*	**TH**
08106a	6787.02	28.3	36.71		139.9	12.2	8.9	**TH**

81111	6788.02	36	40.38	0.12	129.1	1.4	7.7	**TH**
81121	6789.01	35	17.47	1.14	83.1	8.1	1.3	**AF**
81122	6789.01	31.4	16.86	0.13	124.2	34.4	13.5	**TH**
81131	6789.03	32.3	10.12	0.1	199.8	-13.4	9.4	**TH**
81211	6790.06	34.2	5.83	0.1	199.3	7.4	7.9	**TH**
81221	6790.08	33.2	5.79	0.97	196.6	4.7	2.7	**TH**
81231	6792.04	30	25.09	2.25	123.3	16.1	24.1	**AF**
81232	6792.04	25.5	17.69	1.1	281.8	82.8	1.9	**TH**
81241	6792.05	25.9	9.59	0.15	207.3	-0.8	12.7	**TH**
81251	6792.06	28.8	13.44	1.71	174.5	79.4	3.4	**TH**
81311	6793.09	34.4	14.21	0.98	98.3	42.8	10.7	**AF**
81312	6793.09	34.4	21.22	0.12	92.5	0.4	5.6	**TH**
81321	6793.11	32.6	4.1	0.12	85.3	15	1.3	**TH**
81331	6794.02	26.1	2.62	0.11	96.2	17.6	6.9	**TH**
81412	6797	27.1	7.85	0.12	90	34.1	11.9	**TH**
81421	6797.02	28.1	7.31	0.1	99.1	2.6	6.4	**TH**
81422	6797.02	27.8	7.92	0.08	99.7	14	3.1	**TH**
81431	6797.05	28.6	8.56	0.16	92.9	1.8	4	**TH**
81432	6797.05	32.2	10.21	1.01	99.1	44.5	1.3	**AF**
81511	6798	30.3	-0.31	0.06	106.3	27.3	6.8	**TH**
81512	6798	32.8	7.06	0.07	102.8	29.8	3	**TH**
81521	6798.01	29.2	5.32	0.07	103.9	12.1	4.7	**TH**
81522	6798.01	34.4	2.14	0.07	119	10.3	10.5	**TH**
81531	6798.02	30.8	2.99	0.27	97.9	60.1	70.4	**AF**
81532	6798.02	32.4	5.41	0.07	103.4	43.8	14.7	**TH**
81701	6804.7	32.3	2	0.11	**110.7**	**0.6**	**8.2**	**TH**
81702	6804.5	35.5	2	0.14	**118.7**	**6.9**	**11.7**	**TH**
81703	6804.35	32.7	4	0.1	108.4	10.7	9.7	**TH**
81704	6804.2	34.1	0	0.13	**109.2**	**8.5**	**6.1**	**TH**
081704a	6804.2	22.7	4	0.09	94.7	20.4	10.2	TH
81706	6804.08	27.5	18.34		119.9	21.7	7.8	TH
081707b	6804.11	28.8	9.89		132.1	27.6	12.1	TH
081708b	6805.02	27	14.25		94.9	10.4	10	TH
08181a	6805.12	31.1	9.01		**126.7**	**9.4**	**8.9**	**TH**
08182a	6806.02	28	8.49		132.4	-1.3	9	TH
08183b	6806.03	29.4	9.8		*103.3*	*44.2*	*16.1*	*TH*
08184a	6806.05	28.1	19.46		109.8	32.9	10.3	TH
81911	6808.04	32.5	-11.22	0.06	*184.4*	*3.8*	*11.3*	**TH**
81912	6808.04	35.5	-10.03	0.05	144.4	58.3	1.7	**AF**
81921	6808.05	32.2	-10.5	0.04		no good		**TH**
81922	6808.05	30.7	-9.97	0.02	*166*	*15.2*	*13.8*	**TH**
81931	6808.07	34.7	-10.35	0.1	167.5	58.5	4.9	**TH**
82101	6814.8	33	20	0.06	147.2	17.5	6.4	**TH**
82102	6814.8	34.3	10	0.16	138.4	37.2	10.8	**TH**
082103a	6814.07	27.9	20.94		129.6	5.9	5.1	**TH**
082104a	6815.02	29.5	19.98		**108.1**	**-13.4**	**7.5**	**TH**
082202b	6816.1	29.8	16.74		131.4	8.5	4.8	TH

082203a	6817.04	27.5	9.73		122.3	11.4	4.4	TH
90411	6830.04	33.5	9.37	0.23	160.6	-9.6	6.1	**TH**
90412	6830.04	28.6	7.77	0.21	*150.6*	*43.9*	*5.9*	***AF***
90421	6830.06	32.4	4.86	0.23	161.6	-12.4	5.5	**TH**
90422	6830.06	28.8	2.33	0.18	162.6	-11.9	5.9	**TH**
90431	6830.08	31.5	7.66	0.2	162.9	-11.2	5.3	**TH**
090601a	6834.05	30.8	14.41		166	0.1	3.6	**TH**
090602a	6834.07	29.1	13.05		163	2.8	3.4	**TH**
091001a	6845.01	29.2	6.42		52.7	-5.4	7.1	**TH**
091002b	6845.03	30.5	10.42		43.4	20.1	9.2	**TH**
091003a	6845.05	29.6	15.77		60.1	2.3	8.6	**TH**
091004a	6845.08	29.8	20.67		53	8.1	8.8	**TH**
091005b	6846.02	29.1	20		60.9	21.8	5.4	**TH**
91202	6851.6	29.5	16	0.16	162.3	-1	5.9	TH
91311	6852.05	32.4	6.46	0.37	160.4	-10.8	2.5	**TH**
91312	6852.05	27.4	4.21	0.43	160.4	-8.2	2.8	**TH**
91321	6852.07	32.3	9.97	0.29	155.1	-9.3	5.2	**TH**
91701	6862.5	34.7	19	0.77	164.5	16.9	8.3	**TH**
100201	6869.4	34	-10	0.12	*69.1*	*33.6*	*9.1*	**TH**
100301a	6872.11	28.4	19.82		156.3	-7.6	4	TH
100302a	6873.02	29.8	20.35		161.1	-5.5	3.9	TH
100303a	6873.04	30.1	15.13		155.4	-2	4.6	TH
100411	6874.1	30.9	-1.26	0.44	8.8	23.9	3.2	**TH**
100412	6874.1	26.4	-4.62	0.36	7.7	10.4	2	**AF**
100421	6874.09	33.1	7.15	0.43	7.6	20.5	2.4	**TH**
100422	6874.09	27.6	3.74	0.51	6.6	17.6	5.5	**TH**
100431	6874.08	32.7	19.2	0.57	10.4	23.5	2.2	**TH**
100432	6874.08	29.3	10.25	0.58	5.5	15.2	2.3	**TH**
100404a	6874.02	29.5	26.21		165.6	1	3.7	**TH**
100405a	6876.04	27.9	14.79		166.2	-1.9	5.1	**TH**
100406a	6876.06	29.9	10.32		155.8	-7.2	5.1	**TH**
100407b	6876.08	29.6	10.51		172.6	-3.1	5.3	**TH**
110101	6885.2	22.8	-8	0.07	114.3	-22.5	9.9	**TH**
110102	6885.6	30.8	-9	0.14	**153.7**	**-18.5**	**2.3**	**TH**
110103a	6884.4	34.6	4	0.15	**154.4**	**-9.8**	**3.5**	**TH**
110104	6884.4	34.7	-2	0.13	**156.1**	**1.4**	**3.3**	**TH**

FL: 32.4N, -97.2W

Specimen	Depth (feet)	Susceptibility ($X\ 10^{-6}$)	ChRM Directions			Demag type
			Dec °	Inc °	A95	
806706	8067.06	187.9	140	-9.3	5.1	TH / 480
806811	8068.11	66.52	136.4	43.3	10.9	TH / 380
807001	8070.01	61.83	154.8	27.6	15.8	TH / 380
807405	8074.05	72.36	152.2	22.8	16.9	TH / 380
807409	8074.09	117.6	129.6	9.6	1.8	TH / 450
807510	8075.1	153.1	146.6	4.6	6.9	TH / 400
807602	8076.02	154.6	143.8	-3.2	5.2	TH / 450
807604	8076.04	167.5	140.2	-5.3	5	TH / 450
807606	8076.06	120.7	139	-2.9	11.4	TH / 450
808511	8085.11	194.1	169.5	26.3	17.4	TH / 380
808604	8086.04	148.3	179.2	25.7	6.6	TH / 380
808607	8086.07	105.9	179.6	22.5	6.6	TH / 400
809002	8090.02	102.7	147.4	40.4	7.2	TH / 400
810309	8103.09	104.2	179.1	82.2	10.1	TH / 350
810402	8104.02	201	198.1	-5	1.5	TH / 380
810404	8104.04	99.91	180.9	54.9	8	TH / 380
811503	8115.03	87.51	195.3	2.7	4.2	TH / 400
811505	8115.05	110.2	186.6	31.7	8.3	TH / 330
811607	8116.07	116.3	179.4	-45.7	14.1	TH / 350
812511	8125.11	114.5	110.5	54.4	6.7	TH / 350
812604	8126.04	122.8	155.3	7.5	8.5	TH / 380
813200	8132	116.3	87.1	77.4	7.3	TH / 350
813202	8132.02	205.4	136.8	-2.6	10.3	TH / 420
813207	8132.07	214.6	139.1	-2.8	5.8	TH / 450
813211	8132.11	140.6	123.3	47.6	12	TH / 380
813602	8136.02	141.5	136.8	-7.7	7	TH / 500
813702	8137.02	165	131.5	8.8	6.6	TH / 450
813802	8138.02	153.3	131.4	-8	10.9	TH / 500
813803	8138.03	133.4	135.3	-3.2	9.5	TH / 480
813808	8138.08	234.2	135.5	19	10.1	TH / 380
814003	8140.03	74.18	136.7	-6.5	6.4	TH / 420
814005	8140.05	65.33	126.2	-3.6	6	TH / 450
814007	8140.07	55.18	133.9	-11.1	6.6	TH / 450
814502	8145.02	18.78	146.4	-8.9	9.5	TH / 520
814505	8145.05	7.15	143.3	-12.8	2.9	TH / 520
816108	8161.08	18.84	143.7	-8.8	4.5	TH / 520
816203	8162.03	18.17	145.9	-12.9	6.7	TH / 450
816908	8169.08	25.25	155.4	-5.5	6.3	TH / 450
817405	8174.05	15.35	159.8	-2.7	6.6	TH / 450
817602	8176.02	22.23	159.7	0.6	11.7	TH / 420
818207	8182.07	25.41	161.4	-4.7	2.9	TH / 480
818304	8183.04	28.54	140.3	-8.2	10.4	TH / 450
818309	8183.09	27.64	150.8	-6.9	3.8	TH / 520

819703	8197.03	24.36	193.9	-9.9	7.8	TH / 420
819709	8197.09	21.38	198	-9	11.5	TH / 420
821805	8218.05	23.97	339.2	-1.5	4.7	TH / 420
821809	8218.09	33.66	335	1.2	4.1	TH / 420
822202	8222.02	29.68	332.8	1.4	3.9	TH /400
822207	8222.07	26.53	335.5	5.2	4	TH /400
822304	8223.04	21.24	341.5	1.4	12	TH / 420
823409	8234.09	25.12	334.7	-9.6	14.5	TH / 450
823503	8235.03	27.8	343.2	3.4	8.4	TH / 500

SC: 32.4N, -97.2W

Depth	Susceptibility	ChRM Directions			
(feet)	(X 10^{-6})	Dec °	Inc °	a95	Demag type
7733	113.7	255.7	79	8.6	TH/310
7733.07	97.14	118.5	4.6	11.9	TH/380
7734.1	148.5	130.5	9.5	13	TH/380
7748.03	126.9	122.7	-7.2	12.2	TH/380
7748.05	131.3	123.8	-6.3	7.2	TH/420
7748.07	171.8	112.7	7.3	15.3	TH/380
7759.04	168.9	119.5	18.4	13.5	TH/380
7760.09	91.13	84.4	19.9	11.3	TH/380
7762.05	101.3	114.5	-13.5	12.1	TH/400
7766.02	119.8	114.3	-4	3.7	TH/440
7818.02	63.09	140	56.5	5.7	TH/330
7818.06	124.8	332.7	18	12.7	TH/380
7832.11	123.3	87.9	41.3	13.8	TH/330
7834.02	114.7	90.4	-8.1	22.2	TH/350
7834.03	103.3	42.3	6	3.3	TH/330
7847.04	285.7	139.8	-4.1	6.3	TH/400
7849.06	46.99	84.7	62	15.9	TH/350
7849.11	227.2	141.9	-6.5	11.5	TH/400
7858.1	109.7	163.2	0.2	3.5	TH/400
7859.05	230.4	177.6	-10	14	TH/380
7881.05	120.6	137.2	-7	12.6	TH/400
7881.11	91.86	163.6	-13.7	9.1	TH/400
7882.01	158.4	156.4	-3.2	9.9	TH/400
7893.02	152.3	172.6	0.8	9.2	TH/400
7893.06	174.8	169.1	-1.6	9.6	TH/420
7916.08	109.2	165.1	1.6	11.9	TH/420
7916.11	113.8	156.2	-2.9	6.4	TH/420
7917.01	116.3	168.3	1.6	6.1	TH/420
7935.09	146.3	199	-10.4	13.9	TH/350
7962.12	127.3	156.3	-4.5	7	TH/380
7963	142.9	149	1.8	15	TH/380
7963.02	134.5	155.5	3.5	7.3	TH/420

7970.08	74.42	148.2	-6.9	8.4	TH/440
7970.12	74.02	132.5	-11.9	7.9	TH/420
7985.02	53.44	151.6	-7.5	11.4	TH/420
7986.01	46.74	155.1	-1.4	8.1	TH/460
7986.05	65.64	153.5	-0.7	10.9	TH/440